

Influence of Sample Preparation Methods and Interlocking on Sand Behaviour: An Experimental Investigation

by

Xubin Su

A Thesis

Submitted to the School of Graduate Studies
in Partial Fulfillment of the Requirements for
the Degree of Master of Applied Science

McMaster University

March 2007

©Copyright by Xubin Su, 2007

MASTER OF SCIENCE (2007)

(Civil Engineering)

McMaster University

Hamilton, Ontario

TITLE: Influence of Sample Preparation Methods and Interlocking on Sand
Behaviour: An Experimental Investigation

AUTHOR: Xubin Su, M.E. (Tongji University)

SUPERVISOR: Dr. P.J., Guo

NUMBER OF PAGES: xviii, 151

Abstract

This thesis investigates the effects of sample preparation methods, which has substantial influence on the internal structure or fabric of the sample, and interparticle locking on the behaviour of sand through experimental study. Extensive laboratory tests were conducted on two sands (namely, Ottawa sand and crushed limestone) with distinct particle shape and surface texture, using a Bishop-type triaxial testing system.

A total of eight sample preparation methods were used to fabricate specimens with different initial fabric, with specimens being fabricated using water pluviation, moist tamping, and moist rodding. The experimental data reveal that sample preparation methods have significant effect on both deformation characteristics and shear strength of sand, in addition to the density and the effective confining pressure applied to the specimens. More specifically, water pluviation and moist tamping tend to yield specimens of high anisotropy and large dilation, which in turn results in higher friction angle in conventional triaxial compression. The effect of sample preparation methods was also observed from undrained tests on saturated sand.

Laboratory tests on crushed limestone consisting of angular particles demonstrate that strong interparticle locking may develop owing to particle angularity. The shear resistance of sand with angular particles has contributions from interparticle friction, dilatation and interparticle locking. Moreover, interparticle locking, which largely exists at the peak shear resistance of sand but vanishes with dilation at large deformation, exists under both low and high stress levels investigated in this study. A

conceptual model was proposed to take into account the energy consumption associated with breaking interparticle locking during deformation when estimating the dilatancy and strength of granular soils.

The behaviour of sand along proportional strain paths was also investigated, with the focus being placed on strain softening and material instability in the context of Hill's second order work. Depending on the strain path or the deformation history, a dilatant sand displaying hardening and stable behaviour under isochronic (undrained) conditions, which is often used as a reference in soil mechanics, may succumb to unstable flow type behaviour along dilative strain paths. More specifically, when the imposed rate of dilation exceeds the inherent rate of dilation of the material, a dense sand specimen will have flow failure similar to that of a saturated loose specimen subjected to undrained compression. On the other hand, a loose sand may not have a flow failure when it is forced to have contractive volume change along imposed strain paths.

Acknowledgements

I wish to express my sincere and grateful thanks to my supervisor, Dr. Peijun Guo. His guidance and support during these years of research have been invaluable. I am grateful for his exceptional patience and encouragement. His directions, advice and expertise were instrumental in accomplishing this research.

The laboratory program was the major component of this study. The successful completion of this testing program was due in part to the assistance of Mr. Peter Koudys. I would like to express my heartfelt appreciation to him for his tireless support.

The love and support of my parents have always been a source of strength in my work. To them I am deeply grateful.

Table of Contents

Abstract.....	iii
Acknowledgements.....	v
Table of Contents.....	vi
List of Figures.....	ix
List of Tables.....	xiv
Nomenclature.....	xv
List of Symbols.....	xv
Abbreviations.....	xviii
Chapter 1 Preliminaries.....	1
1.1 Background and motivations.....	1
1.2 Objectives.....	5
1.3 Thesis outline.....	6
Chapter 2 Literature review.....	8
2.1 Strength properties of granular material.....	8
2.1.1 Three fundamental representations of shear strength.....	8
2.1.2 Development of stress-dilatancy theory.....	9
2.1.3 Contribution of interparticle locking to shear strength.....	13
2.2 Influence of sample preparation method on sand behaviour.....	15
2.2.1 Overview.....	15
2.2.2 Influence of sample preparation method on sand behaviour: static loading	17
2.2.3 Sample preparation method on sand behaviour: cyclic loading.....	20
2.2.4 Sample preparation method and critical state.....	21
2.3 Instability and strain softening.....	22
2.3.1 Introduction.....	22
2.3.2 Experimental observation of instability phenomenon.....	24
Chapter 3 Testing materials, equipment and procedures.....	30
3.1 Introduction.....	30

3.2 Description of testing equipment	30
3.3 Tested materials.....	32
3.4 Sample preparation methods	32
3.4.1 Water / moist / dry pluviation.....	33
3.4.2 Water / moist / dry tamping.....	34
3.4.3 Moist / dry rodding.....	36
3.5 Testing procedures	36
3.5.1 Sample setup.....	36
3.5.2 Saturation.....	37
3.5.3 Consolidation.....	38
3.5.4 Shearing.....	39
3.6 Discussion of test errors	39
3.6.1 Errors in void ratio measurement	39
3.6.2 Membrane penetration.....	42
3.6.3 End restraint.....	44
3.7 Performance of testing system and repeatability of tests	46
Chapter 4 Influence of sample preparation method on stress-strain-strength response of sands.....	54
4.1 Introduction	54
4.2 Behaviour of Ottawa sand prepared by MT	55
4.2.1 Drained behaviour	55
4.2.2 Stress-dilatancy characteristics.....	57
4.2.3 Peak strength and the angle of dilation.....	58
4.3 Undrained behaviour of saturated Ottawa sand	60
4.4 Influence of sample preparation method on sand behaviour.....	61
4.4.1 Static drained triaxial response.....	61
4.4.2 Static undrained response	68
4.5 Summary	69

Chapter 5 Influence of interparticle locking on strength properties of granular material	83
5.1 Introduction	83
5.2 Experimental results and discussions	85
5.2.1 Stress-strain and volume change responses	85
5.2.2 Limiting envelopes in p-q space	88
5.2.3 Stress-dilatancy plots	89
5.2.4 Contributions to shear strength of granular materials	91
5.3 Energy dissipation associated with interlocking degradation	93
5.3.1 Theoretical background	93
5.3.2 Energy dissipation due to interlocking: Experimental data	95
5.4 Summary	97
Chapter 6 Strain softening and material instability along proportional strain paths.....	109
6.1 Introduction	109
6.2 Hill's material instability along proportional strain paths.....	111
6.3 Material Instability along proportional strain path.....	112
6.3.1 Stress-strain responses	112
6.3.2 Strain softening along proportional strain path	116
6.3.3 Strain softening and material instability	118
6.4 Instability domain along imposed proportional strain paths	121
6.5 Summary	121
Chapter 7 Summary and Conclusions.....	133
Bibliography	138
Appendix A Formulae used for the data analysis	149
A.1 Right cylinder assumption and strain localisation.....	149

List of Figures

Figure 2.1: Influence of sample preparation method on sand responses (data after Oda, 1972)	28
Figure 2.2: Peak stress-dilatancy plot in plane strain tests for Toyoura sand (modified from Tatsuoka <i>et al.</i> , 1986).....	28
Figure 2.3: Influence of sample preparation methods on undrained responses of Nevada sand	29
Figure 2.4: Influence of sample preparation methods on undrained responses of Masado sand	29
Figure 2.5: Typical instability in (a) drained test on dense sand, and (b) undrained test on very loose sand.....	29
Figure 3.1: Schematic layout of the triaxial testing system	48
Figure 3.2: Photograph of triaxial testing system	49
Figure 3.3: Schematic of particle shape of testing materials: (a) Sand O; (b) Sand L.....	49
Figure 3.4: Particle size distribution curves.....	50
Figure 3.5: Magnitude of membrane penetration of loose Sand O.....	50
Figure 3.6: Schematic of adopted sample preparation procedures	51
Figure 3.7: Comparison of drained response of Sand L with lubricated and regular end: (a) stress-strain response; (b) volumetric-strain response.....	52
Figure 3.8: Snapshot of dense Sand L specimen at shearing with regular end, $Dr=94\%$, $\sigma_3=100$ kPa: (a) $\varepsilon_a=6.25\%$; (b) $\varepsilon_a=16.85\%$	52
Figure 3.9: Repeatability of triaxial compression drained tests:.....	53
Figure 4-1: Drained triaxial compression test results of Ottawa sand at $\sigma_3 = 100$ kPa :..	71
Figure 4-2: Triaxial compression drained test results of Ottawa sand at $e_0 = 0.73$:.....	71
Figure 4-3: Influence of initial void ratio and the confining pressure on peak friction angle of Ottawa sand.....	72
Figure 4-4: Influence of initial void ratio on stress-dilatancy plot of Ottawa sand at $\sigma_3 = 100$ kPa	72

Figure 4-5: Influence of initial void ratio on stress-dilatancy plot of Ottawa sand at $\sigma_3 = 500$ kPa	73
Figure 4-6: Influence of confining pressure on stress-dilatancy plot of dense Ottawa sand at $e_0 = 0.62$	73
Figure 4-7: Peak stress ratio versus peak dilatancy for Ottawa sand, Moist tamping	74
Figure 4-8: Influence of density to undrained behaviour of Ottawa sand at $\sigma_{30} = 200$ kPa: (a) stress-strain curve; (b) stress path.....	74
Figure 4-9: Influence of confining pressure to undrained behaviour of Ottawa sand at initial relative density of 42%:(a) stress-s ratio versus axial strain; (b) stress path.....	75
Figure 4-10: Influence of sample preparation on drained behaviour of loose Ottawa sand sheared at $\sigma_3 = 100$ kPa : (a) Stress-strain response; (b) Volumetric strain response.....	75
Figure 4-11: Influence of sample preparation on drained behaviour of Sand L sheared at $\sigma_3 = 100$ kPa : (a) Stress-strain response; (b) Volume change response.....	76
Figure 4-12: Influence of sample preparation on drained behaviour of Sand L sheared at $\sigma_3 = 100$ kPa : (a) Stress-strain response; (b) Volume change response.....	76
Figure 4-13: Influence of sample preparation on peak friction angle of Ottawa sand at $\sigma_3 = 100$ kPa	77
Figure 4-14: Influence of sample preparation on peak friction angle of Sand L at $\sigma_3 = 100$ kPa	77
Figure 4-15: Influence of sample preparation method on characteristic friction angle of Sand O: $\sigma_3 = 100$ kPa	78
Figure 4-16: Influence of sample preparation method on characteristic friction angle of Sand L: $\sigma_3 = 100$ kPa	78
Figure 4-17: Stress-dilatancy plots of Ottawa sand at $\sigma_3 = 100$ kPa ($Dr = 31\%$)	79
Figure 4-18: Influence of sample preparation methods on $D_{max}-R_{max}$ relationship of Ottawa sand at $\sigma_3 = 100$ kPa	79

Figure 4-19: Influence of sample preparation methods on dilatancy of Sand L at $\sigma_3 = 100$ kPa	80
Figure 4-20: Influence of sample preparation methods on the maximum angle of dilation	81
Figure 4-21: Dependency of peak friction angles on the maximum angle of dilation	81
Figure 4-22: Influence of sample preparation method on undrained response of Ottawa sand	82
Figure 4-23: Influence of sample preparation method on undrained triaxial response of Ottawa sand ($e_0 = 0.73$): (a) stress-strain curve; (b) stress path	82
Figure 5.1: Pre- and post- test check on particle size distribution sheared at $\sigma_3 = 500$ kPa	100
Figure 5.2: Typical data of stress ratio $R = \sigma_1 / \sigma_3$ and volumetric strain plotted against axial strain for Sand O and Sand L at $\sigma_3 = 100$ kPa	100
Figure 5.3: Measured contribution to shear strength of Sand O and Sand L of different void ratios at $\sigma_3 = 100$ kPa	101
Figure 5.4: Limiting envelopes in p - q space: (a) Sand O, and (b) Sand L	101
Figure 5.5: Stress-dilatancy plots at $\sigma_3 = 100$ kPa	102
Figure 5.6: Influence of stress level on stress-dilatancy plots: (a) Sand O, $D_r = 62\%$; and (b) Sand L, $D_r = 72\%$	103
Figure 5.7: Influence of interparticle locking on shear strength of granular materials...	104
Figure 5.8: An alternative conceptual model for shear strength of granular materials...	104
Figure 5.9: Empirical relationship between φ_μ and φ_{cv} based on data in the literature .	105
Figure 5.10: Variation of Φ_U of Sand O during triaxial compression at different confining pressures ($e_0 = 0.56$)	105
Figure 5.11: Rate of energy dissipation due to fabric degradation of Sand L at different effective confining pressures	106

Figure 5.12: Rate of energy dissipation at peak of Sand L sheared at different effective confining pressures Φ_U (kPa)	107
Figure 5.13: Rate of energy dissipation due to fabric degradation of Sand L specimens fabricated by dry pluviation at $\sigma_3=100$ kPa.....	107
Figure 5.14: Rate of energy dissipation due to fabric degradation of Sand L specimens fabricated by water pluviation at $\sigma_3=100$ kPa	108
Figure 5.15: The effect of sample preparation methods on energy dissipation due to interlocking	108
Figure 6.1: Measured strain paths: (a) Dense Ottawa sand; (b) Loose Ottawa sand.....	123
Figure 6.2: Behaviour of dense water pluviated Ottawa sand sheared along imposed proportional strain paths: (a) Stress-strain curves; (b) Effective stress path.	124
Figure 6.3: Behaviour of loose moist tamped Ottawa sand sheared along imposed proportional strain paths: (a) Stress-strain curves; (b) Effective stress path.	125
Figure 6.4: Dependency of phase transformation line on initial void ratio and imposed rate of volume change \mathcal{G}	126
Figure 6.5: Softening/hardening domain in strain path tests	127
Figure 6.6: Evolution of second-order work, $\sigma_1 - \sigma_3 / \mathcal{R}$, and deviatoric stress along $\mathcal{G} = -0.18$	127
Figure 6.7: Stress path and evolution of d^2W for loose Ottawa sand ($e_0 = 0.81$) sheared along $\mathcal{G} = 0, -0.18$ and -0.34	128
Figure 6.8: Effective stress paths and evolution of d^2W of medium dense Ottawa sand ($e_0 = 0.68$) sheared along $\mathcal{G} = -0.18, -0.34$ and -0.46	129
Figure 6.9: Comparison of onset of static liquefaction and instability in $\eta - \mathcal{G}$ space ..	129
Figure 6.10: Effective stress paths and evolution of d^2W along strain paths of $\mathcal{G} = -0.26, -0.31$ and -0.33	130

Figure 6.11: Evolution of second-order work, $\sigma_1 - \sigma_3 / \mathfrak{R}$, deviatoric stress along strain path: $\mathcal{G} = -0.26$; $e_0 = 0.58$	130
Figure 6.12: Stress path and evolution of the second-order work along strain path: $e_0 = 0.68$, $\mathcal{G} = 0, -0.12$, and -0.18	131
Figure 6.13: Stress paths and evolution of d^2W along various strain path: loose sand ($e_0 = 0.81$), $\mathcal{G} = 0.08, 0.22$, and 0.28	131
Figure 6.14: Stress paths and evolution of d^2W along various strain path: dense sand ($e_0 = 0.51$), $\mathcal{G} = -0.51$	132
Figure 6.15: Instability domain along imposed proportional strain paths	132

List of Tables

Table 2.1: Sample preparation methods of sand in laboratory	27
Table 3.1: List of adopted sample preparation methods	47
Table 3.2: Volume changes during saturation for MT samples.....	47
Table 5.1: Reference data for φ_{μ} and φ_{cv} in literature	99

Nomenclature

As all the stresses used in this thesis are effective stresses, the word “effective” has been omitted in referring to the friction angle, and no prime sign (\prime) has been used in the symbol φ , or the relevant stress components p, σ_3 , etc. Each symbol is declared upon its first appearance. A list of symbols is also included below.

List of Symbols

e_0 = initial void ratio

Dr = initial relative density

e_{\max} = maximum ASTM void ratio

e_{\min} = minimum ASTM void ratio

e_{cr} = the critical void ratio

G_s = specific gravity

G = shear modulus

ε_1 = major principal strain

ε_3 = minor principal strain

ε_r = radial strain

ε_a = axial strain

$\varepsilon_v = \varepsilon_1 + \varepsilon_2 + \varepsilon_3$ volumetric strain

$\gamma = \varepsilon_1 - \varepsilon_3$ shear strain

$$\varepsilon_q = \frac{2}{3}(\varepsilon_1 - \varepsilon_3) \text{ shear strain}$$

σ_1 = major principal stress

σ_3 = minor principal stress

u = pore water pressure

Δu = excess pore water pressure

$p = (\sigma_1 + \sigma_2 + \sigma_3)/3$ mean principal stress

$q = \sigma_1 - \sigma_3$ deviatoric stress

$R = \sigma_1 / \sigma_3$ effective stress ratio

$\eta = q / p$ effective stress ratio

φ_m = mobilized friction angle

φ_{mc} = mobilized friction angle at characteristic state

φ_{PT} = friction angle at phase transformation

φ_{cv} = friction angle at constant volume

φ_f = friction angle at onset of dilation

φ_μ = interparticle friction angle

φ_{peak} = peak friction angle

ψ = dilation angle

ψ_{max} = maximum dilation angle

$D = 1 - d\varepsilon_v / d\varepsilon_1$ dilatancy factor

$\mathcal{G} = d\varepsilon_v / d\gamma$ strain increment ratio

$\eta_{asy} = (q / p)_{asy}$ asymptotic stress ratio

$\mathfrak{R} = -d\varepsilon_1 / (2d\varepsilon_3)$ constant for a given axisymmetric strain path

Abbreviations

CSL = critical state line

PT = phase transformation

IL = instability line

SS = steady state

QSS = quasi-steady state

CID = isotropically consolidated drained test

CIU = isotropically consolidated undrained test

WP = water pluviation

WT = water tamping

MT = moist tamping

MR = moist rodding

MP = moist pluviation

DP = dry pluviation

DT = dry tamping

DR = dry rodding

Chapter 1

Preliminaries

1.1 Background and motivations

Granular materials, such as sand, are an assembly of distinct, irregular-shaped particles that are in contact with each other to form a particle network that provides internal transmission of interparticle forces and carries the mechanical loads. On the scale of particle size level, network of particles creates a so-called internal structure (or fabric) that is a function of the interconnectivity of particles, as well as their size, shape, surface texture and mechanical properties. These microscopic features have significant influence on the macro-mechanical response of a granular material subjected to external loads. For example, the deformation and failure of the granular material is closely related to relative particle sliding and rolling at the grain scale. Even though the material is considered as continuum with the discrete attributes being ignored in general engineering practice, a better understanding of the mechanical behaviour, including both deformation and failure characteristics, requires adequate consideration of the discrete nature of granular materials.

The salient difference of granular material behaviour relative to that of ordinary solids can be observed during the volume change under pure shear and its dependency on stress state. For example, a loose granular specimen (high initial void ratio) will contract continuously upon application of a deviatoric stress. On the other hand, a dense specimen (low initial void ratio) may only contract initially, and thereafter, dilate (expand) due to a

tendency for the particles to slip against and override each other as deformation occurs. This well-known phenomenon coined as stress-induced dilatancy, or simply, dilatancy was first recognized by Reynolds (1885) in his famous experiment on sand. The mechanical behaviour of granular materials naturally centres around stress-dilatancy that is governed by a number of factors such as fabric, void ratio, confining stresses, previous deformation history as well as stress or strain paths.

Traditionally, the shear strength of granular soils is considered to be due to interparticle friction and dilation. For example, Taylor (1948) and Rowe (1962) recognized that the mobilized friction angle must take into account the sliding resistance at contacts as well as dilation owing to particle rearrangement and overriding each other. Particle crushing, which increases in importance as confining pressure increases and void ratio decreases, also contributes to the shear strength of soil. According to Rowe (1962), the mobilized friction angle at the onset of dilation, φ_f , varies with particle packing arrangements and the number of sliding contacts. Depending on the confining pressure and density, φ_f varies in the range of $\varphi_\mu \leq \varphi_f \leq \varphi_{cv}$ with φ_μ being the interparticle friction angle (or “true friction”) associated with the resistance to interparticle sliding, and φ_{cv} being the friction angle at constant volume. Nevertheless, the ultimate failure and flow of granular materials are governed almost entirely by frictional factors. In other words, when the critical state is reached and shearing continues at constant volume with constant stress level, the shear strength is linked to stress level by a coefficient of friction.

Various methods have been developed to fabricate identical specimens in the laboratory, which includes moist tamping, water pluviation, dry pluviation, and vibration. Given that dilatancy is closely related to the fabric, which depends on the interconnectivity of the particles, one expects that different sample preparation methods develop different fabric, which in turn results in different mechanical behaviour even when the specimens with identical physical properties are subjected to the same stress conditions. As reported by Oda (1972), sand specimens prepared using moist-tamping tend to have relatively higher shear strength and more dilation than that of specimens prepared by dry deposition in drained triaxial compression tests. Under undrained conditions, Zlatovic and Ishihara (1997) observed that specimens prepared by dry deposition are more prone to flow failure than those prepared by moist-tamping. The influence of sample preparation method on the mechanical behaviour of sand is attributed to different patterns of particle arrangements developed during compaction. For engineering practice, however, it is important to estimate the range of variability of laboratory experimental data obtained from specimens prepared using different methods. Thus there is a need to systematically investigate the influence of sample preparation method on the macroscopic mechanical properties of granular materials.

Particle shape is also considered as an important factor affecting the behaviour of granular materials. Experimental evidence reveals that granular materials comprising angular-shaped particles usually have higher macroscopic shear strength at a given confining pressure than those comprising round particles. For example, Koerner's work (Koerner, 1970) on single mineral soils shows that the angularity of particles may result

in a variation in ϕ_{cv} as much as 8° (Koerner, 1970), because the angularity of particles may cause an interlocked fabric, or interparticle locking, in addition to providing extra restraint to particle rotation and hence delay the occurrence of dilation. Herein, interparticle locking is referred as the contribution to shear strength in the absence of volume change to distinguish it from dilatancy-related quotation, *e.g.*, Taylor (1948). The concept of locked sand has been introduced to characterize the behaviour of natural sand with strong locked fabric; see, Dusseault and Morgenstern (1979) and Barton (1993). However, it is also argued that intact samples of locked sand as defined by Dusseault and Morgenstern (1979) cannot be created artificially, since most locked sands acquire some degree of cementation (Barton, 1993) and it is relatively rare to find a purely locked sand without any trace of cementation (Cresswell and Barton, 2003). It should be noted that even though the connotation with the term ‘interparticle locking’ is explicit (as it typically signifies geometrical interlocking), very little is known of its influence on failure mechanism under compression, still less to quantify it. As such, it is important to carry out experimental study to identify this mechanism and possibly to quantify it.

Traditionally, the mechanical behaviour of granular materials is experimentally investigated by performing drained tests along various stress paths or undrained tests when the material is fully saturated. Since the volume change of grains and pore water are negligible, the undrained shear test on saturated sand corresponds to zero volume change. The response of sand along imposed strain paths, however, may provide additional information on understanding the instability of granular material deformation, as discussed by Chu and Lo (1993). Since a given strain path in fact prescribes an

imposed rate of volume change with respect to shear strain, the overall response of granular materials will be affected substantially by the internal capability of dilation, or “locked dilation”. Depending on the imposed rate of volume change and the inherent locked dilation, granular materials may have complicated stress-strain responses. More specifically, an initially dense specimen, which has stable deformation under undrained conditions, may become unstable along some strain paths, similar to the behaviour of loose sand. However, limited knowledge about the behaviour of sand along imposed strain paths are available, particularly in terms of the influence of fabric and sample preparation method.

1.2 Objectives

Motivated by the issues identified in the above, this these seeks to experimentally investigate the stress-dilatancy behaviour of sand, focusing on the influence of sample preparation method, interparticle locking, as well as the response of granular materials along various imposed strain paths. All experimental work is limited to triaxial stress conditions. The prime objectives of this research are as follows:

- To study the influence of sample preparation methods on the behaviour of granular materials;
- To explore the importance of particle shape on shear strength via testing materials comprising primarily rounded- and angular-shaped particles, respectively. More specifically, the contribution to shear strength from particle shape is investigated through detailed exploration of the dilatancy characteristics with respect to particle shape.

A series of tests are carried out to investigate the instability of granular material deformation along various strain paths. Based on the experimental results, some important issues related to strain softening and material instability are re-examined within the framework of thermodynamics.

1.3 Thesis outline

The outline of this thesis is as follows:

Chapter 2 consists of a literature review of the strength properties of granular materials, with focus being placed on material instability and the influence of sample preparation method. The importance of proportional strain path tests is also included in this literature review. From the literature review the need for the current research is established and the specific issues addressed in this study are stipulated.

Chapter 3 describes the laboratory testing program, materials as well as the details of various sample preparation methods used in this study. This is followed by a discussion and assessment of test errors, and methods used to minimize them. Typical experimental results are presented in order to demonstrate the consistency and repeatability of the test results.

Chapter 4 explores the influence of sample preparation method on stress-strain-strength behaviour of granular materials under both drained and undrained conditions. Attempts are made to establish a link between sample preparation methods and the measured strength and dilatancy properties of the tested materials.

Chapter 5 investigates the influence of interparticle locking on the strength and deformation of coarse sand. A new conceptual model about the contributions to shear

strength from different mechanisms is proposed based on the experimental results. A modification to a modified Rowe's stress-dilatancy model is proposed to incorporate the influence of interparticle locking.

Chapter 6 investigates the deformation instability of granular materials when sheared along a variety of proportional strain path tests using Hill's criterion for the sign of the second order work. It was thus shown that the difference between material dilatancy potential and imposed dilatancy factor governs the salient stress-strain behaviour, as well as the transition between strain softening and onset of instability. The difference between strain softening and instability is thus identified.

Chapter 7 closes the thesis with a summary of conclusions and the work considered necessary in the future.

Chapter 2

Literature review

2.1 Strength properties of granular material

2.1.1 Three fundamental representations of shear strength

Historically, the shear strength of soil, τ_f , was expressed as a linear function of the applied normal stress σ_f on the shear plane according to Coulomb's law (Coulomb, 1773)

$$\tau_f = c + \sigma_f \tan \varphi \quad (2.1)$$

where c and φ are the cohesion and the angle of friction, respectively. For triaxial stress conditions, when adopting Terzaghi's effective stress principle, the failure criterion is usually expressed by Mohr-Coulomb's law

$$\frac{\sigma_1 - \sigma_3}{2} = \frac{\sigma_1 + \sigma_3}{2} \sin \varphi + c \cos \varphi \quad (2.2)$$

with σ_1 and σ_3 being the axial and lateral stresses in triaxial compression tests.

The cohesion intercept c in terms of effective stresses is obtained conventionally by extrapolation of the straight line envelope of the Mohr-circles towards the zero normal stress level. For granular soils, the value of c is usually zero. The experimental evidence clearly shows that the failure envelope is curved for almost all types of soils (Taylor 1948, Bishop 1965, Vesic and Clough 1968, Marachi *et al.* 1972, Marsal 1973, among others) owing to stress level dependency, which may result in an "apparent cohesion" for

granular soils when a linear regression is performed. The apparent cohesion can also be induced by suction when the specimen is partially saturated. Following the concept of Taylor's interlocking (Taylor, 1948), Schofield (1999) explained that soil could exhibit apparent cohesion as it flows, particularly at peak strength, while Coulomb's law was still satisfied. His friction angle was broken down into a dilational component and a frictional component as $\varphi_m = \varphi_{cv} + \psi$ with φ_m being the mobilized friction angle, φ_{cv} the friction angle at the critical state of deformation, and ψ the angle of dilation, respectively.

Based on an examination of experimental data in the literature, Bolton (1986) suggested the following empirical relation to characterize the friction angle at failure in triaxial compression tests:

$$\varphi - \varphi_{cv} = 0.8\psi = 3I_D(10 - \ln p_f) - 3 \quad (2.3)$$

where I_D is the relative density and p_f is the mean effective stress at failure, respectively. One observes that in Bolton's empirical relation, the angle of dilatancy is expressed as a function of sand density and the effective confining stress level.

It should be noted, however, the simple representations of shear strength by Schofield (1999) and Bolton (1986) may be difficult to reflect the sophisticated soil behaviour, such as strength anisotropy as discussed by Tatsuoka (1987).

2.1.2 Development of stress-dilatancy theory

2.1.2.1 Rowe's stress-dilatancy theory

It has been known for a long time that dense sand tends to increase in volume, or dilate, when sheared (Reynold, 1885). This phenomenon is termed as dilatancy that is a

major difference between granular materials and classical solid materials. In the early days of geomechanics, the concept of “energy correction” was used to correlate the shear resistance to the angle of dilation and the grain-to-grain friction angle (Taylor 1948, Bishop and Eldin 1953). This method breakdowns the friction angle into a dilational component and a frictional component, with the latter being perceived to be a fundamental property of granular materials.

Rowe (1962) discussed dilatancy in the framework of modern continuum mechanics. He considered the deformation mechanism of an assembly of spherical particles subjected to biaxial or triaxial stress conditions. By adopting the hypothesis of minimum energy ratio, Rowe obtained a relation of the mobilized stress ratio, the rate of plastic strains and the interparticle friction angle (or “true friction”) φ_μ in the form of

$$\frac{\sigma_1}{\sigma_3} = K_\mu \left(1 - \frac{d\varepsilon_v}{d\varepsilon_1}\right) \text{ with } K_\mu = \tan^2(45^\circ + \varphi_\mu/2) \quad (2.4)$$

Where σ_1 and σ_3 are the major and minor principal effective stresses, respectively; $d\varepsilon_v$ and $d\varepsilon_1$ are the rate of volumetric strain and the axial strain in triaxial compression, respectively. By invoking the mobilized friction angle φ_m as $\sin\varphi_m = (\sigma_1 - \sigma_3)/(\sigma_1 + \sigma_3)$ via the Mohr-Coulomb criterion, Eq. (2.4) can be rewritten as

$$\sin\psi = \frac{\sin\varphi_m - \sin\varphi_f}{1 - \sin\varphi_m \sin\varphi_f} \quad (2.5)$$

Although Rowe's work provided a reasonable relationship between stress ratio and volume changes for both contractive and dilative behaviours of sand, it did have

limitations. The assumption of a minimum energy ratio cannot be proved theoretically, owing to the difficulties in proving the extreme principle when friction is involved (de Josselin de Jong, 1976), even though the assumption was supported by experimental data (*see*, Rowe 1962 and Horn 1965 among others). Recent work by Wan *et al.* (2005) shows that the hypothesis of minimum energy ratio can be relaxed when establishing the stress-dilatancy model.

However, it must be understood that Eq. (2.4) is only a lower limit for dilatancy behaviour of sand. In other words, a deforming assembly of granular particles may not necessarily obey such a limit. In fact, it has been found that Eq. (2.4) is valid only for very dense sand at small strains. As such, in response to this shortcoming, Rowe (1971) suggested using a characteristic friction angle φ_f which takes various values for sands of different density at various strain levels. φ_f is the mobilized friction angle at the onset of dilation, and it varies with particle packing arrangements and the number of sliding contacts. Depending on the confining pressure and density, φ_f varies in the range of $\varphi_\mu \leq \varphi_f \leq \varphi_{cv}$. It is important to note that Rowe's equation cannot be used for general stress conditions.

2.1.2.2 Influence of void ratio, pressure, and fabric on dilatancy

Following Rowe's work, different stress-dilatancy formulations were proposed based on energy principles without explicit consideration of microstructure (Newland and Alley 1957, Roscoe *et al.* 1963, Gutierrez *et al.* 1991, and Muhunthan *et al.* 1996). Microstructural information can be taken into account in the determination of dilatancy

by treating it as a constraint imposed by internal grain geometry on macroscopic deformations (Matsuoka 1974, Tokue 1979, Ueng and Lee 1990, Goddard and Bashir 1990). The importance of stress level, density, and stress path has been clearly demonstrated (Pradhan *et al.* 1989, Houlsby 1991, Gudehus 1996, Nakai 1997, Wan and Guo 1998, Li and Dafalias 2000). There are also some models coupling dilatancy with particle crushing at high stress levels (McDowell and Bolton 1998, Ueng and Chen 2000, Indraratna and Salim 2002). However, experimental studies of stress-dilatancy with a focus on fabric issues are scarce, probably because fabric is difficult to be quantified in standard laboratory tests.

While the description of the influence of fabric on dilatancy is primarily qualitative, mathematical relations are available for the dependency on void ratio and stress level. For example, Wan and Guo (1998) modified Rowe's dilatancy model to describe the mechanical behavior of granular materials at different stress levels and densities. This modified dilatancy is expressed as

$$\sin \psi = \frac{\sin \phi_m - (e / e_{cr})^\alpha \sin \phi_{cv}}{1 - \sin \phi_m (e / e_{cr})^\alpha \sin \phi_{cv}} \quad (2.6)$$

where e is the current void ratio, e_{cr} denotes the critical void ratio in the e - p plane corresponding to the current mean effective stress p and α is a parameter derived from testing.

Li and Dafalias (2000) introduced a general state dependent dilatancy expression of the form:

$$d = d(\eta, e, Q, C) \quad (2.7)$$

where Q and C denote internal state variables other than the void ratio e , $\eta = q/p$ and $d = \sin \psi$. Eq. (2.7) must satisfy the requirement that dilatancy is zero at both the critical state and the phase transformation (PT) point, which is achieved by introducing the state parameter $(e - e_{cr})$ proposed by Been and Jefferies (1985) into Eq. (2.7) as

$$d = d(\eta, e - e_{cr}, Q, C) = 0 \quad (2.8)$$

herein e_{cr} is the critical state void ratio corresponding to the current p , and phase transformation refers to the state at zero pore pressure change, *e.g.*, $du=0$.

2.1.3 Contribution of interparticle locking to shear strength

In addition to interparticle friction and dilatancy, particle shape, particle angularity and interparticle locking also affect the strength of sand. According to Barton (1993), different structures may develop in granular soils. For example, sand particles can develop bonds between them (*i.e.* cementation) that results in a bonded structure, or can be interlocked, forming an interlocked structure or fabric. In general, particle interlocking becomes noticeable only for granular materials consisting of angular particles.

Experimental evidence reveals that the critical state friction angle ϕ_{cv} cannot be uniquely determined from mineral-to-mineral friction angle ϕ_{μ} dominated by particle roughness, but depends on particle shape as well. As reported by Chan and Page (1997), ϕ_{cv} generally decreases with increasing particle roundness. Granular materials comprising angular-shaped particles usually have higher macroscopic shear strength at a given confining pressure than those comprising round particles. For example, Koerner's work on single mineral soils showed that the angularity of particles may result in a

variation in φ_{cv} as much as 8° (Koerner, 1970) because the angularity of particles may cause an interlocked fabric in addition to providing extra restraint to particle rotation and hence enhancing dilation. The concept of locked sand has been introduced to characterize the behaviour of natural sand with strong locked fabric, *e.g.*, Dusseault and Morgenstern (1979) and Barton (1993). The influence of interparticle locking or fabric structure on the mechanical behaviour of locked sand, either bounded or unbounded, has been examined more recently by Cuccovillo and Coop (1999), Wong (2001), Cecconi and Viggiani (2001), Cresswell and Barton (2003), and Cresswell and Powrie (2004). The results of these studies confirm that interparticle locking is an important component of shear resistance, which cannot be quantified by the stress-dilatancy model developed for classical sand. However, it is also argued that intact samples of locked sand as defined by Dusseault and Morgenstern (1979) cannot be created artificially, since most locked sands acquire some degree of cementation (Barton, 1993) and it is relatively rare to find a purely locked sand without any trace of cementation (Cresswell and Barton, 2003).

Cresswell and Powrie (2004) performed a series of drained triaxial compression tests to investigate the influence of fabric structure on Reigate silver sand. This is a purely locked sand with minimal cementation, large grain contacts, and a relative density index of 136%. The experimental results showed that the intact samples were associated with much higher dilation rates compared to the reconstituted samples by pluviation. Significant delay of dilation within the intact samples was observed that was attributed to the effect of particle interlocking. The intact samples, however, were consistently denser

than the reconstituted samples, so it is not known to what extent the difference seen is a result of the effect of structure.

2.2 Influence of sample preparation method on sand behaviour

2.2.1 Overview

When fabricating granular specimens in the laboratory, the conditions applied to sand grains during deposition and densification, such as tapping, tamping, or rodding of particles under various moisture conditions, affect the orientation and contact configurations of particles, which in turn induces different fabric in the specimens. Consequently, the response of reconstituted specimens in the laboratory changes with sample preparation methods. The fabric developed during sample preparation is referred as the initial fabric. Any directional dependency of material properties owing to initial fabric is termed as inherent anisotropy, defined by Casagrande and Carrillo (1944) as “a physical characteristic inherent in the material and entirely independent of the applied strains”, compared to induced anisotropy that depends on applied stresses and corresponding strains.

In general, sample preparation methods can be categorized according to the water content of the sample (dry, moist, or saturated) and the densification procedures (*e.g.*, tamping, rodding, tapping or vibrating). Table 2.1 summarizes the sample preparation methods used in the literature, each of which has its advantages and disadvantages. For example, water pluviation method can produce relatively homogeneous specimens with the experimental results highly repeatable. This method, however, has difficulty to produce very loose or very dense samples. For well-graded granular materials, the

potential of particle segregation during deposition may reduce the homogeneity of the specimen. The method of moist tamping (MT), which is another common procedure in many geotechnical laboratories, can produce specimens of various densities, from very loose to very dense, with the average density being easily controlled. The specimens, however, are less uniform (Mitchell 1976, Vaid *et al.* 1999, Frost and Park 2003), with local densities of high standard deviation with respect to the global average density (Marcuson and Gilbert, 1972). More specifically, when each layer is compacted to a nominal thickness, the bottom layers tend to be over-compacted during the compaction of succeeding layers, with the heterogeneities between layers being clearly observed from X-ray images Mulilis *et al.* (1977) and Vaid *et al.* (1999).

With regard to reproducing in-situ soil fabric, water pluviation is considered to effectively simulate the deposition processes in hydraulically placed fills and in alluvial environments. For cases in which moist sand is truck dumped as fill material and subsequently compacted, however, the moist tamping method is more representative. Dry pluviation best models the natural deposition process of wind blown Aeolian deposits, which generally consist of well-sorted sand or silt (Kuerbis and Vaid, 1988).

Uniformity of specimens is essential for an element test. The uniformity of reconstituted sand samples can be quantified using various procedures. Quantities such as local void ratio and particle orientation can be measured by destructive methods including freezing or introduction of some impregnating substance and then thin sectioning (Oda 1972, Vaid *et al.* 1999), or by nondestructive techniques such as magnetic resonance imaging, ultrasonic testing, X-ray radiography and X-ray computed

tomography (Frost, 2000). Using these approaches, critical assessments on uniformity of reconstituted samples have been carried out by a number of investigators (*e.g.*, Castro 1969, Emery *et al.* 1973, Mulilis *et al.* 1977, Vaid and Negussey 1988, Frost and Park 2003). These studies demonstrate that the specimens reconstituted by moist tamping (MT) tend to be less uniform than those prepared by pluviated samples (WP, MP, and DP). Water pluviated specimens are much closer to be uniform with height (Vaid and Negussey 1988). The local relative density varies by as much as $\pm 10\%$ from the average of the entire specimen when moist tamping method is used. Similar serious non-uniformities have been reported by Castro (1969) in moist tamped specimens. The local deviation of relative density from the average may be noted to be much smaller (within about 3%) for water or dry pluviated sands. As shown by Frost *et al.* (1998), however, even specimens prepared by highly controlled dry pluviation could not avoid nonhomogeneity of void ratio distribution.

2.2.2 Influence of sample preparation method on sand behaviour: static loading

2.2.2.1 Drained behaviour

Bishop (1954) was one of the earliest researchers to emphasize that dissimilar soil structures resulting from different sample preparation methods could be the reason for differences in reported mechanical behaviour. He conducted drained triaxial compression and extension tests on fully saturated and dry specimens of Folkestone Bed sand, which was a well-graded medium to fine sand. The specimens were prepared by water and dry pluviation. At a confining pressure of 37 kPa, Bishop found that the friction angles from dry and fully saturated specimens were different; the friction angles for the dry specimens

were 2 degrees higher for loose sand and 5 degrees for dense sand. Although water content is thought to be the major reason of different shear resistance, Bishop asserted that “..... The results suggest that the presence of water at the intergranular contacts may alter the coefficient of friction mobilized during sliding, but also that the structure of the sand depends on the method of deposition”.

Oda (1972) observed that, at identical initial void ratios, Toyoura sand specimens prepared by tapping exhibited higher strength and stiffness than those prepared by rodding (or plunging in Oda 1972). Microscopic analyses on the distribution of the orientation of particle axes showed that the longitudinal axes of particles tended to be aligned in the horizontal direction when using tapping method, and the particles were more randomly distributed in specimens fabricated using rodding method.

Miura and Toki (1982) compared the triaxial test results of Toyoura sand specimens prepared using multiple sieve pluviation, dry tapping, and moist rodding. They observed that sample preparation methods affected the results of triaxial extension tests more than those of triaxial compression. For example, for tests carried out on samples with the relative density of 53-57% at a confining pressure of 196 kPa, specimens prepared by multiple sieve pluviation were stronger than those prepared by dry tapping. The moist tamped samples had the strongest response in all sample preparation methods. However, an opposite trend was observed in drained triaxial extension tests.

The influence of initial fabric on sand behaviour was also studied by exploring the variation of deformation characteristics when shearing specimens in different directions. Tatsuoka *et al.* (1986) reported results on loose and dense Toyoura sand with inclined

bedding planes in plane strain compression, with the samples being isotropically consolidated at mean pressures of 4.9, 9.8, 49, 98 and 392 kPa. When defining δ as the angle between the normal to the bedding plane and the vertical axis (i.e., $\delta = 0^\circ$ for a vertical bedding plane and $\delta = 90^\circ$ for a horizontal bedding plane, respectively), they found that the drained strength generally increases with increasing δ , with the minimum strength observed at about $\delta = 30^\circ$. The bedding plane orientation was also found to significantly affect the peak stress-dilatancy relationship, as shown in Figure 2.2. Similar results were reported by others (e.g., Wong and Arthur 1985, Miura *et al.* 1998).

2.2.2.2 Undrained behaviour

Several studies (e.g., Ladd 1874, Miura and Toki 1982, DeGregorio 1990, Zlatovic and Ishihara 1997, Vaid *et al.* 1999, Papadimitriou *et al.* 2005) have reported that the undrained behavior of clean sands can be greatly influenced by specimen reconstitution method. Figure 2.3 shows the undrained triaxial compression responses of Nevada sand samples prepared by two different methods (MT and DP) at the same initial void ratio; i.e., $e_0 = 0.80$ (Zlatovic and Ishihara, 1997). An interesting observation is that the sample prepared by moist placement displays a hardening behaviour with the development of increasing strength. On the other hand, the dry deposited sample exhibited a quasi-steady state (QSS) behaviour described by temporary collapse (region AB), followed by a brief phase of limited flow (point B) before regaining strength with increased deformations. The significant difference in behaviour of samples prepared by different methods highlights the importance of fabric effects. More importantly, the initial fabric of the sample also influences the point at which the rate of pore pressure

change temporarily equals zero; *i.e.*, corresponding to the phase transformation or quasi-steady state. This observation suggests that QSS is a material characteristic controlled by some internal parameter such as fabric.

More subtle differences due to different sample preparation methods are found in the development of excess pore pressure. The point at which the rate of pore pressure generation is temporarily zero coincides with the so-called phase transformation state marking the transition from contractive to dilative behaviour. Figure 2.4 illustrates the role played by fabric in the undrained response of Masado sand under both triaxial compression and extension; *see, e.g.*, Tsukamoto *et al.* (1998). For the same initial void ratio, different stress-strain curves are obtained in spite of achieving the same ultimate strength. Based on triaxial compression tests, the phase transformation state is reached at higher strains for water sedimentation (or water pluviation in this study) prepared samples.

2.2.3 Sample preparation method on sand behaviour: cyclic loading

The sample preparation method also makes a difference in the cyclic behaviour of granular soils, particularly the resistance to liquefaction of saturated sand subjected to cyclic loading under undrained conditions.

Mitchell (1976) investigated the effect of sample preparation methods on the undrained strength and volume change properties of saturated soils in cyclic triaxial tests. They indicated that samples prepared by pluviation had the lowest strength of all of the samples prepared by various methods. Silver *et al.* (1980) compared the cyclic resistance of specimens prepared by dry pluviation and wet tamping. They observed that the cyclic

undrained strength of sand prepared by moist tamping was higher than that of samples fabricated by air pluviation, which is consistent with the observations of Mitchell (1976).

Tatsuoka *et al.* (1986) examined the factors affecting cyclic undrained triaxial strength of sand, including sample preparation methods. For specimens of various densities, lower strength was obtained for specimens prepared using multiple sieve pluviation while the dry pluviation and water vibration gave stronger specimens. Miura and Toki (1982) also observed that specimens prepared by moist tamping had higher resistance to liquefaction than those prepared by dry rodding, with the cyclic resistance of multiple sieve pluviated samples being less than those fabricated by moist tamping or dry rodding.

The influence of sample preparation method was more evident for dense specimens. Both Miura and Toki (1982) and Tatsuoka *et al.* (1986) noted that, similar to static triaxial strength tests, the influence of sample preparation is more evident for dense specimens than for loose ones.

In summary, under undrained cyclic triaxial loading, specimens prepared by the water pluviation method are generally weaker than those prepared by the dry pluviation method; likewise specimens prepared by dry pluviation are generally weaker than specimens prepared by the moist tamping method.

2.2.4 Sample preparation method and critical state

The dependency of the critical (or steady) state line in the $e - p$ space on initial fabric is still controversial in the literature.

It is generally believed that the initial fabric is most likely destroyed at large strains, even though it has substantial influence on the peak strength. As a result, the critical state is most likely not affected by the initial fabric, as observed by Ishihara (1993), Verdugo and Ishihara (1996), Zlatovic and Ishihara (1997). On the contrary, Alarcon and Leonards (1988), Dennis (1988) and DeGregorio (1990) observed in laboratory tests that the critical state of sandy soils may be sensitive to sample preparation method. It is likely that the initial fabric related to sample preparation method is not completely eliminated at the critical state in these tests.

Even though the critical state soil mechanics has been well-developed, some researchers have questioned if the critical state is an over-simplification. For example, Mooney *et al.* (1997, 1998) showed dependence of the critical state line in the $e - p$ space on loading direction and loading history, while Yoshimine and Ishihara (1998) observed the same for the ultimate steady-state line in undrained tests on sand.

2.3 Instability and strain softening

2.3.1 Introduction

Instability of material deformation is defined as a condition that occurs when a soil element subjected to a small perturbation cannot sustain the current stress state imposed on it, resulting in a runaway deformation (Lade 1989, Lade and Pradel 1990). In general, material manifests unstable behaviour when the stress state of a material element reaches the failure state. Many flow slides have been observed in coastal and offshore areas (Terzaghi 1956, Andersen and Bjerrum 1968) as a result of instability in natural deposits. The description of the circumstances surrounding the great majority of these

slides indicates that some relatively sudden perturbation, such as lowering of the water level outboard of the slope, was observed almost immediately prior to the initiation of the flow slides.

Several modes of instability are observed in laboratory tests and field investigations. For example, in conventional drained triaxial tests on dense sand at constant confining stress, the state corresponding to the peak deviator stress (Point A in Figure 2.5a) signifies the onset of instability, particularly in stress controlled tests. Instability may also occur during undrained loading of loose sand prior to the attainment of the state of maximum obliquity. This type of instability has been referred to as pre-failure instability (Lade and Pradel 1990, Chu *et al.* 1993, and Sasitharan *et al.* 1993), as Point A shown in Figure 2.5b.

In general, material instability is related to strain softening. According to tests on sand along imposed strain paths corresponding to partially undrained conditions, Chu and Lo (1993, 1994) and Vaid and Eliadorani (1998) argued that the mechanisms for pre-failure strain softening and instability are the same, except that strain softening and instability occur in strain-controlled and stress controlled modes, respectively. On the other hand, hinging on Hill's stability criterion, Darve *et al.* (1995) showed numerically that instability might occur either before or after strain softening, which was verified by Lancelot *et al.* (2004) via testing loose Hostun RF sand along proportional strain paths at low confining pressures (20 to 100 kPa).

Different definitions for strain softening within the context of plasticity theory have been proposed in the past. These definitions normally require the choice of the yield

function and the plastic potential, *a priori*, in elasto-plastic constitutive modeling. The behaviour associated with $dq < 0$, or defined by Valanis (1985) as $d\sigma_{ij} \cdot d\varepsilon_{ij} < 0$, has been referred to as strain softening (Prevost 1975, Read 1984, Chu *et al.* 1992). As the strain softening occurs before the effective stress path reaches the failure line, it has been called pre-failure strain softening (Chu *et al.* 1992).

When material instability is concerned, Drucker's postulation is usually adopted, which states that stability is assured if the second order plastic work is positive; *i.e.*, $d^2W^p = d\sigma_{ij} \cdot d\varepsilon_{ij}^p > 0$. Bishop and Hill (1951) and Hill (1958) extended the condition of stability slightly beyond that proposed by Drucker by expressing it in terms of total strain increments as $d^2W = d\sigma_{ij} \cdot d\varepsilon_{ij} > 0$.

2.3.2 Experimental observation of instability phenomenon

Sladen *et al.* (1985) found that, for loose sand in undrained triaxial tests at different initial confining pressures, the points of peak deviator stress q on effective stress paths in the p - q plane are on the same line. The position of this line varies with the initial density of sand, thus defining a collapse surface in the p - q - e space. In the context of Hill's non-negative second order work, Lade (1992) identified an instability line, which can be approximated by the line joining the points of peak deviator stress on effective stress paths in undrained tests. Similar phenomena were observed in more general proportional strain paths (Chu *et al.* 1993), with the instability line being strain path dependent.

Lade *et al.* (1988) showed that dense dilative sand remained stable when loaded into a region of high shear stresses where Drucker's stability postulate is violated. However, loose contractive sand became unstable when subjected to the same loading condition but prevented from drainage. Instability involved a sudden increase in pore pressure and axial strain with the development of a runaway condition that brought the sample to failure without further loading. However, when the sample was loaded to low shear stress level, it remained stable and developed only small axial strain and excess pore pressure that was attributed to a small volumetric creep. Under fully drained conditions, however, the sample remained stable regardless of its density and the stress level imposed. Following a procedure similar to that of Lade *et al.* (1988), Chu *et al.* (1993) showed that instability may occur in dilative sand in strain path tests. They concluded that a material becomes unstable if the imposed rate of dilation exceeds a certain limit, which is approximately the rate of dilation exhibited by the soil itself. Similar observation was made by Uchida and Vaid (1994) and Vaid and Eliadorani (1998) in tests along proportional strain paths.

Chu *et al.* (1992) observed that pre-failure strain softening depends on several factors including the initial confining pressure. A higher confining pressure yields a greater tendency for softening, provided that the imposed rate of dilation remains the same. By conducting tests under stress-controlled and strain-controlled conditions, Chu *et al.* (1993) showed that instability occurred under stress-controlled condition in samples that exhibited softening under strain-control. They concluded that strain softening is a necessary condition for the occurrence of instability. Chu *et al.* (1992, 1993) also

concluded that, as suggested by Vardoulakis (1979), the strain softening observed in drained triaxial compression tests on dense sand was not a material property, but a result of non-uniform strains and shear band. However, the position of the “instability line” is not an intrinsic property of sands. For example, Doanh *et al.* (1997) reported that Lade’s instability line for triaxial compression is strongly influenced by the stress history such as the isotropic or anisotropic consolidation, the overconsolidation or the drained axial strains before undrained shearing.

Lancelot *et al.* (2004) performed a series of tests along proportional strain paths at low confining pressures (20 to 100 kPa) using Hostun RF sand. He interpreted the instability line as the locus of zero Hill’s second order work, and found that it did not coincide with the peak deviator stress states on the corresponding effective stress paths. Moreover, the instability line was strain-path dependent, with a smaller $d\varepsilon_v/d\varepsilon_1$ value leading to a larger inclination of the instability line.

Table 2.1: Sample preparation methods of sand in laboratory

Water content	Deposition method	Densification procedures	Name denoted by various authors
Saturated (submerged in water)	Pluviation or sedimentation through water	No densification	Water Pluviation (WP) or Water Sedimentation (WS), other specific method such as Slurry Deposition method for loose sample(Kuerbis, 1988)
		Horizontal tapping or vibration of split mould	Moist or wet tamping (MT or WT)
Moist (Varies from 3% to 8%, typically 5%)	Placement by spoon, funnel, etc.	Vertical tamping on the top of the material	Moist or wet Vibration (MV or WV)
		Horizontal tapping or vibration of split mould	Moist or wet rodding (MR or WR)
		Rodding	Dry or dry pluviation (DP, AP) or Dry deposition (DD), other specific method such as multiple sieving pluviation method (Miura, 1982,1984)
Dry	Pluviation or deposition through air	No densification procedure	Dry tamping (DT)
		Vertical tamping on the top of the soil	Dry or dry pluviation (DP, AP) or Dry deposition (DD)
		Horizontal tapping or vibration of split mould	Dry rodding (DR)
		Rodding	

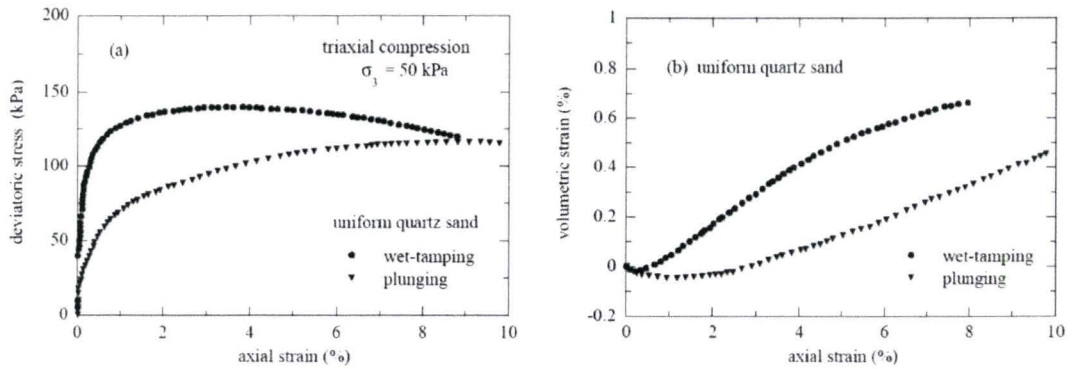


Figure 2.1: Influence of sample preparation method on sand responses (data after Oda, 1972)

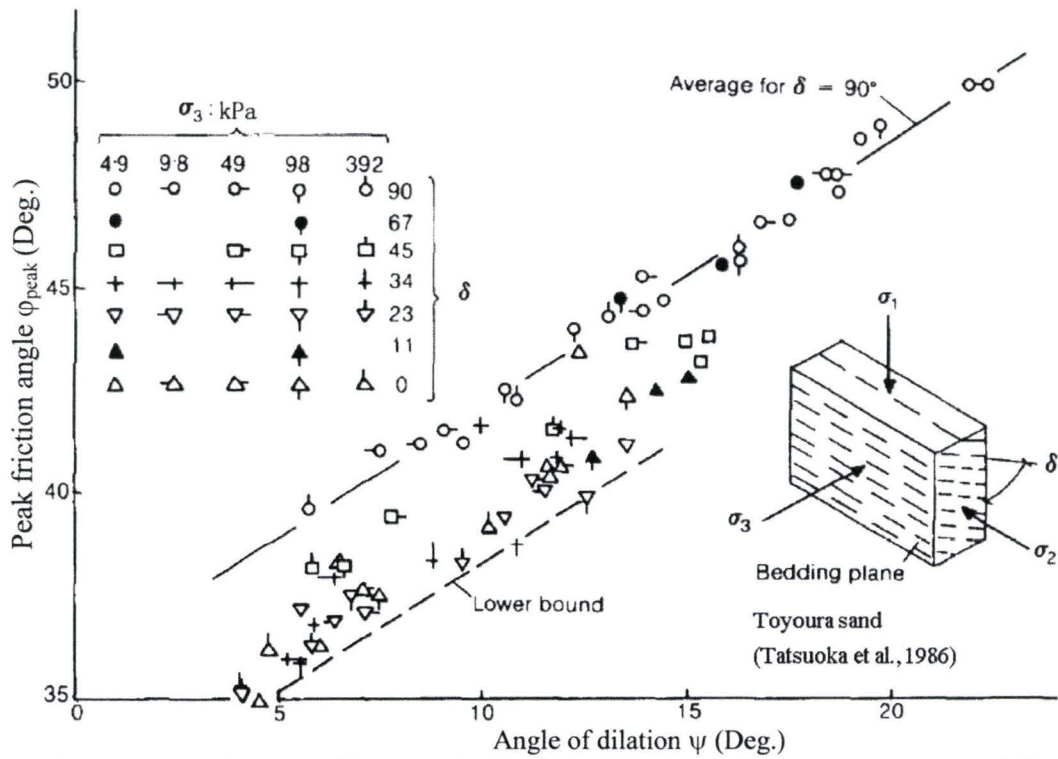
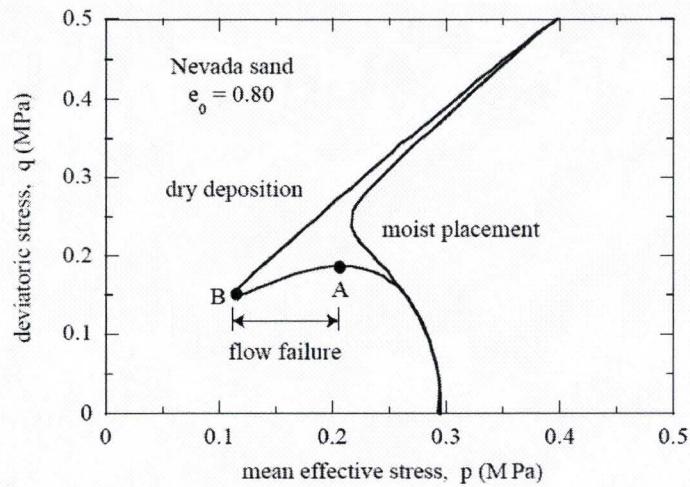
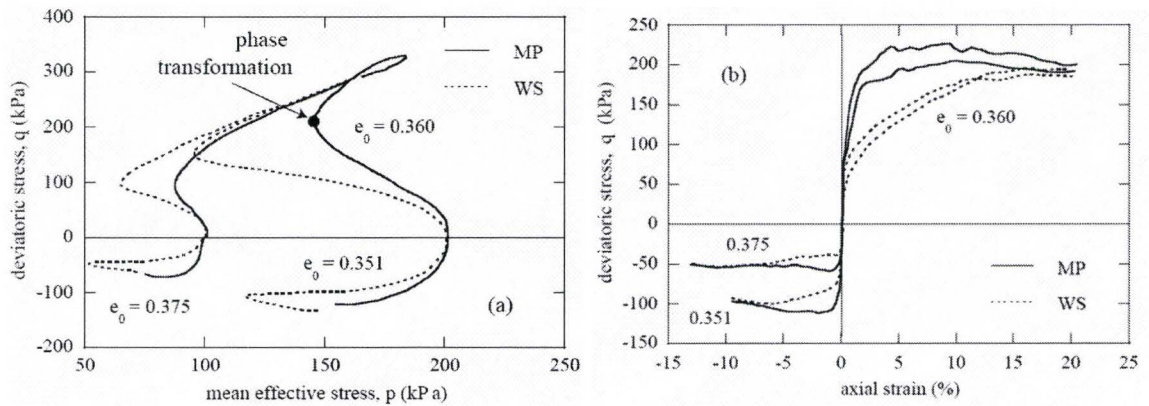


Figure 2.2: Peak stress-dilatancy plot in plane strain tests for Toyoura sand (modified from Tatsuoka *et al.*, 1986)



dry deposition = dry pluviation; moist placement = moist tamping

Figure 2.3: Influence of sample preparation methods on undrained responses of Nevada sand



water sedimentation = water pluviation; moist placement = moist tamping

Figure 2.4: Influence of sample preparation methods on undrained responses of Masado sand

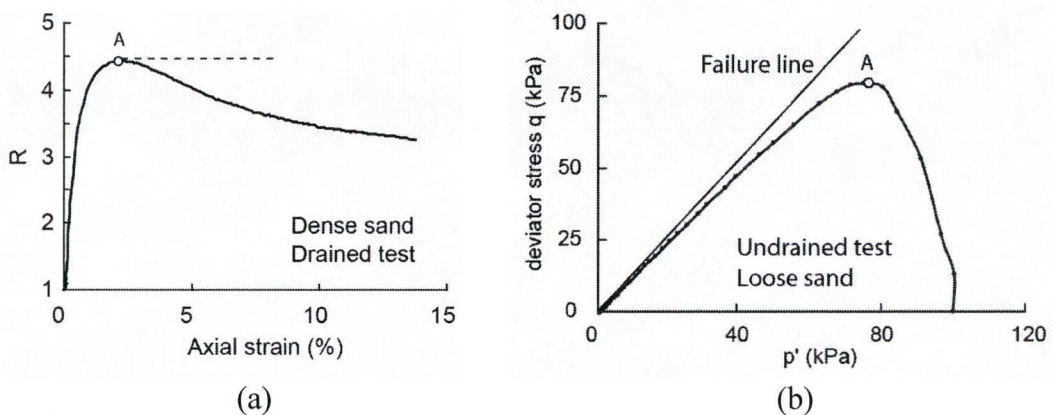


Figure 2.5: Typical instability in (a) drained test on dense sand, and (b) undrained test on very loose sand

Chapter 3

Testing materials, equipment and procedures

3.1 Introduction

In order to study the influence of sample preparation method, interparticle locking and material instability, a series of conventional drained and undrained, proportional strain path triaxial compression tests were performed on two materials with different particle shapes and surface textures. This Chapter presents a description of the equipment used to perform these tests, the procedure for sample preparation and testing, and a summary of the tests performed.

3.2 Description of testing equipment

Figure 3.1 presents a schematic representation of the Bishop-type triaxial testing system employed in this study. Axial load, axial displacement, pore water pressure, volume change and cell pressure, were measured by different types of transducers, including load cell, Linear Variable Differential Transducer (LVDT), pore pressure transducers, and volume change transducer. All data were acquired by a computer controlled acquisition system.

Cylindrical specimens of 50 mm in diameter and 100 mm in height were used in all triaxial tests. In conventional triaxial compression tests (both drained and undrained), loading was controlled by constant rate of axial displacement, with the displacement and the corresponding axial load being measured by a load cell and a LVDT, which were both mounted outside the triaxial chamber. DC silicon oil was applied to the rod to reduce the

piston friction, which was evaluated by performing a system calibration with a precision of 0.1 N.

In all drained tests, single drainage through the porous stone at the bottom of the specimen was used. Special care was taken to ensure that no leakage occurred from the drainage lines. In order to ensure no air bubbles being trapped in the drainage system, the drainage lines were flushed by de-aired water thoroughly before the specimen setup. The volume change of a specimen was obtained by measuring the volume of water flowing into or out of the specimen using a volume change transducer.

In the proportional strain path tests, a volume change controller was used to control the volume change of the specimen independently. Figure 3.1 illustrates the major components of the volume change controller, which consisted of a water cylinder, a motor, and a control panel. The volume change of specimens during shearing was precisely controlled by controlling the speed of the motor with the control panel, and monitored by the volume change transducer. The rate of volume change with respect to the speed of the motor was calibrated in advance so that appropriate strain ratios could be controlled using the control panel.

The data acquisition system consisted of a scanner and multimeter. A computer controlled the model 59309A HP scanner, which acquired the signals from different transducers. After being amplified by the model 34401A HP voltmeter, the outputs were sent to the computer and displayed on the monitor. The data was scanned continuously at an interval of 0.2s during the test. All channels were calibrated by adjusting the electrical signal to a convenient range accepted by the scanner. An overall view of the triaxial

testing system is shown in Figure 3.2.

3.3 Tested materials

The tests were performed on Sand O (Ottawa sand C-109) and Sand L which was derived from crushed limestone aggregate. Ottawa sand is a commercially available, clean medium sand with rounded to sub-rounded grains, while Sand L is a coarse sand with angular particles. Figure 3.3 shows the particle shapes of these two materials.

Following ASTM test methods D 4254-00 and D 4253-00, the maximum and minimum void ratios of Sand O were measured as 0.811 and 0.503, with those of Sand L being 1.201 and 0.520, respectively. Sand O has a specific gravity (G_s) of 2.65, a mean grain size (D_{50}) of 0.375 mm and the coefficient of uniformity (C_u) of 1.80, with those of Sand L being 2.75, 1.637 mm and 1.94, respectively. The particle size distribution curves of the two materials are presented in Figure 3.4.

3.4 Sample preparation methods

In order to explore the influence of sample preparation method on the mechanical behaviour of sand, eight different preparation methods were adopted to produce samples of different initial fabric. Table 3.1 lists the sample preparation methods utilized in this study for each material, and details of each method can be found in Table 2.1, and further illustrated in Figure 3.6. Three representative preparation methods, namely, water pluviation (WP), moist tamping (MT), and moist rodding (MR), were used for Sand O, while all eight methods were used for Sand L.

3.4.1 Water / moist / dry pluviation

3.4.1.1 Water pluviation

In the water pluviation (WP) procedure, sand is deposited in a water-filled split mold. The sand may be deposited by pluviation from a funnel (Ishihara 1996) or a sealed flask (Finn *et al.* 1971), or by spooning. Before the specimen preparation, the sand sample and the porous stones were boiled for at least 10 minutes to remove any trapped air bubbles and then allowed to cool down to room temperature. All drainage lines connected to the volume change transducer and the base of triaxial cell were carefully checked by flushing de-aired water through. A 0.3-mm thick membrane was then mounted to the base pedestal and secured by O-rings. After the membrane and the split mould were put in position, the mould was filled to the top using de-aired water. The sand was then poured into the mould using a spoon. During this process, care was taken so that sand grains were not exposed to air at any time. The approximate desired density was achieved by adjusting the speed of underwater deposition. When preparing dense samples, the split mould was tapped gently from outside by a hammer. This method, however, does not provide precise control over the specimen density. The top platen was mounted with care so that no air bubbles were trapped between the platen and the specimen. Thereafter, the membrane was secured to the top platen with O-rings. A small suction of 10 kPa was applied to dense specimens (2 kPa for loose samples) so that the specimen could stand when the slit mould was removed and the triaxial chamber was installed.

3.4.1.2 Moist pluviation

The procedure for moist pluviation (MP) is as follows. A predetermined amount of moist sand at a water content of 4 percent was placed in the mould in five layers. For each layer, a surcharge was applied on the moist sand by a weight of 200 grams, the split mould was then gently tapped from out by a steel tamper. When the sample was densified to an expected thickness, the surface of the sample was gently scratched to eliminate obvious layering at the interface of different Sand Layers. Following that, the material for the next layer was placed and the above procedure was repeated.

3.4.1.3 Dry pluviation

Specimens reconstituted by dry pluviation (DP) were formed by depositing dry sand in 5 layers in the mould. The density of the specimen was controlled by controlling the falling height of sand grains. For dense samples, each layer was densified to the specified thickness by tapping from outside of the split mould.

3.4.2 Water / moist / dry tamping

3.4.2.1 Moist tamping

In this method, moist sand at 4 percent of moisture content was loosely placed in five layers in the mould. For each layer, vertical tamping was applied to the deposit using a flat tamper with the diameter of 26 mm, which was a half of that of the sample.

Moist tamping method was frequently used in 1980's since it could easily control the average void ratio of the specimen. This method, however, was strongly criticized, since it tended to produce specimens with a non-uniform void ratio distribution over the height of the specimen. More specifically, when each layer was compacted to a nominal

thickness, the bottom layers tended to be over-compacted during the compaction of succeeding layers. X-ray images taken by researchers including Mulilis *et al.* (1977) and Jang (1997) clearly demonstrated the heterogeneities between layers.

Various approaches were used to minimize the local void ratio non-uniformity. In this study, the undercompaction procedure proposed by Ladd (1974) was adopted to compensate for the extra compactive effort applied on a layer by the compaction of the succeeding layer. This was accomplished by compacting the bottom layers to a lower density than the target value. In this study, each layer was compacted at a relative density of 2 percent higher than the preceding one.

Another limitation of moist tamping is the non-uniformities created in the same layer. In order to minimize this effect, the top of each layer was scarified by approximately 2 mm after tamping. Although this method helped in mitigating the non-uniformity in the same layer, it could not completely eliminate the non-uniformity.

3.4.2.2 Water tamping

When water tamping method was used, the specimen was densified by tamping the specimen vertically when all sand grains were underwater. This method is different to the water pluviation in which horizontal tapping from outside of split mould was applied.

3.4.2.3 Dry tamping

This method is similar to moist tamping, except that dry sand was used in compaction. In particular, dry sand was loosely placed in five layers in the mould. Each thin layer was tamped to the desired height. Although relative high densities could be

obtained in this method, similar disadvantages as those for moist tamping are to be expected.

3.4.3 Moist / dry rodding

3.4.3.1 Moist rodding

Moist rodding is very similar to moist tamping, however, the specimen was densified to desired height using a steel rod (6 mm in diameter) in the axisymmetric manner rather than the tamper of 26 mm in diameter. More specifically, moist sand with 4 percent water content was placed in five layers in the mould. Each layer was densified to desired height using the steel rod. The end of the rod was rounded in a half-spherical shape. To reduce the local non-uniformity, a large number of roddings were needed.

3.4.3.2 Dry rodding

This procedure was essentially the same as moist rodding except that sample was prepared using dry sand.

3.5 Testing procedures

3.5.1 Sample setup

After the specimen was prepared using one of the methods described in the previous section, the top platen was carefully seated on the leveled surface and the membrane secured on it by an O-ring. A suction of 10 kPa was applied to the specimen (2 kPa for loose water pluviated specimens), then the split mould was dismantle and the dimension of the sample was carefully measured as follows:

First, the sample diameter was determined using the perimeter tape method

similar to that described by Sasitharan (1994) and Verdugo and Ishihara (1996). A total of three measurements were taken along the sample height. The measurements were averaged and the membrane thickness was accounted for to obtain a good representation of the sample diameter.

Secondly, the sample height was determined by placing the triaxial apparatus under a dial gauge. Three measurements were taken at different locations. The height of the specimen was obtained by comparing the gauge readings with those for a dummy sample of known height.

After the dimensions of the specimen were obtained, the triaxial cell was assembled and securely clamped under the loading rod. When the cell was filled with water, a cell pressure of 10 kPa was applied and the suction was removed at the same time. The transducers for the measurements of load, pore pressure, cell pressure, axial and volumetric deformations were then set to their initial zero level, and these initial readings were recorded.

3.5.2 Saturation

In order to accurately measure the volume changes and pore pressures during shearing, all samples were fully saturated before being sheared. Depending on the sample preparation methods, the following two methods were used to saturate the specimen:

3.5.2.1 Specimens prepared using WP or WT

For specimens prepared using WP or WT, the porous stones were boiled for at least 10 minutes so that no air bubbles were trapped in the pores. Then they were cooled down to room temperature before being submersed onto the triaxial base. The saturation

of the sand was guaranteed by boiling with water or de-aired using high vacuum. Special care was taken so that no air was introduced when the saturated porous stone were placed on the pedestal of triaxial chamber and when the sand was placed in the split mould.

3.5.2.2 Specimens prepared using neither WP nor WT

Saturation of specimen fabricated by neither WP nor WT was undertaken in three stages: carbon dioxide flushing, de-aired water flushing and back pressure saturation. When carbon dioxide gas was flushed through the specimen in the upward direction, air trapped in the pores was replaced by carbon dioxide. Following the flushing of de-aired water, back pressure was applied while an effective stress of 10 kPa was maintained so that any carbon dioxide in the sample would be dissolved in water under pressure. Full saturation of the soil specimen was ensured by insisting on Skempton's B value no less than 0.96, with B being defined as

$$B = \frac{\Delta u}{\Delta \sigma_3} \quad (3.1)$$

where Δu denotes measured pore pressure increment due to applied cell pressure increment, $\Delta \sigma_3$. In most cases, a back pressure of 100 kPa was required for $B \geq 0.96$.

3.5.3 Consolidation

In this study, isotropic consolidation was performed. During consolidation, the effective stress was brought to desired values by increasing the cell pressure gradually with the back pressure being kept at 100 kPa.

3.5.4 Shearing

Displacement control of axial displacement was used in all tests with the cell pressure being held constant during shear. The majority of tests were performed at the rate of axial displacement 0.76 mm/min. A slower shearing rate with 0.15 mm/min was also used for comparison purpose only. It should be noted that displacement control allowed post peak behaviour to be obtained when the specimen, particularly dense sand, suffered from strain softening.

3.6 Discussion of test errors

3.6.1 Errors in void ratio measurement

Error in the determination of average void ratio mainly arises from errors in measurement of the weight and dimensions of the specimen, as well as any volume change in the process of flushing and saturation. In general, errors from the weight and dimension measurements are inherent and usually caused by poor resolution of measuring tools. For the specimens prepared under saturated conditions, the specimen dimensions were measured after a suction of 10 kPa was applied to the specimen. Any volume change owing to cell pressure adjustment and consolidation was measured by the volume change transducer. For the specimens prepared under dry or moist conditions, the specimen dimension was measured under a suction of 10 kPa before carbon dioxide gas and water were flushed through the sample. In this case, any volume change induced by carbon dioxide gas and water flushing as well as saturation was often ignored. The volume change during flushing was reported as large, especially for loose specimens prepared under moist conditions (*e.g.*, Sasitharan, 1994).

In this study, the void ratio after consolidation was taken as the initial void ratio, e_0 , which can be expressed as:

$$e_0 = \frac{\pi D^2 H / 4 - (V_{\text{flu}} + \Delta V_{\text{sat}} + \Delta V_{\text{con}})}{m_s / G_s} - 1 \quad (3.2)$$

where

D – Average diameter of the specimen from three measurements deducted by the thickness of the membrane

H – Measured height of the specimen

m_s – Dry mass of soil

G_s – Specific gravity of soil

ΔV_{flu} – Volume change during carbon dioxide gas and water flushing

ΔV_{sat} – Volume change during saturation

ΔV_{con} – Volume change during consolidation

Generally, the mass of a specimen can be measured to ± 0.01 g, compared with the sample weight of more than 300 g. As a result, the error in the measurement of mass is negligible. In other words, the error in the initial void ratio can be related to any error in dimension and volume change measurement. By differentiating the above equation, the maximum error propagation in e_0 is given as:

$$\delta e_0 = (1 + e_0) \left(\left| \frac{2\delta D}{D} \right| + \left| \frac{\delta H}{H} \right| \right) + (|\delta V_{\text{flu}}| + |\delta V_{\text{sat}}| + |\delta V_{\text{con}}|) G_s / m_s \quad (3.3)$$

note that volume change during consolidation can be precisely measured, *etc.*, $\delta V_{\text{con}} = 0$, one has

$$\delta e_0 = (1 + e_0) \left(\left| \frac{2\delta D}{D} \right| + \left| \frac{\delta H}{H} \right| \right) + (|\delta V_{\text{flu}}| + |\delta V_{\text{sat}}|) G_s / m_s \quad (3.4)$$

The first part of the above equation, $(1 + e_0) \left(\left| \frac{2\delta D}{D} \right| + \left| \frac{\delta H}{H} \right| \right)$, determines the error in e_0 owing to dimension measurement, while the second part, $(|\delta V_{\text{flu}}| + |\delta V_{\text{sat}}|) G_s / m_s$, contributes to the errors in volume change measurement during flushing and saturation, which varies with sample preparation methods.

3.6.1.1 Errors in dimension measurement

For a specimen with the nominal dimension of 50 mm × 100 mm, its diameter and height can be measured to 0.5 mm using the perimeter tape method (corresponding to an error in diameter measurement of $0.5/\pi$ mm) and 0.01 mm using the height gauge method, respectively. If the void ratio of a specimen is 0.7, the maximum error assessed from Equation (3.4) in the overall void ratio is about 0.006, which is less than 1% of the expected void ratio.

3.6.1.2 Errors in volume change measurement during saturation

For an initially saturated specimen prepared using WP or WT method, the volume change of the specimen at each step can be measured by the volume change transducer precisely, *etc.*, $\delta V_{\text{flu}} = \delta V_{\text{sat}} = 0$.

However, for those prepared using other than the WP or WT procedures, *e.g.*, MT, saturation is undertaken in two stages: water flushing and back pressure saturation. The sample dimension is first measured under a low suction (10 kPa in this study) before carbon dioxide gas and de-aired water is flushed through the sample. Volume change

during flushing and saturation is often ignored, which contributes to an additional source of error in e_0 .

The volume change of specimens during water flushing and saturation was calculated based on the height changes monitored by an external LVDT attached on the loading rod and under the assumption of no change in the specimen diameter during saturation. The results of four tests using MT method reported in Table 3.2 indicate that, the error in void ratio due to ignoring the volume change during saturation decreases when the relative density increases. For very loose Ottawa sand with a relative density of 3.6 %, the error in e_0 is 0.018, which is slightly smaller than 0.023 for loose Unimui sand with initial relative density of 4.3 % reported by Zhang and Garga (1997). For medium to dense Ottawa sand, the error rapidly reduces to $\delta e_0=0.005$ for $Dr=32.5\%$, and $\delta e_0=0.003$ for $Dr=60.4\%$. In other words, for medium to dense sand specimens prepared using other than the WP or WT procedures, ignoring the volume change of specimens during saturation stage only leads to a minor error in e_0 .

3.6.2 Membrane penetration

A change in effective confining pressure during a triaxial test causes the membrane enclosing the soil specimen to change its peripheral configuration by either indentation or rebound. For conventional drained triaxial compression tests, a constant effective confining pressure was maintained during shearing and hence the volume measurement was not affected by membrane penetration. The effect of membrane penetration, however, can be substantial in undrained or proportional strain path tests in

which the effective confining stress continuously changes. As a result, the membrane may withdraw out of the interstices of sand grains during increasing pore water pressure or penetrate into them during decreasing pore water pressure. This is equivalent to partial drainage, and would invariably influence the developed excess pore water pressure and the effective stress state in the specimen.

The soil grain size and its gradation have been found to be the most dominant factors that control the magnitude of membrane penetration. All studies concur that the magnitude of membrane penetration decreases with denser packing of sand particles and the influence of density is relatively small compared to influence of mean particle size D_{50} . Also the dependence of membrane penetration on grain angularity and fabric are negligible (Banerjee *et al.* 1979, Nicholson *et al.* 1993).

In this study, the membrane compliance testing for Sand O was performed using 0.3 mm and 0.6 mm thick membranes. Isotropic consolidation tests were performed to evaluate the magnitude of membrane penetration, with the specimens having a comparable initial void ratio of about 0.73 ($D_r=26\%$). The results shown in Figure 3.5 indicate that the membrane thickness significantly affects the membrane penetration. The usage of 0.6 mm thick membrane does not eliminate, but mitigates, the error introduced by membrane penetration. The membrane penetration for the 0.3 mm membrane was about 2.5 times that for the 0.6 mm membrane. Although post-test correction may be performed to account for the influence of membrane penetration, however, such correction may also introduce certain unknown factors. The experimental data reveal that the error induced by membrane penetration effects is quite small in Ottawa sand if the

membrane with the thickness of 0.6 mm is used. Therefore, the membrane induced volume changes were not corrected in subsequent undrained and strain path tests on Ottawa sand reported in the following chapters.

According to the correction suggested by ASTM D4767-04, the deviatoric stress due to membrane restraining in the Ottawa sand samples with 0.6 mm thick membrane is about 10 kPa at an axial strain of 15%. However, it was observed that a latex membrane wrinkled at large strains, indicating that the membrane did not support any axial stress. Consequently, no membrane restraining correction was applied when determining the steady state strength of the Ottawa sand.

3.6.3 End restraint

The development of the frictional forces at the interface between loading platens and the soil specimen can result in premature development of non-homogeneous deformations during shearing. In order to estimate the effect of end restraint, as a preliminary investigation, tests on specimens of dense Sand L were carried out using both regular and lubricated loading platens.

The lubricated ends were prepared using the method proposed by Rowe *et al.* (1964). Two layers of latex disks were cut and lubricated on one side with a thin film of high vacuum grease. They were placed on the enlarged platens with a diameter of about 70 mm. Small air bubbles trapped between the latex disks and platens were carefully removed. The platens with the lubricated end were then subjected to a load of 500 N for about 15 minutes followed by 10 kN for about 30 minutes to obtain a uniform grease film.

Figure 3.7 compares stress-strain and volumetric strain response of very dense Sand L specimens (crushed limestone) with regular ends and lubricated ends. One may observe that the volumetric response is essentially identical for both lubricated and regular ends. Slight differences in deviatoric stress response are due to bedding error corrections pertinent to the lubricated ends used. It should be noted that the chosen density for comparison is close to the densest attainable. Nevertheless, considering the stress-strain and volumetric strain response, the results as shown are considered satisfactory. Figure 3.8 illustrates two pictures taken during a test on a very dense specimen with regular ends. It was observed that even if regular ends are used, the specimen still had uniform deformation up to an axial strain of about 15%. Further shearing, however, caused budging of the specimen owing to end restraints. Furthermore, shear bands were not observed in such dense specimen throughout the testing. The possible reasons for the absence of shear band could be:

(1) The extremely angular grain shape of Sand L inhibits rotation of particles during shearing, which is considered as a basic component of deformation within a shear band (Bardet 1994). Because of rotational frustration, localization or shear band development is less likely to be observed in the presence of angular particles. When shear bands do form it is at higher strains (Alshibli and Sture 2000).

(2) Relatively large grain size to specimen dimension ratio. Therefore, it was speculated that end restraint had minimum effect on promoting non-uniform deformations.

Though the use of lubricated ends is desirable, extreme care is required in

preparing these ends. Moreover, the latex disks could introduce unknown amount of bedding error. Therefore, the choice was made in favor of regular end platens to simplify test procedures. For the sake of consistency, all test results presented in the following chapters were conducted using regular ends.

3.7 Performance of testing system and repeatability of tests

To verify the repeatability of the specimen preparation method, preliminary drained triaxial compression tests were performed on two control specimens of Ottawa sand prepared using MT method. The initial average void ratio of the specimens was approximately 0.715 with the relative density being 75%. A back pressure of 100 kPa was applied during the stage of saturation and the specimens were consolidated at an effective cell stress of 100 kPa. The specimens were then subjected to axial compression loading at a strain rate of 0.015% per minute. These tests were performed using strain control to enable capturing the post-peak stress-strain responses. The experimental data presented in Figure 3.9 show excellent repeatability of stress-strain and volumetric strain responses.

Table 3.1: List of adopted sample preparation methods

Material	Adopted sample preparation methods	Tests
Sand O	WP, MT, MR	CID [†] , CIU*, Strain path
Sand L	WP, WT, MT, MP, MR, DP, DT, DR	CID

[†]CID – Isotropically consolidated triaxial compression drained test;

*CIU – Isotropically consolidated triaxial compression undrained test.

Table 3.2: Volume changes during saturation for MT samples

Initial void ratio, e_0	Initial relative density, $Dr(\%)$	Volume change during flushing, $\delta V_{flu}(\text{cm}^3)$	Volume change during saturation, $\delta V_{sat}(\text{cm}^3)$	Total δe_0
0.625	60.4	0.05	0.32	0.003
0.711	32.5	0.24	0.41	0.005
0.773	12.4	0.85	0.65	0.014
0.800	3.6	1.50	0.54	0.018

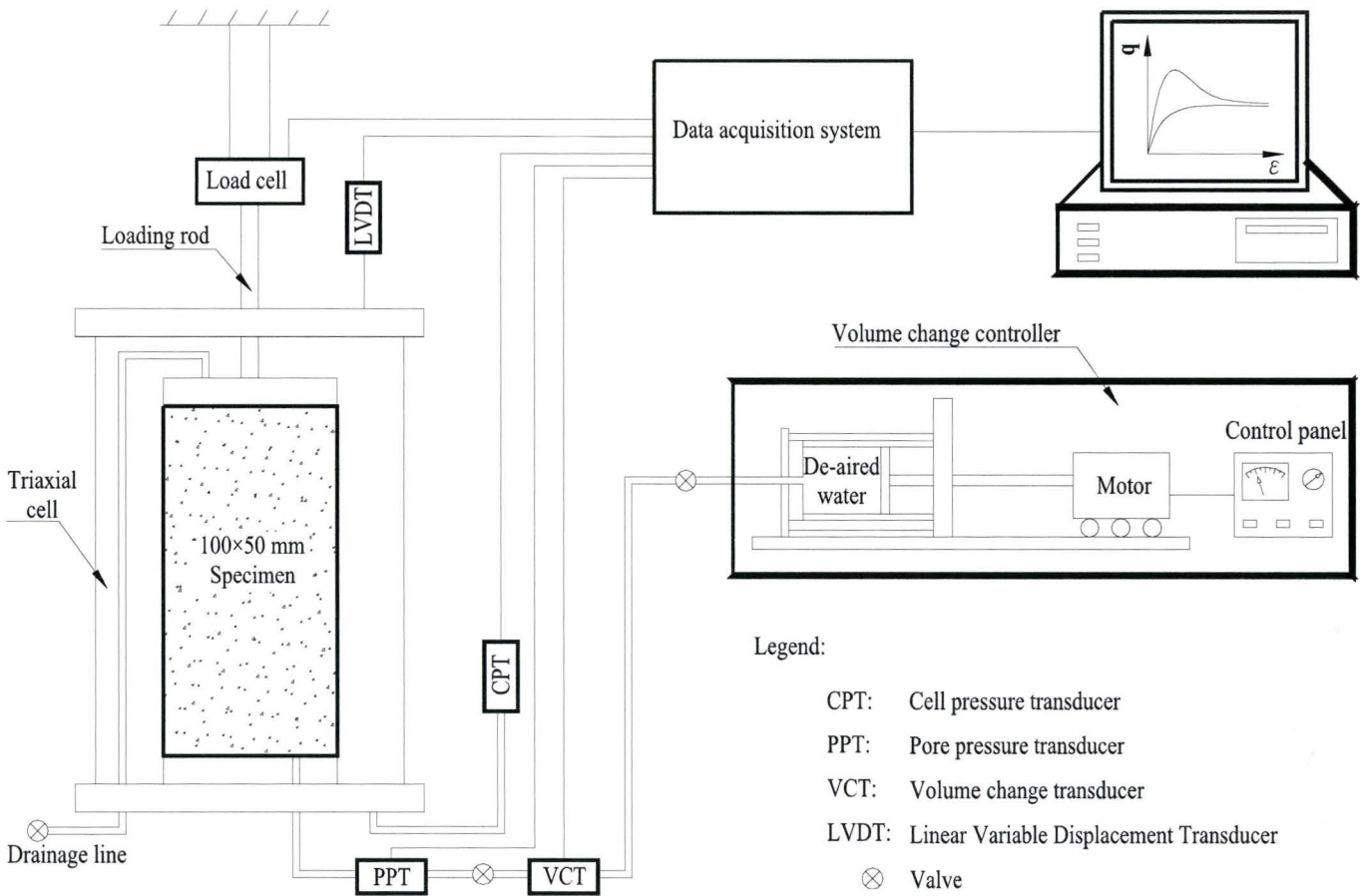


Figure 3.1: Schematic layout of the triaxial testing system

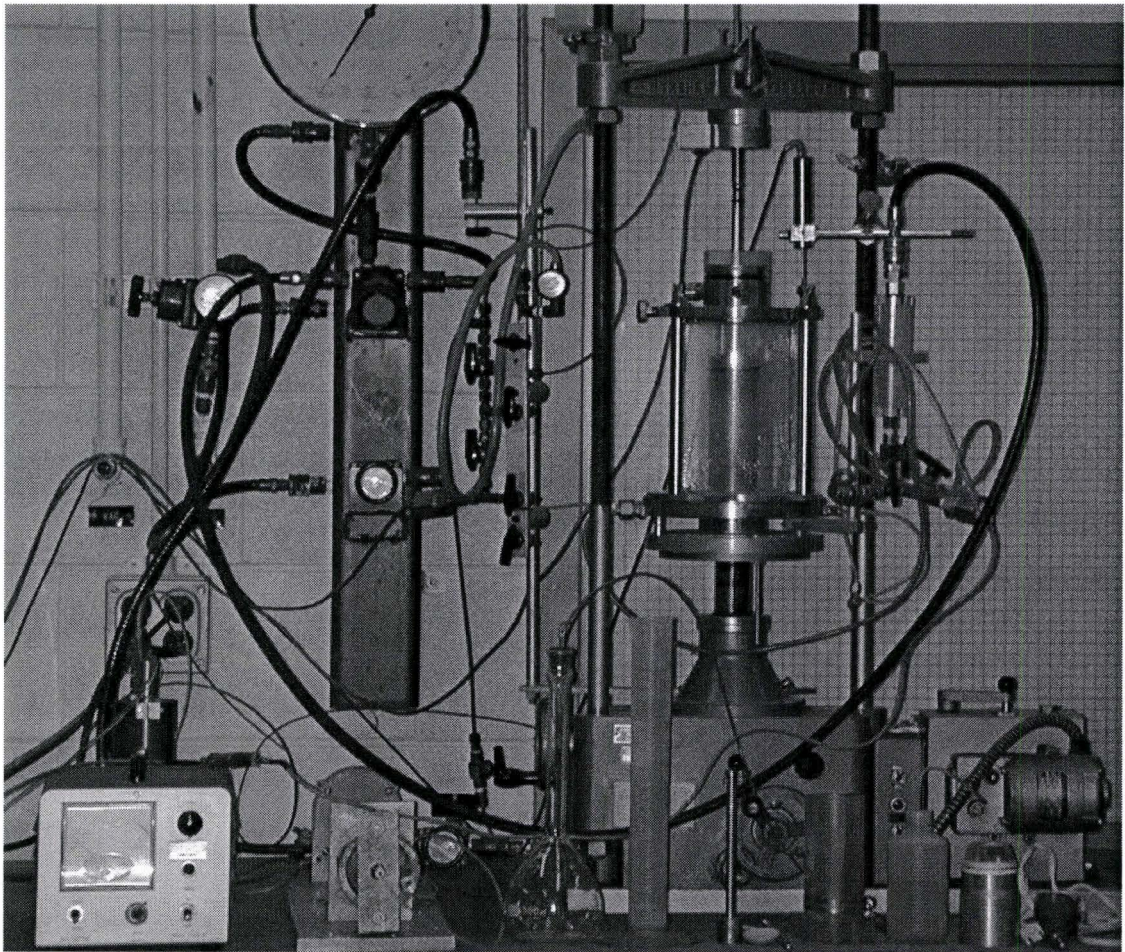


Figure 3.2: Photograph of triaxial testing system

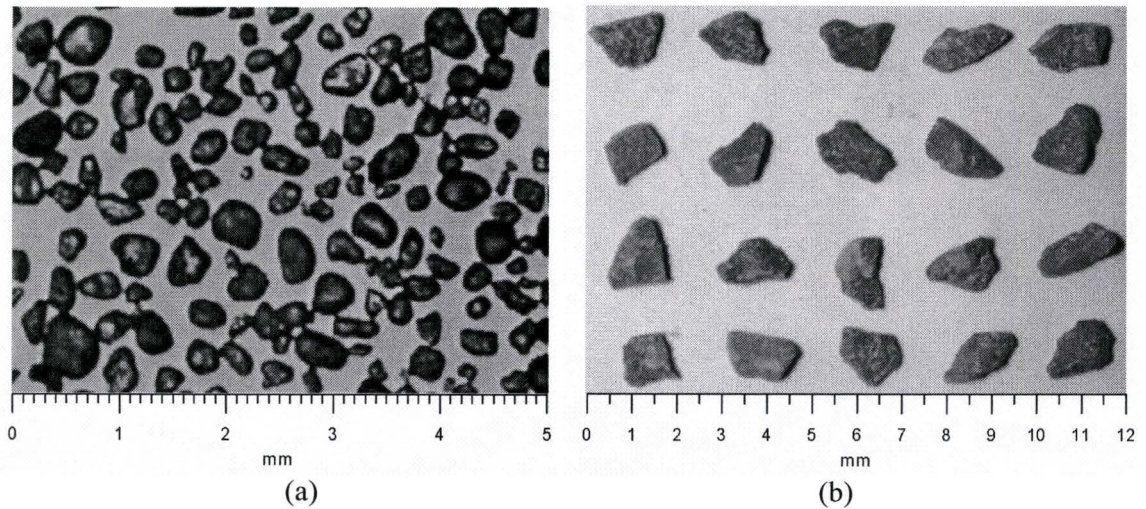


Figure 3.3: Schematic of particle shape of testing materials: (a) Sand O; (b) Sand L.

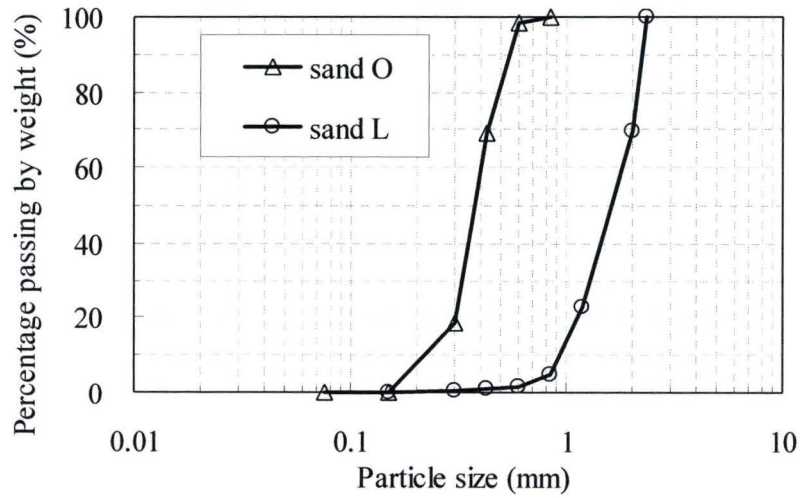


Figure 3.4: Particle size distribution curves

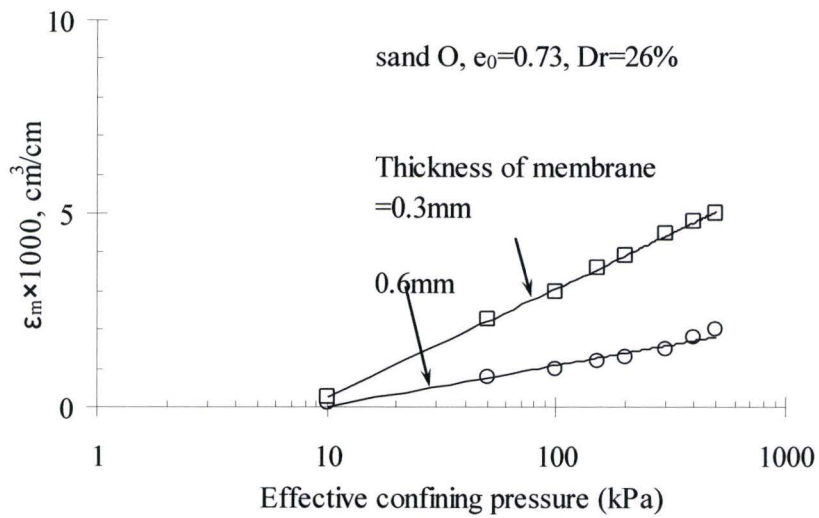


Figure 3.5: Magnitude of membrane penetration of loose Sand O

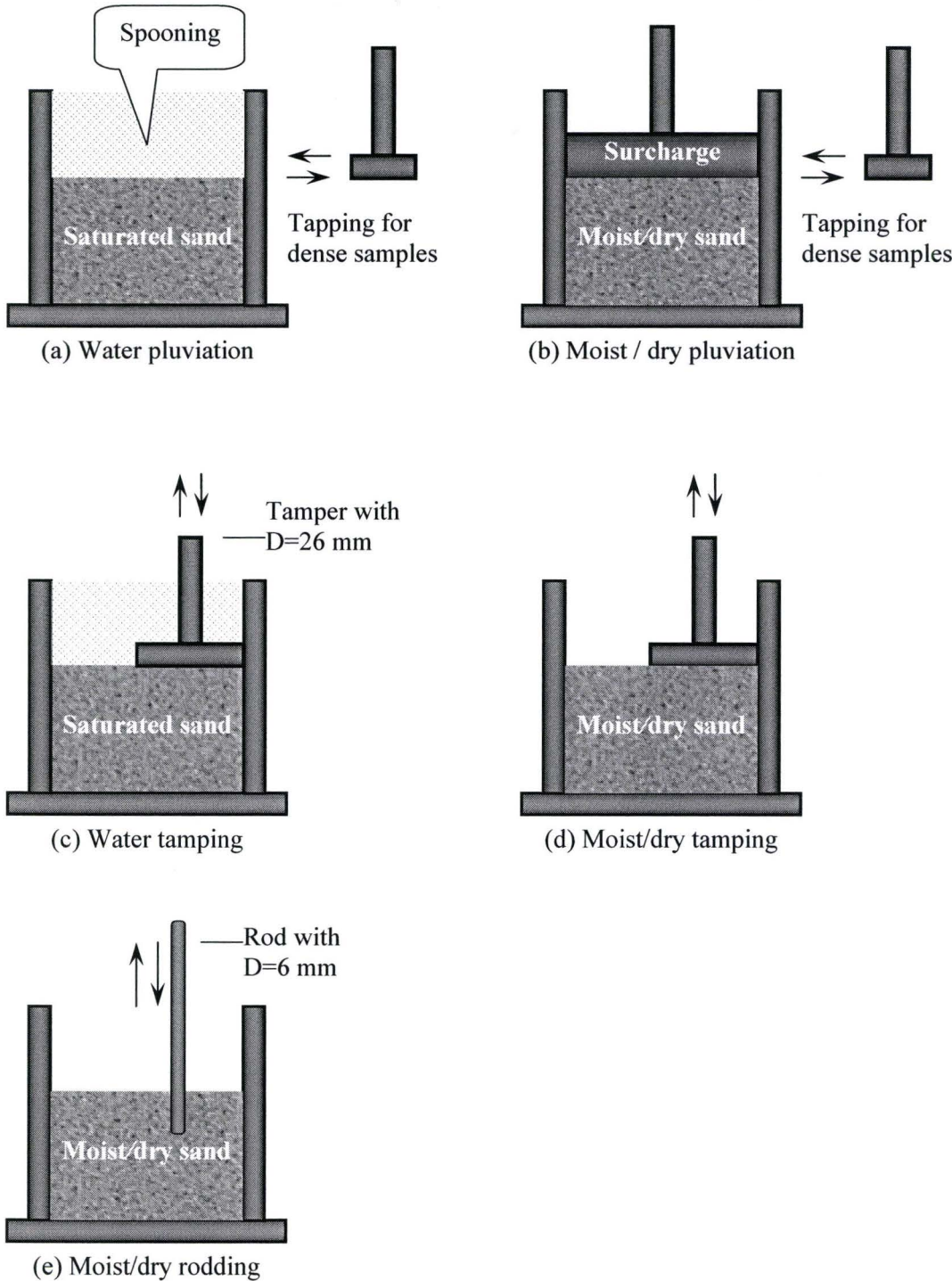


Figure 3.6: Schematic of adopted sample preparation procedures

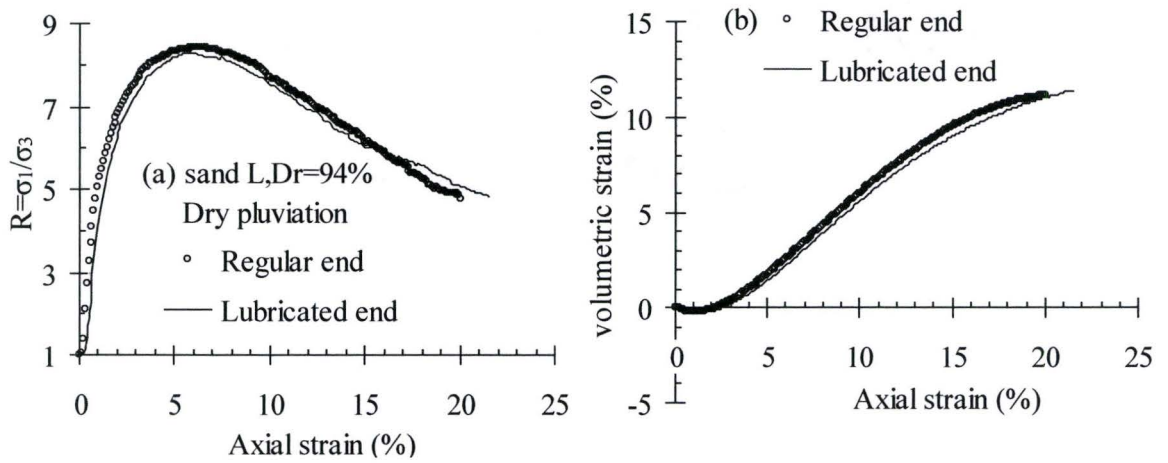


Figure 3.7: Comparison of drained response of Sand L with lubricated and regular end: (a) stress-strain response; (b) volumetric-strain response.

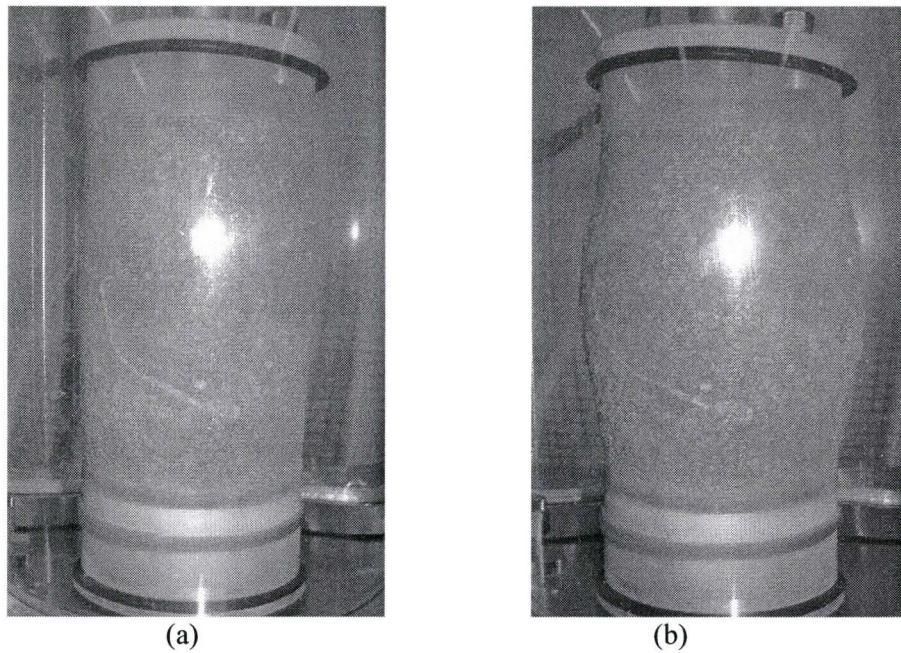


Figure 3.8: Snapshot of dense Sand L specimen at shearing with regular end, $Dr=94\%$, $\sigma_3 = 100$ kPa: (a) $\epsilon_a = 6.25\%$; (b) $\epsilon_a = 16.85\%$.

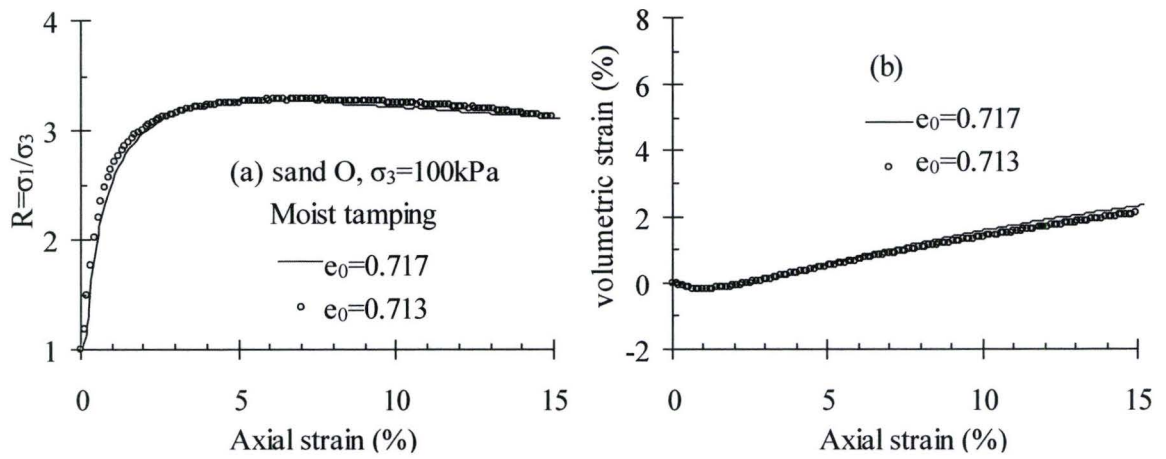


Figure 3.9: Repeatability of triaxial compression drained tests:
 (a) stress-strain response; (b) volumetric-strain response.

Chapter 4

Influence of sample preparation method on stress-strain-strength response of sands

4.1 Introduction

The fundamental understanding of the mechanical behavior of granular materials has evolved mostly from the results of laboratory tests on uniformly reconstituted specimens under homogeneous states of strain and stress. Over the years, numerous studies on the mechanical behavior of sands were performed using various sample preparation methods, from which the influence of initial fabric induced by reconstitution procedures on the stress-strain-strength responses could be recognized; *see, e.g.*, Oda 1972, Mahmood *et al.* 1976, Mulilis *et al.* 1977, Tatsuoka *et al.* 1979, Miura and Toki 1982, Zlatovic and Ishihara 1997, Jang and Frost 1998 and Vaid *et al.* 1999. However, systematic investigations on the influence of sample preparation method on experimental results are scarce.

This chapter presents a comprehensive experimental study on the influence of sample preparation method. A series of conventional triaxial compression tests, both drained and undrained, were carried out on high-quality reconstituted specimens of Ottawa sand (Sand O) and crushed limestone (Sand L) prepared using eight different techniques, namely, water pluviation (WP), moist tamping (MT), moist rodding (MR), dry pluviation (DP), dry tamping (DT), dry rodding (DR), moist pluviation (MP), and water tamping (WT). The behaviour of Ottawa sand specimens prepared by the MT

method will be discussed first and will be used as benchmark to evaluate the influence of sample preparation method.

4.2 Behaviour of Ottawa sand prepared by MT

4.2.1 Drained behaviour

4.2.1.1 Effect of density and stress level on stress-strain responses

Figure 4.1 shows the stress-strain and volumetric strain responses of Sand O sheared at the effective cell pressure of 100 kPa with the initial void ratio ranging from 0.773 to 0.650, which corresponds to variation of relative density from 12% to 52%. The stress-strain responses are presented in terms of the effective principal stress ratio $R = \sigma_1 / \sigma_3$ against the axial strain. As would be expected, for dense specimen ($D_r=74\%$), following the initial volumetric compression at small axial strain, significant dilation occurs when the mobilized stress ratio approaches its maximum value. After the occurrence of peak, both the stress ratio and volumetric strain decrease when deformation approaches the critical state. The peak stress ratio and the amount of volumetric strain, which tend to reduce with an increase of initial void ratio, vanish completely for the loose specimen ($D_r=12\%$). With an increase of initial density, much steeper initial slopes of stress-strain curves are observed, which indicate that the initial stiffness of the material increases with density. At large axial strains, the critical state is approached and the three curves tend to converge to the same critical state stress ratio $(\sigma_1 / \sigma_3)_{cv} = 3.0$, which corresponds to a critical friction angle of $\varphi_{cv} = 29.5^\circ$ (which will be discussed in Chapter

5 in detail). In other words, Figure 4.1 indicates much higher strength and initial stiffness of dense materials, as well as strong evidence of strain hardening and softening effects.

Figure 4.2 shows the influence of effective confining pressure on the responses of a loose Sand Of $e_0 = 0.73$ ($D_r = 26\%$). In general, with an increase of confining pressures, the peak stress ratio (or equivalently the peak friction angle) decreases with the tendency of dilation also decreasing. This is because an increase in confinement tends to suppress the tendency of dilation, which in turn reduces the shear strength of the specimen. Moreover, the initial slope of the stress ratio against axial strain curves tends to decrease with increasing confining pressure. However, comparison of Figures 4.1 and 4.2 reveals that the initial void ratio has a greater influence on the behaviour of Ottawa sand.

4.2.1.2 Peak friction angle

As can be seen from Figure 4-3, the peak effective stress ratio decreases with initial void ratio for a given confining pressure. In other words, the peak friction angle of Ottawa sand is affected by the initial void ratio of the material. Figure 4-3 summarizes the measured peak friction angles of specimens with the initial void ratio and confining pressure. The following conclusions can be drawn from the results presented in Figure 4-3:

- The peak friction angle φ_{peak} decreases with an increase in the initial void ratio e_0 ;
- With an increase of the initial void ratio, φ_{peak} approaches 30° , which is identical to the critical friction angle φ_{cv} .

- φ_{peak} is not sensitive to the effective confining pressure in the range of 100 to 500 kPa.

4.2.2 Stress-dilatancy characteristics

The stress-dilatancy characteristics of sand is usually presented as the variation of the mobilized stress ratio $R = \sigma_1 / \sigma_3$ against the dilatancy factor D , which is defined as $D = 1 - d\varepsilon_v^p / d\varepsilon_1^p$ with ε_v^p and ε_1^p being the plastic volumetric and axial strains, respectively. For granular materials, it is difficult to separate plastic deformation from the total deformation. The elastic strain during deformation, however, is only a small fraction of the total strain, particularly at large deformation. For simplicity and without loss of generality, the dilatancy factor is determined according to the total strain components in the following sections.

Figure 4-4 through Figure 4-6 present the stress-dilatancy plots of Ottawa sand subjected to different confining stresses at various initial void ratios. When defining

$$K_\mu = \tan^2\left(\frac{\pi}{4} + \frac{\varphi_\mu}{2}\right) \text{ and } K_{cv} = \tan^2\left(\frac{\pi}{4} + \frac{\varphi_{cv}}{2}\right) \text{ with } \varphi_\mu \text{ being the interparticle friction angle}$$

that is assumed to be 25° , the R/D ratios of all specimens are $K_\mu \leq \frac{R}{D} \leq K_{cv}$. Graphically,

the dilatancy plots are located between two straight lines $R = K_{cv}D$ (K_{cv} -line) and

$R = K_\mu D$ (K_μ -line), respectively. For very loose sand ($e_0 \approx 0.81$) at a given stress level,

the stress–dilatancy plots are best represented by the K_{cv} - line. For dense sand with $e_0 =$

0.61 at $\sigma_3 = 100$ kPa (see Figure 4-4) the stress–dilatancy plots first evolves along the

K_μ -line. The peak stress ratio is reached when the maximum value of dilatancy factor is mobilized. Following the peak point of the curve, the stress ratio R decreases simultaneously with D , giving a “hook” in the curve as it drops to the critical state. The R - D plot for a medium dense sand with $e_0 = 0.71$ is located between those of loose and dense specimens. The data shown in Figure 4-4 also suggest that, while the friction angle at the onset of dilation φ_f (*i.e.*, the mobilized friction angle when $D = 1$), is different from φ_{cv} as implied by Rowe’s original stress-dilatancy relation (Rowe, 1962). Instead, φ_f varies between φ_μ for dense sand and φ_{cv} for loose sand. Figure 4-5, which presents the dilatancy plots of Sand O sheared at $\sigma_3 = 500\text{kPa}$, shows the same trend as that observed from Figure 4-4.

The effect of confining pressure on stress-dilatancy plot is also observed from the experimental data. As shown in Figure 4-6, for dense sand specimens with $e_0 = 0.62$, both the peak stress ratio R_{max} (or the peak friction angle) and the maximum dilatancy factor D_{max} decrease with an increase in the confining pressure, while φ_f (the friction angle at the onset of dilation) tends to increase.

4.2.3 Peak strength and the angle of dilation

The stress-dilatancy plots presented in Figure 4-4 through Figure 4-6 clearly show that, in addition to the confining stress and the initial void ratio, the peak stress ratio and the corresponding friction angle are closely related to the maximum rate of dilatancy. Figure 4-7 summarizes the relation between R_{max} and the corresponding dilatancy factor D_{max} . One observes that, irrespective of the difference in the initial void ratio and the

confining pressure, the experimental data can be represented by a straight line located between the K_{μ} - and K_{cv} -lines as

$$R_{\max} = R_{cv} + 1.45 D_{\max} \quad (4.1)$$

When one defines the angle of dilation as

$$\sin \psi = -\frac{d\varepsilon_v^p}{d\gamma^p} = -\frac{d\varepsilon_1^p + 2d\varepsilon_3^p}{d\varepsilon_1^p - d\varepsilon_3^p} \quad (4.2)$$

with ε_1^p and ε_3^p being the axial and lateral plastic strains, respectively, the relation between the peak friction and the maximum angle of dilation may then be approximated as

$$\varphi_{peak} - \varphi_{cv} = 0.6437\psi_{max} \quad (4.3)$$

in which the friction angle at critical state is $\varphi_{cv} = 30^\circ$ for Ottawa sand. This relation is very close to that proposed by Bolton (1986):

$$\varphi_{peak} - \varphi_{cv} = 0.8\psi_{max} \quad (4.4)$$

It should be noted that when calculating the angle of dilation, the increments of total strain components instead of plastic strain components were used, owing to difficulties in separating the plastic and elastic deformations of the specimens. This assumption is reasonable since the elastic strains usually are very small compared with the plastic strains.

4.3 Undrained behaviour of saturated Ottawa sand

Figure 4.8 shows typical undrained response of Ottawa sand consolidated under an effective pressure of 200 kPa at various initial void ratios. For a loose specimen of $e_0 = 0.798$ ($D_r = 5\%$), one observes that the deviatoric stress q increases at the beginning of shearing and reaches its maximum at a small axial strain of approximately 0.8% (Figure 4.8b), and that continuous shearing induces a decrease of q . During this process, the mean effective stress p monotonically decreases with the excess pore pressure increasing, indicating that the specimen is contractive during the whole process of undrained shear. The effective stress path gradually approaches the critical state line (CSL) in the $p - q$ space when both p and q approach zero. When a medium dense specimen ($e_0 = 0.683$, $D_r = 41.6\%$) is sheared, both p and q increase monotonically and the effective stress path eventually approaches the CSL, as shown in Figure 4.8a. The excess pore water pressure, however, increases at the beginning and then decreases with negative values developing at large strain. This observation is consistent with the drained behaviour of dense sand shown in Figure 4.1, in which the dense specimen has contractive volumetric strain at small strains followed by substantial dilation. Under undrained conditions, the tendency of volume contraction causes an increase in excess pore pressure, while dilation induces negative pore pressure. For the specimen with $e_0 = 0.732$, the deviatoric stress decreases following an initial increase at the beginning of shearing, regain of q is observed when the effective stress path approaches the CSL. The point at which both p and q reach their minimum values and the effective stress path turns upward is called the state of phase transformation. These observations are consistent with previous experimental studies;

see, for example, Ishihara (1993). Figure 4.9 compares the undrained responses of a medium dense sand ($e_0 = 0.68$, $D_r = 42\%$) subjected to different initial effective confining pressure σ_3 . No significant difference in the effective stress paths is observed when σ_3 varies from 100 kPa to 500 kPa. However, the variation of the effective stress ratio $R = \sigma_1 / \sigma_3$ against the axial strain reveals that a peak stress ratio develops when $\sigma_3 = 100$ kPa, with a decrease in R being observed when both p and q increase. For the specimen subjected to $\sigma_3 = 500$ kPa, however, the effective stress ratio increases monotonically with the axial strain. The difference in the evolution of R with respect to the axial strain at different σ_3 reflects the influence of mean effective stress level on the friction angle of granular materials, which is consistent with the drained triaxial compression test results.

4.4 Influence of sample preparation method on sand behaviour

4.4.1 Static drained triaxial response

4.4.1.1 Stress-strain-volume change responses

For discussion purposes, three typical data sets for both Sand O and Sand L sheared at an effective confining pressure of 100 kPa are re-plotted in Figure 4-10 through Figure 4-12. More specifically, Figure 4-10 compares the stress-strain and volumetric strain curves for Sand O specimens with the initial void ratio $e_0 = 0.71$ (or $D_r = 31\%$), but fabricated using WP (water pluviation), MT (moist tamping) and MR (moist rodding), respectively. Figure 4-11 and Figure 4-12 compare the behaviour of medium dense specimens of Sand L ($e_0 = 0.77$ and 0.68 , respectively) fabricated using different methods.

As can be seen from Figure 4-10, for the loose specimen of Sand O with $e_0 = 0.71$, the responses of all three specimens are almost identical at small axial strains (less than 0.3%), which implies that the initial stiffness is likely not affected by sample preparation method. However, this might be owing to the accuracy of small strain measurement in triaxial tests at low strain levels. When the axial strain is larger than 0.3%, the specimen fabricated by the WP method has the largest mobilized stress ratio at the given axial strain with the MR prepared specimen having the lowest. With the increase of axial strain, the differences in the mobilized effective stress ratio decrease and the three curves converge into the same one with R approaching the constant volume stress ratio R_{cv} . In other words, when specimens of the same nominal initial void ratio are subjected to the same initial stress state, the difference in the fabric associated with sample preparation methods results in different responses at relatively low strain level. At large strains, however, owing to the particle rearrangement induced by shearing, initial fabric is eliminated and all specimens show the same responses.

The sample preparation method also affects the volume change characteristics of Ottawa sand. As shown in Figure 4-10b, the specimen prepared by WP tends to have more dilation than those prepared by MT and MR. On the other hand, MR is likely to result in an internal structure with more shear-induced compaction and less dilation during shearing. The experimental results presented in Figure 4-10 confirm again that the shear resistance of Ottawa sand is substantially affected by sample preparation method and is closely related to dilatancy of the samples.

Figure 4-11 and Figure 4-12 show the effect of sample preparation method on the stress-strain-volume change responses of Sand L, which is a sand comprising angular particles derived from crushed limestone. The experimental data in Figure 4-11 show that the specimen ($e_0 = 0.77$) fabricated using MR (moist rodding) has the most gentle stress-strain curve with less dilation, while WP and MT tend to produce samples that yield more dilation and higher shear resistance. However, when compared with the results of Sand O presented in Figure 4-10, one observes that WP and MT only cause small variations in the behaviour of Sand L. Figure 4-12 further compares the behaviour of Sand L ($e_0 = 0.68$) prepared from dry sand using different compaction methods. Similar to the experimental data shown in Figure 4-11, the specimen densified by rodding (*i.e.*, DR) has lower shear resistance and less dilation compared with the corresponding samples prepared by the pluviation and tamping methods.

In summary, the test results presented herein clearly indicate that the drained stress-strain-volume change responses of both Sand O and Sand L sand are significantly affected by sample preparation methods, which resulted in different initial internal structure (or fabric) or inherent anisotropy. An interpretation with regard to the influence of densification methods (herein pluviation, tamping and rodding) on sand behaviour is given as follows. According to Oda (1972), when sand grains fall into the split mould from a certain height, the longer axis of a non-spherical particle tends to align in the horizontal direction. For moist tamping method, the orientations of particles are random when the particles are placed into the mould. The tamping, however, may induce certain preferential orientations of particles, but less significant when compared to orientations

obtained via the pluviation method. Rodding tends to yield more random distribution of sand grains in space and the sample will most likely be isotropic. The inherent anisotropy derived from different sample preparation methods is reflected in the differences of the experimental curves presented in Figure 4-10 through Figure 4-12.

4.4.1.2 Peak friction angle

Another appraisal on the influence of sample preparation methods on sand behaviour is presented in Figure 4-13 and Figure 4-14, which summarize the variation of peak friction angle φ_{peak} with respect to the initial void ratio at $\sigma_3 = 100$ kPa for Sand O and Sand L samples prepared by WP, MT and MR, respectively. Irrespective of the difference in particle shape, the WP method yields the highest peak friction angle with $\varphi_{peak,MP} > \varphi_{peak,MT} > \varphi_{peak,MR}$ at a given initial void ratio for both materials. The influence of sample preparation method vanishes for very loose specimens.

4.4.1.3 Characteristic friction angle

The characteristic friction angle φ_{mc} of sand under drained conditions is referred to as the mobilized friction angle at which the volumetric deformation changes from compaction to dilation with the rate of volumetric strain being temporarily zero (*i.e.*, $d\varepsilon_v = 0$). Figure 4-15 presents the variation of φ_{mc} with respect to the initial void ratio of Ottawa sand subjected to the effective confining pressure of 100 kPa. φ_{mc} generally increases with an increase in the initial void ratio, with the maximum $\varphi_{mc}^{max} = \varphi_{cv}$ being reached for loose sand. For dense specimens, dilation starts at a mobilized friction angle smaller than φ_{cv} . Moreover, φ_{mc} is substantially affected by sample preparation methods.

More specifically, WP tends to cause a larger variation of φ_{mc} with regard to initial void ratio, with $\varphi_{mc} \cong \varphi_{cv}$ for all specimens fabricated using moist rodding, which tends to yield mostly isotropic structure. For dense specimens obtained via WP and MT, on the other hand, the preferential arrangement of grains results in more stable but anisotropic structures. Any particle movement, even at lower shear stress level, is accompanied by particle rotation and particles overriding each other, and hence dilation. This finding implies that, in addition to the initial void ratio, fabric should also be taken into account when determining the characteristic friction angle.

The measured characteristic friction angle φ_{mc} for Sand L also shows the influence of sample preparation methods, as can be seen from Figure 4-16. Different from the data for Ottawa sand in Figure 4-15, φ_{mc} of Sand L is consistently larger than its critical friction angle φ_{cv} , with specimens prepared by WP having the largest φ_{mc} at a given void ratio. This can be attributed to the interlocking of angular particles of Sand L, since extra shear stresses are required to overcome interparticle locking before relative displacements between particles and hence dilation can take place. As such, one may conclude that the influence of sample preparation methods may manifest itself as different particle arrangements (*i.e.*, fabric) and interparticle locking.

4.4.1.4 Dilatancy characteristics

The influence of sample preparation methods on sand behaviour presented in Figure 4-10 to Figure 4-13 can be alternatively presented in terms of the stress-dilatancy plots.

Figure 4-17 compares the dilatancy plots of Sand O prepared by MT, MD and MR, corresponding to the experimental results presented in Figure 4-10. For a given stress ratio prior to its maximum, the specimens prepared using WP and MR have the highest and the lowest potential of dilation, respectively. One also observes that the specimen prepared by WP starts to dilate at much smaller shear stress than the specimen prepared by MR.

Even though the peak friction angles and the stress-dilatancy plots are significantly affected by the sample preparation method, the relation between R_{max} and D_{max} is not sensitive to sample preparation methods. As shown in Figure 4-18, a unique $R_{max} - D_{max}$ relation can be reasonably defined for all specimens at a given effective confining pressure (herein $\sigma_3 = 100$ kPa). Similar conclusions can be drawn from the experimental data of Sand L, as shown in Figure 4-19.

It should be noted that the experimental stress-dilatancy data for Sand O, shown in Figure 4-17, normally do not lie on the K_{cv} line as implied by the original Rowe's stress-dilatancy equation (Rowe, 1962), but fall on a line found between the K_{cv} - and K_{μ} -lines, which is consistent with the experimental data in the literature (*e.g.*, Bishop, 1972; Wan and Guo, 1999). For Sand L, however, all data points are above the K_{cv} -line and the data points deviate more from the K_{cv} -line for dense specimen at small stress ratios, as shown in Figure 4-19.

In addition to the influence on stress-dilatancy plots, sample preparation methods affect the maximum angle of dilation ψ_{max} as well. Figure 4-20 shows the influence of sample preparation methods (WP, MT and MR) on the variation of ψ_{max} with initial void

ratio for Ottawa sand subjected an effective confining pressure of 100 kPa. For a given initial void ratio, the water pluviation method yields higher dilation angle than MT and MT, with the difference being as high as 8° for dense samples. This feature of Sand L has been attributed to interlocking owing to the angularity of particle (Guo and Su, 2006).

4.4.1.5 Peak friction angle and the maximum angle of dilation

Figure 4-13, Figure 4-14 and Figure 4-20 reveal that sample preparation methods have significant effects on both φ_{peak} and ψ_{max} . When the relation between φ_{peak} and ψ_{max} is concerned, one can easily obtain the variation of φ_{peak} with respect to ψ_{max} from the $R_{max} - D_{max}$ relation presented in Figure 4-18 and Figure 4-19. As shown in Figure 4-21, for both Sand O and Sand L, regardless of the sample preparation methods and the effective confining stresses, linear relations can be used to describe the relation between φ_{peak} and ψ_{max} :

$$\text{Sand L: } \varphi_{peak} - \varphi_{cv} = 0.99\psi_{max}, \quad \varphi_{cv} = 37.5^\circ \quad (4.5)$$

$$\text{Sand O: } \varphi_{peak} - \varphi_{cv} = 0.6437\psi_{max}, \quad \varphi_{cv} = 30^\circ \quad (4.6)$$

in which the critical friction angles for both materials are given in Chapter 3. It should be noted that Eqs. (4.5) and (4.6) have the same form as the empirical relation proposed by Bolton (1986):

$$\varphi_{peak} - \varphi_{cv} = 0.8\psi_{max} \quad (4.7)$$

which is based on the experimental data of 18 river / marine sands.

Eqs. (4.5) and (4.6) indicate that, even though the peak friction angle φ_{peak} and ψ_{max} are affected by sample preparation methods, their relations are almost unaffected by sample preparation method. In other words, the influence of sample preparation methods on the strength of sand is the consequence of variation in dilatancy owing the different fabrics associated with sample preparation methods.

4.4.2 Static undrained response

In this section, only MT and WP specimens are used to investigate the influence of sample preparation on the undrained behaviour of Ottawa sand. Figure 4-22 compares the undrained behaviour of very loose Sand O specimens under an initial effective confining pressure of 100 kPa. The specimens, with the initial void ratios ranging between 0.793 and 0.798 ($D_r \approx 5\%$), were prepared by water pluviation and moist tamping, respectively. Even though both specimens were extremely loose, the one prepared by WP method exhibits dilative behaviour, which corresponds to the turning upward of the effective stress path. The specimen prepared by MP, however, displayed typical contractive response that manifests itself as continuous decrease in the effective stress, which leads to static liquefaction during undrained triaxial compression. The effect of sample preparation method was also observed under different initial consolidated pressures. As shown in Figure 4-23, when the consolidated pressure is changed, MT prepared specimens are more prone to contractive behaviour and hence static liquefaction. Similar results are reported by DeGregorio (1990), Zlatovic and Ishihara (1997), and Vaid *et al.* (1999). The strain softening response of the moist tamped sand is

primarily due to the collapsible ‘honeycomb-like’ structure that ensues upon reconstitution by moist tamping (Casagrande, 1975). In addition, considerable variations from the average void ratio occur in the specimen.

4.5 Summary

The influence of sample preparation method was assessed from drained and undrained triaxial compression tests on two sands with distinct grain characteristics. Based on the experimental results presented in this chapter, the following conclusions are drawn:

- The differences in drained stress-strain-strength behavior at medium straining level between reconstituted specimens at the identical initial state (void ratio and mean effective stress) may be dramatic. Such manifestation of fabric on strength and deformation characteristics of granular material almost always exists, but differs quantitatively with particle shape. It is thus presumed that contact normal distribution attributes to the strength anisotropy behaviour of Ottawa sand with regard to rounded to subrounded particles. Conversely, both preferred orientation of the longitudinal axis of the sand grains in the horizontal direction and contact normal distribution accounts for the observed anisotropy of crushed limestone with very angular grains.
- For both Ottawa sand and crushed limestone, the peak friction angles and the characteristic friction are influenced by sample preparation methods. However, a unique relation between the peak friction angle and the maximum angle of dilation is defined for each material.

- The stress-dilatancy plots of Ottawa sand, which has rounded particles, are bounded by the K_{μ} - and K_{cv} -lines. For Sand L, which has angular particles, the stress-dilatancy plots are always above the K_{cv} -line, owing to the effect of interparticle locking associated with particle angularity.
- With all sample preparation methods used in this study, moist tamping seems to form the most non-uniform specimens. There are distinguishable interfaces between layers appearing in MT specimens. Both WP and MR tend to yield relatively uniform specimens. However, dense specimens fabricated using WP exhibits substantial anisotropic behaviour.

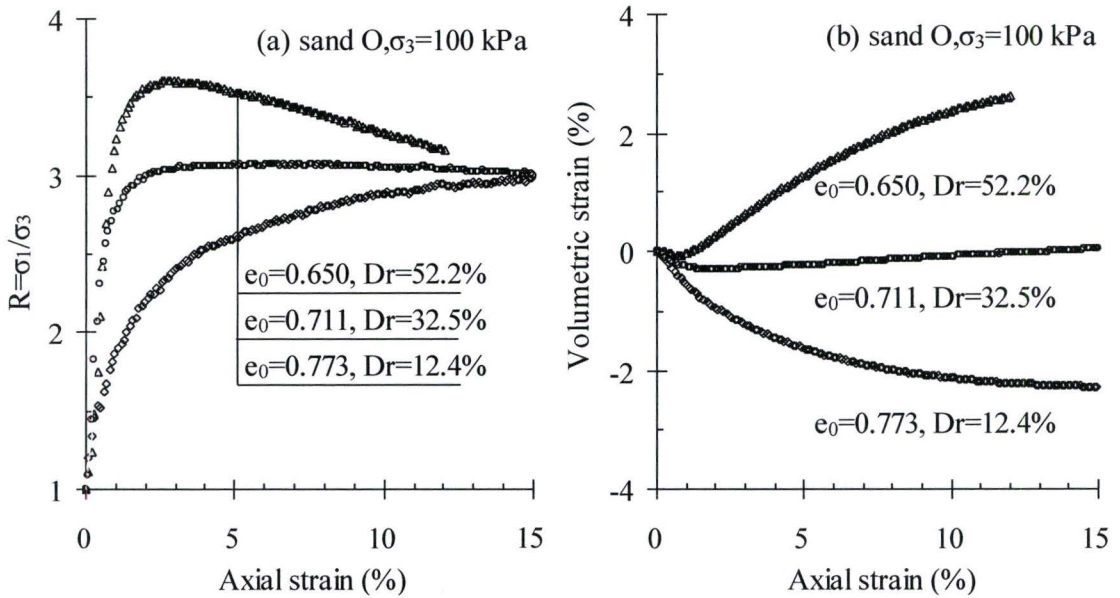


Figure 4-1: Drained triaxial compression test results of Ottawa sand at $\sigma_3 = 100$ kPa :
 (a) Stress-strain response; (b) Volumetric strain response.

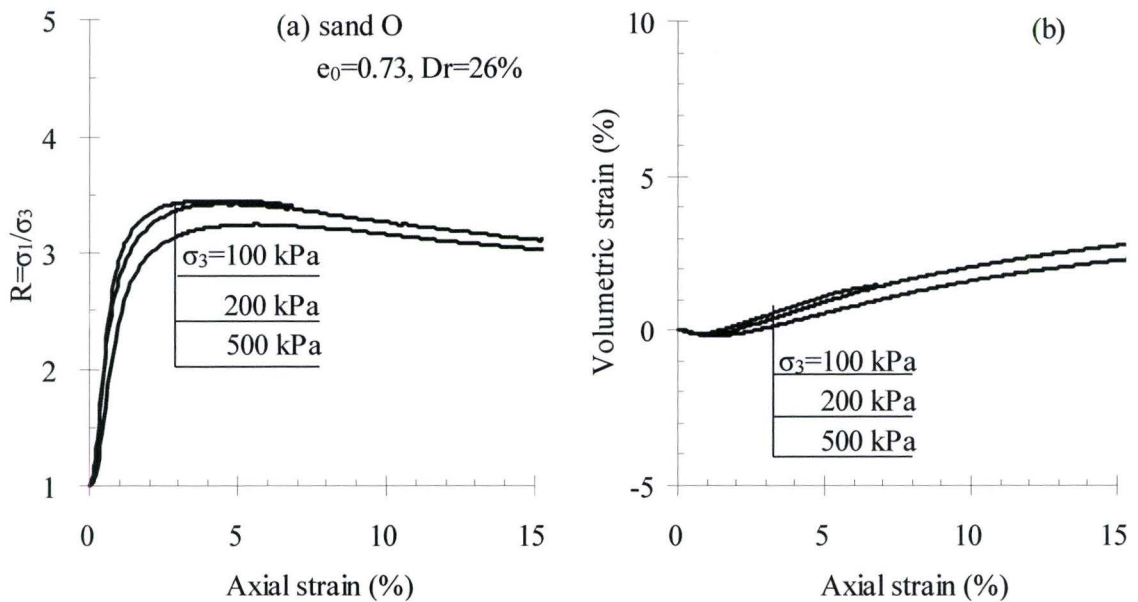


Figure 4-2: Triaxial compression drained test results of Ottawa sand at $e_0 = 0.73$:
 (a) Stress-strain response; (b) Volumetric strain response.

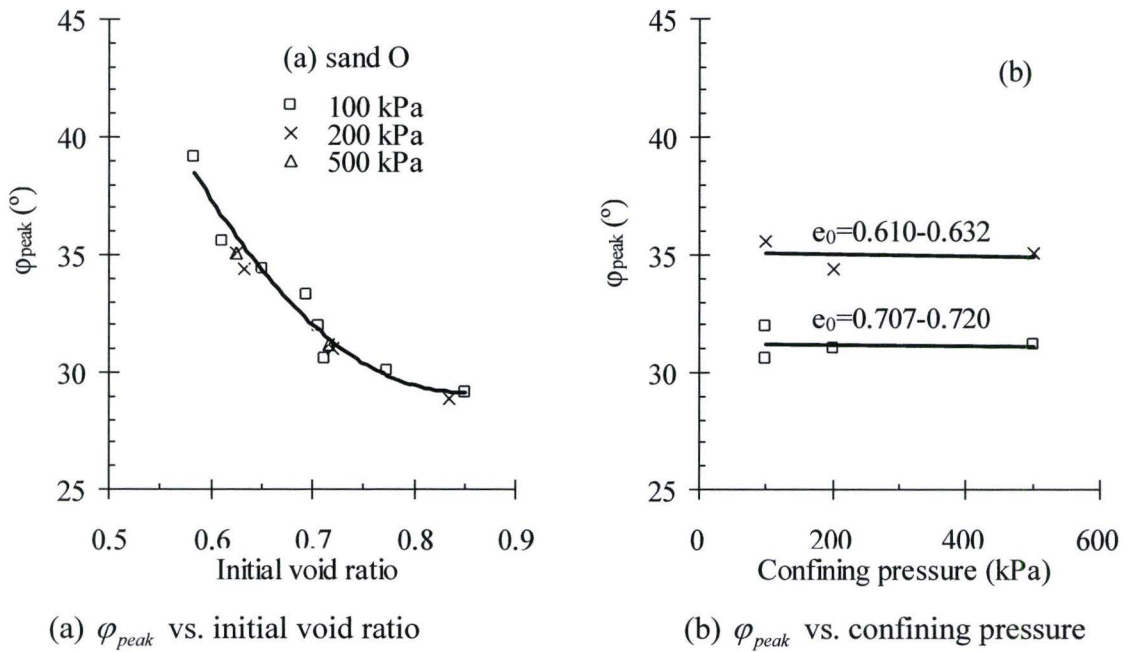


Figure 4-3: Influence of initial void ratio and the confining pressure on peak friction angle of Ottawa sand

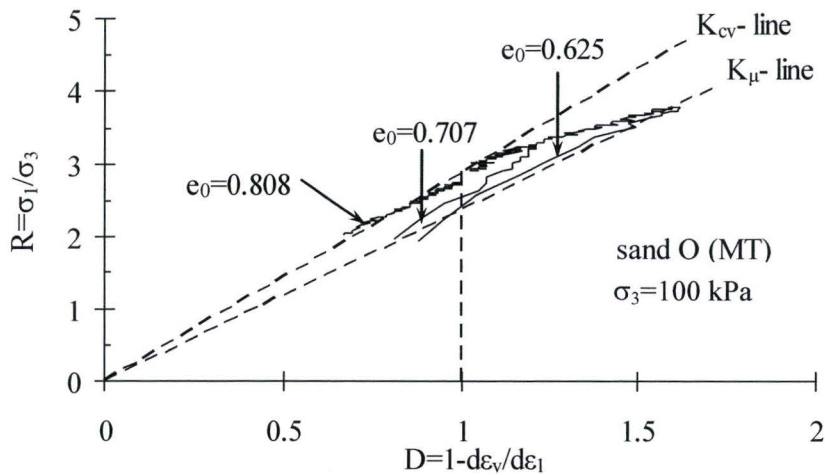


Figure 4-4: Influence of initial void ratio on stress-dilatancy plot of Ottawa sand at $\sigma_3 = 100$ kPa

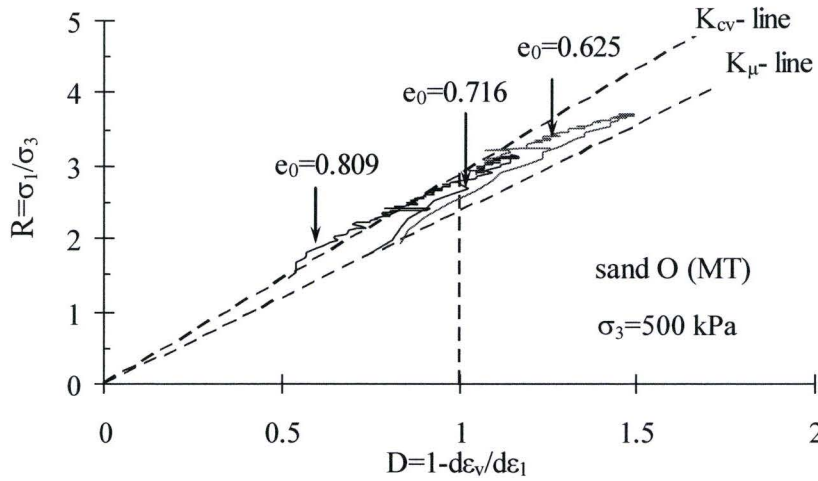


Figure 4-5: Influence of initial void ratio on stress-dilatancy plot of Ottawa sand at $\sigma_3 = 500 \text{ kPa}$

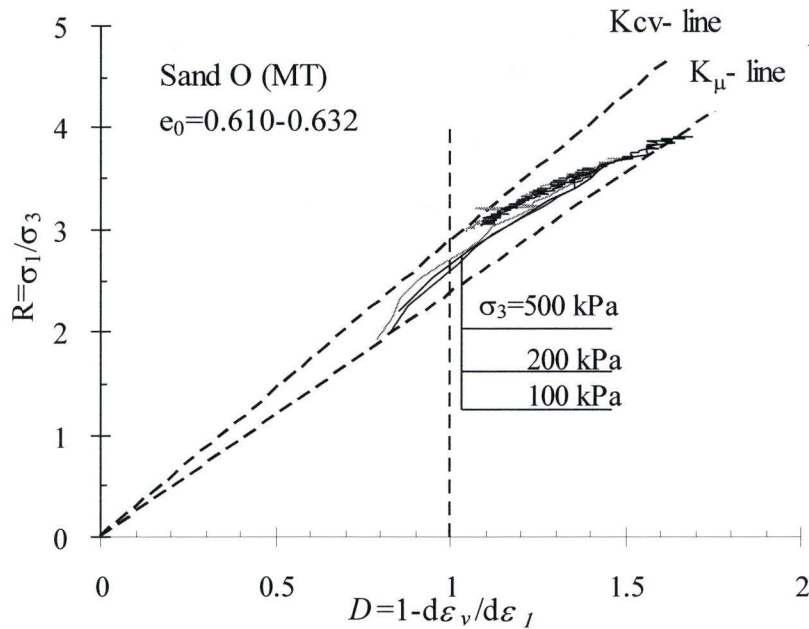


Figure 4-6: Influence of confining pressure on stress-dilatancy plot of dense Ottawa sand at $e_0 = 0.62$

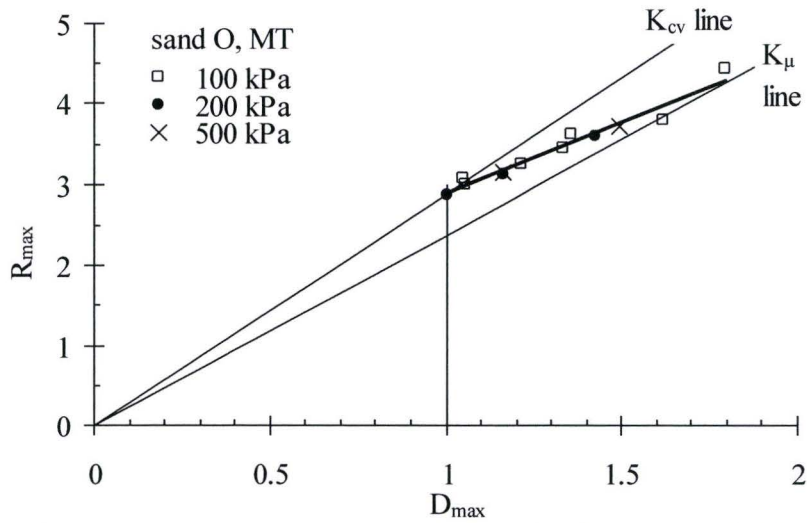


Figure 4-7: Peak stress ratio versus peak dilatancy for Ottawa sand, Moist tamping

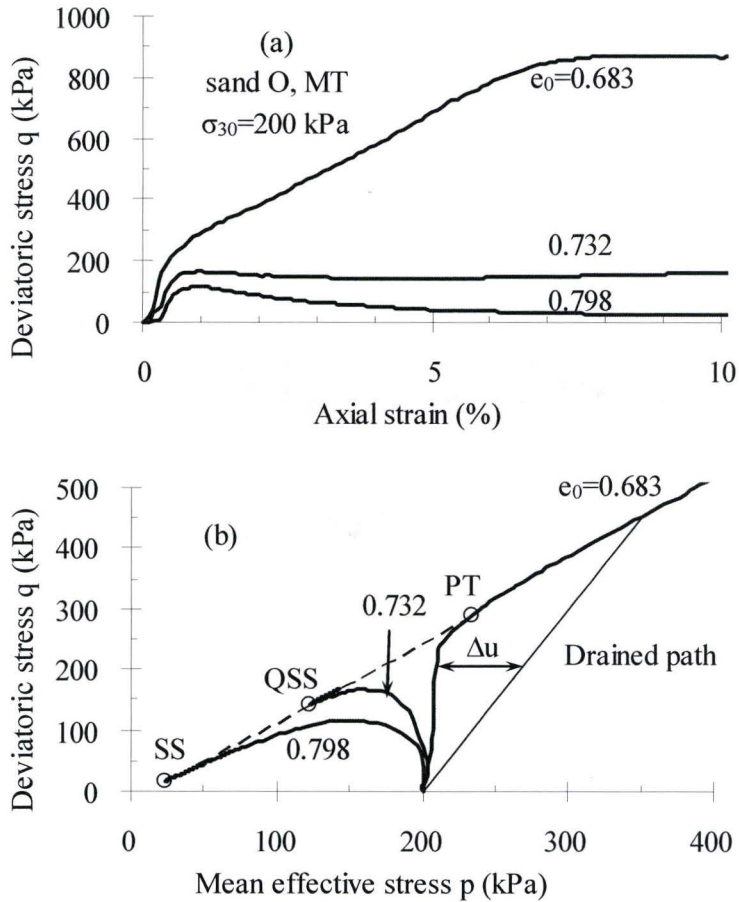


Figure 4-8: Influence of density to undrained behaviour of Ottawa sand at $\sigma_{30} = 200\text{kPa}$:
 (a) stress-strain curve; (b) stress path.

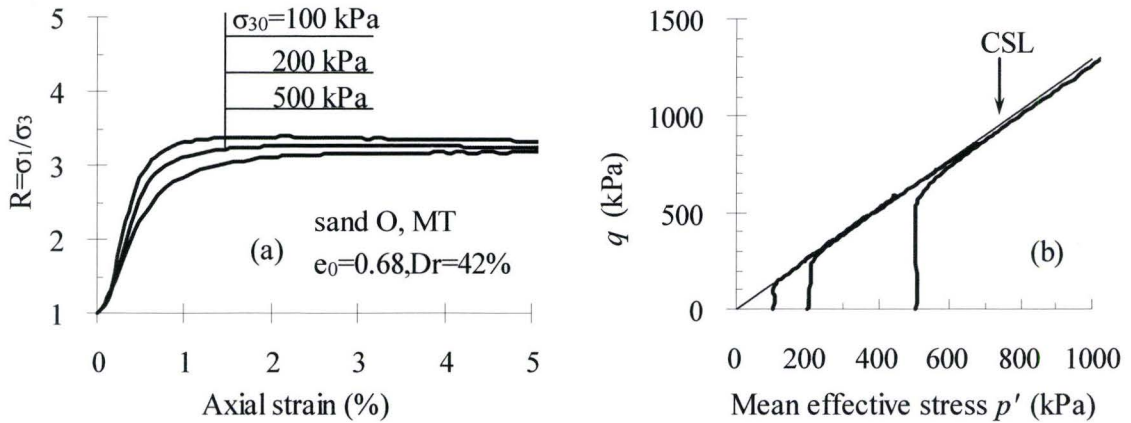


Figure 4-9: Influence of confining pressure to undrained behaviour of Ottawa sand at initial relative density of 42%:(a) stress-s ratio versus axial strain; (b) stress path.

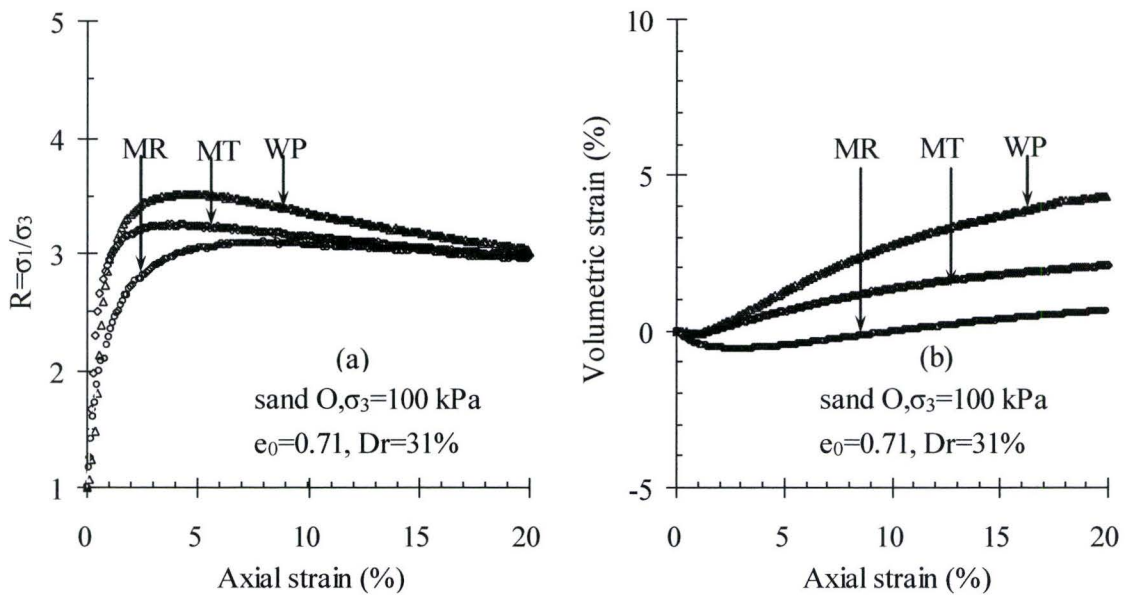


Figure 4-10: Influence of sample preparation on drained behaviour of loose Ottawa sand sheared at $\sigma_3 = 100$ kPa : (a) Stress-strain response; (b) Volumetric strain response

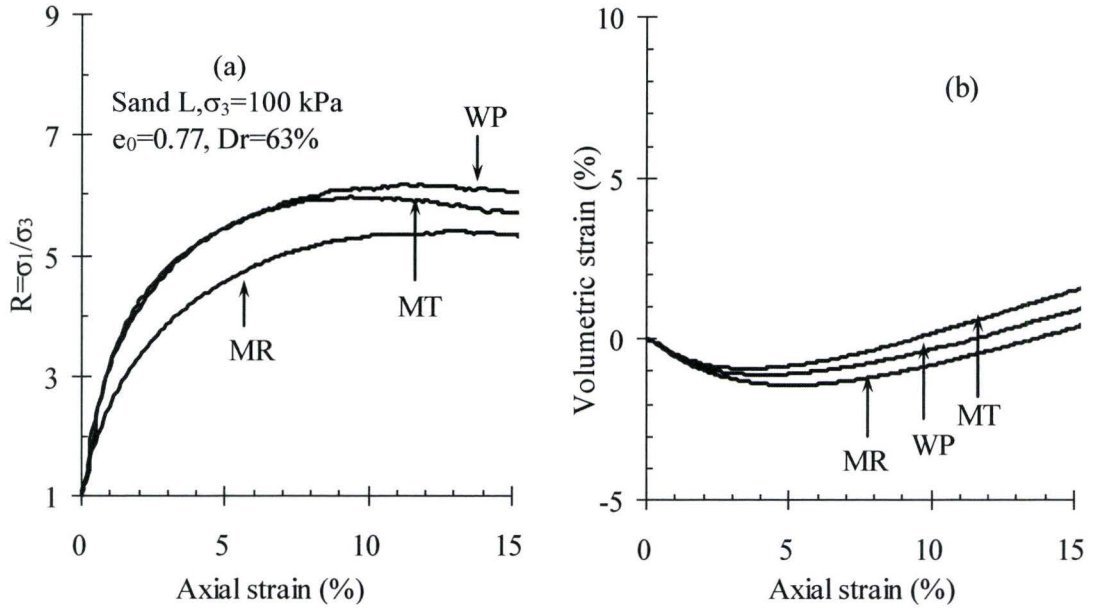


Figure 4-11: Influence of sample preparation on drained behaviour of Sand L sheared at $\sigma_3 = 100$ kPa : (a) Stress-strain response; (b) Volume change response

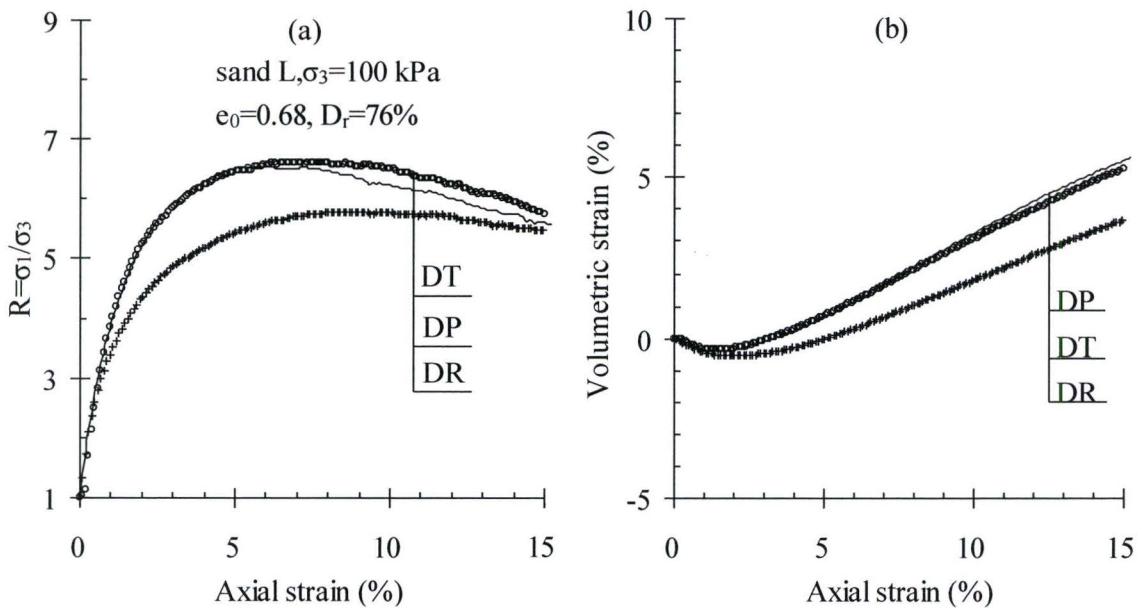


Figure 4-12: Influence of sample preparation on drained behaviour of Sand L sheared at $\sigma_3 = 100$ kPa : (a) Stress-strain response; (b) Volume change response

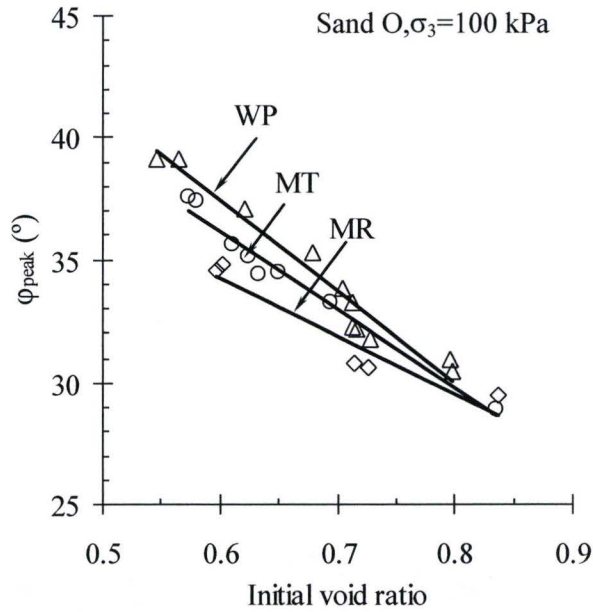


Figure 4-13: Influence of sample preparation on peak friction angle of Ottawa sand at $\sigma_3 = 100$ kPa

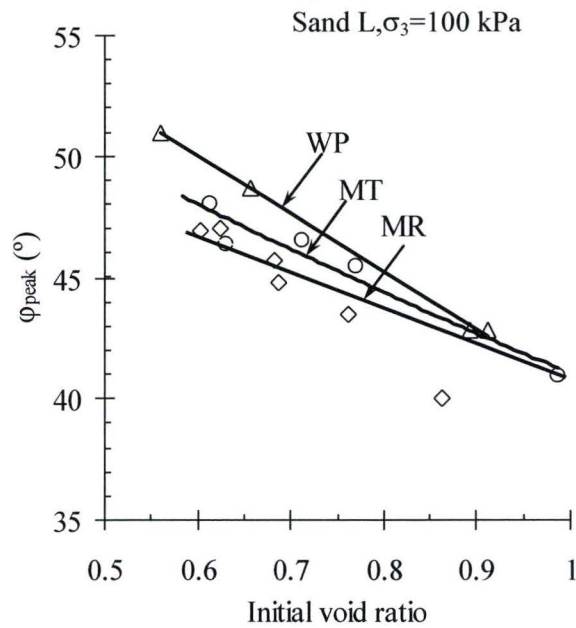


Figure 4-14: Influence of sample preparation on peak friction angle of Sand L at $\sigma_3 = 100$ kPa

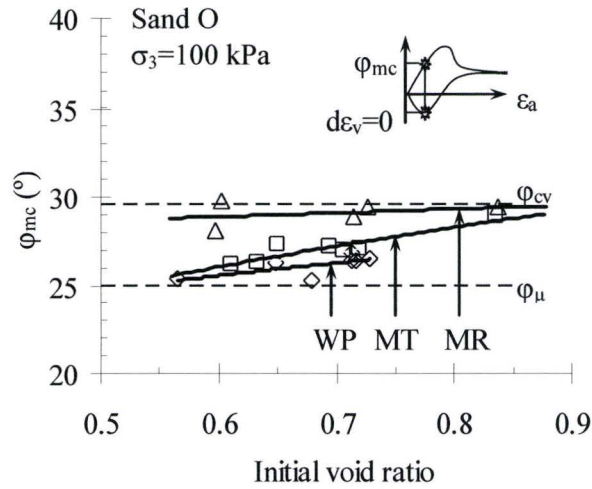


Figure 4-15: Influence of sample preparation method on characteristic friction angle of Sand O: $\sigma_3 = 100 \text{ kPa}$

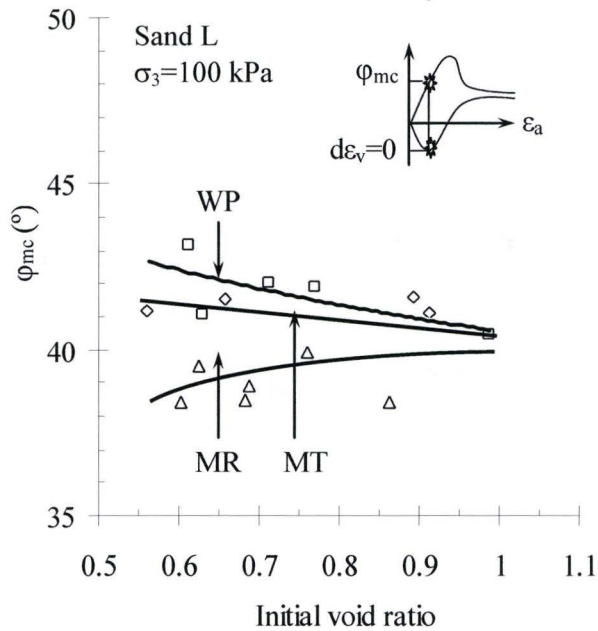


Figure 4-16: Influence of sample preparation method on characteristic friction angle of Sand L: $\sigma_3 = 100 \text{ kPa}$

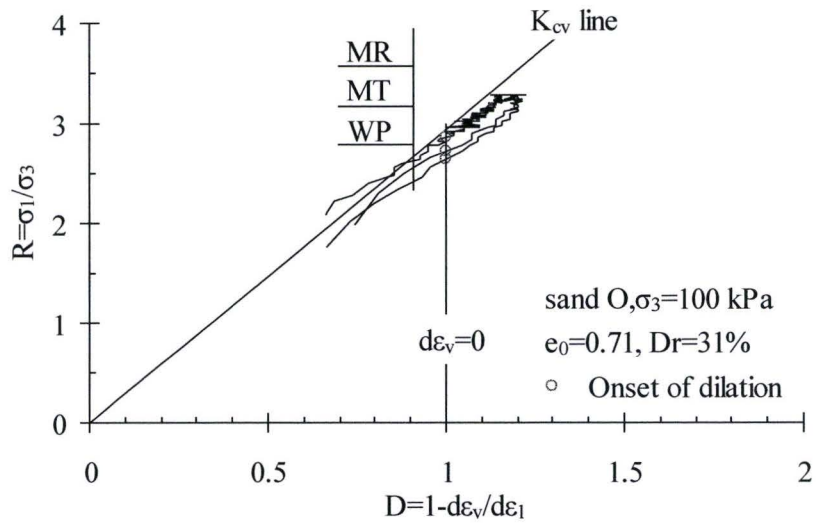


Figure 4-17: Stress-dilatancy plots of Ottawa sand at $\sigma_3 = 100$ kPa ($Dr = 31\%$)

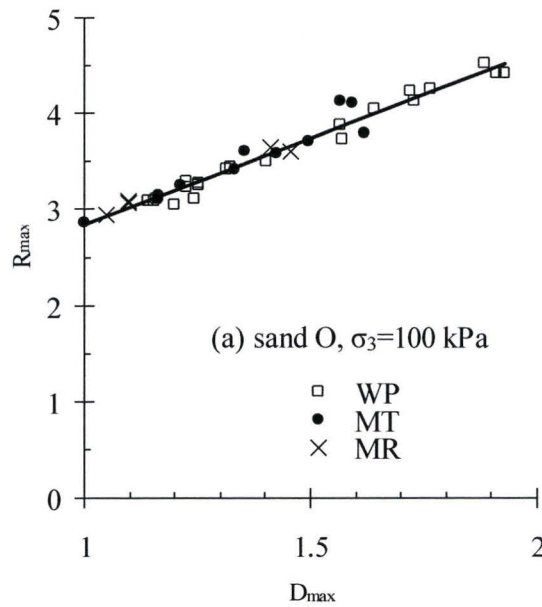
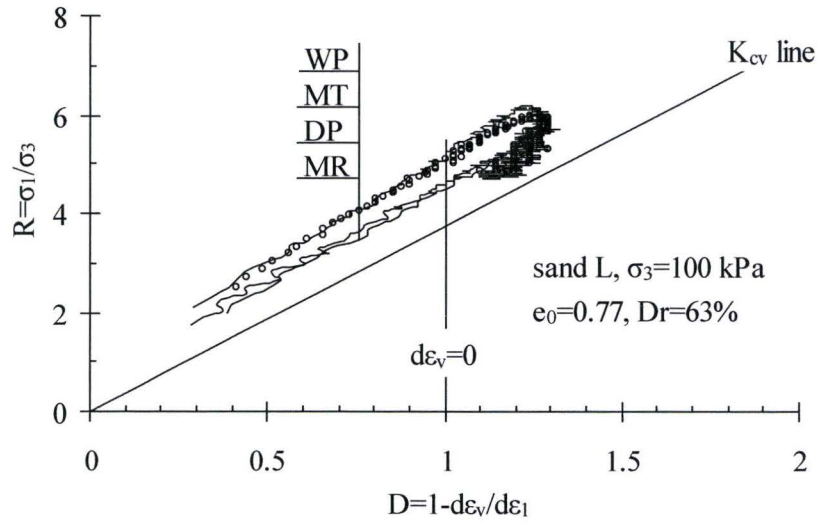
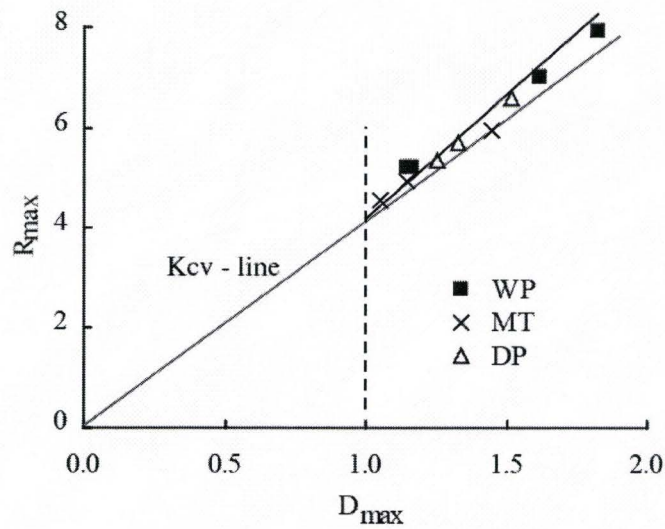


Figure 4-18: Influence of sample preparation methods on $D_{max}-R_{max}$ relationship of Ottawa sand at $\sigma_3 = 100$ kPa



(a) Stress-dilatancy plots



(b) D_{max} - R_{max} relation

Figure 4-19: Influence of sample preparation methods on dilatancy of Sand L at $\sigma_3 = 100$ kPa

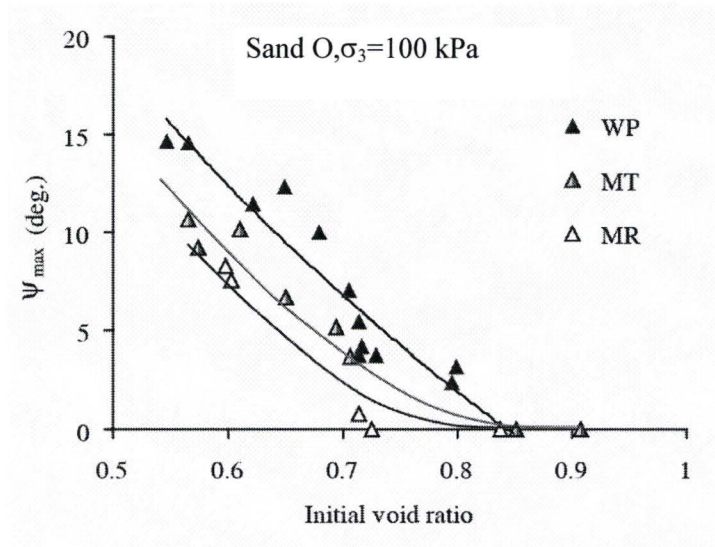


Figure 4-20: Influence of sample preparation methods on the maximum angle of dilation

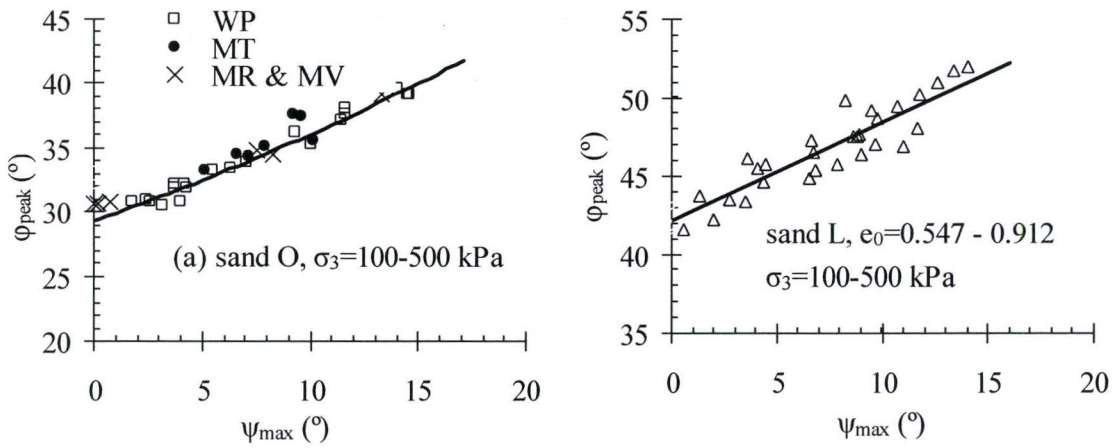


Figure 4-21: Dependency of peak friction angles on the maximum angle of dilation

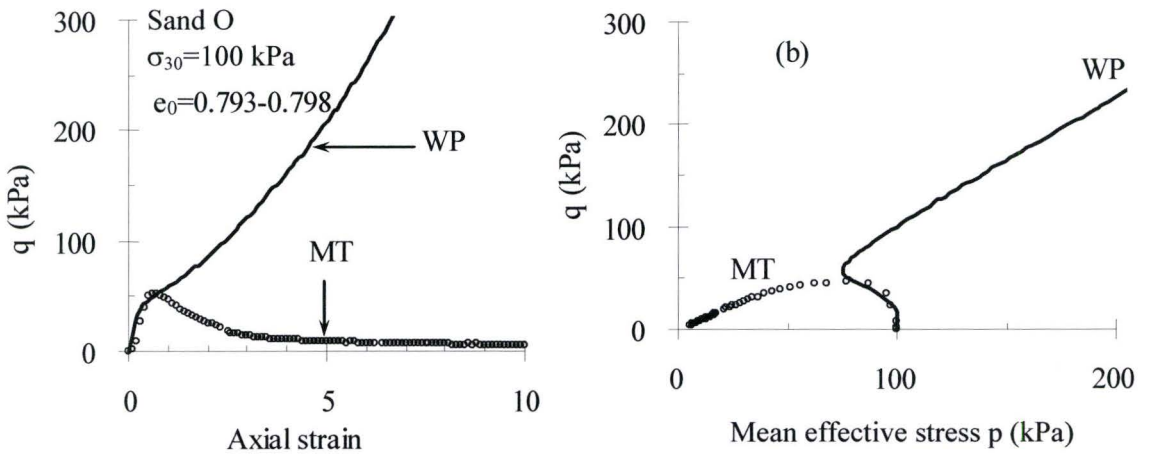


Figure 4-22: Influence of sample preparation method on undrained response of Ottawa sand

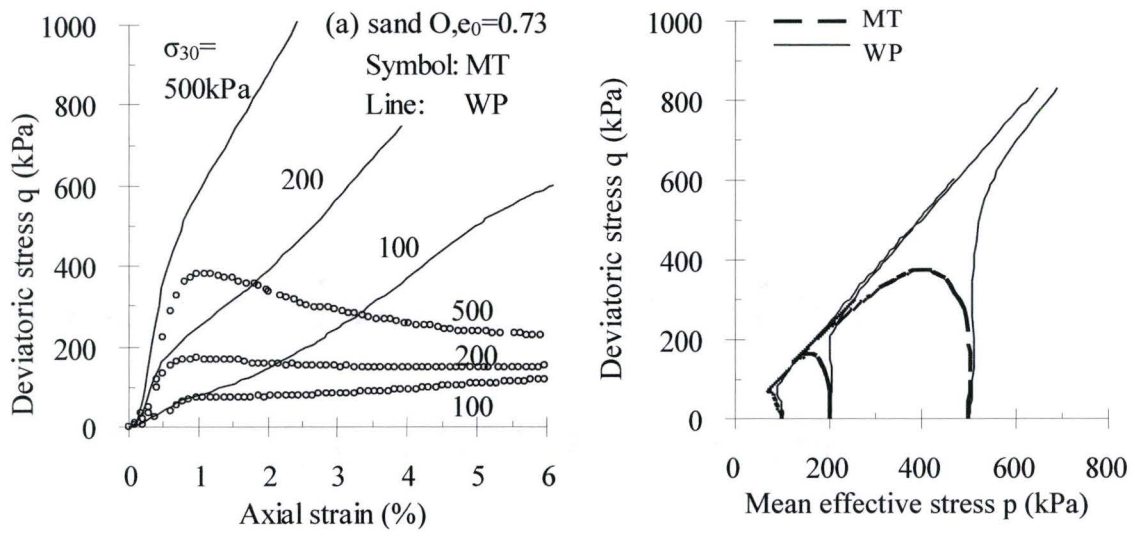


Figure 4-23: Influence of sample preparation method on undrained triaxial response of Ottawa sand ($e_0 = 0.73$): (a) stress-strain curve; (b) stress path

Chapter 5

Influence of interparticle locking on strength properties of granular material

5.1 Introduction

The shear strength of granular materials is affected by many factors, including interparticle friction and particle shape. In general, interparticle friction varies with particle texture (or roughness), which refers to the small asperities present on the surface of a particle. The particle shape, which dominates spatial arrangement of particles and interparticle locking, is characterized by angularity, *i.e.*, the sharpness or roundness of the corners at the boundary of a particle. In addition, the texture elements are usually smaller in size than the ones constituting particle angularity (Barret, 1980).

Traditionally, the shear strength of cohesionless soils is considered to be due to interparticle friction and dilation. For example, Taylor (1948) and Rowe (1962) recognized that the mobilized friction angle must take into account the sliding resistance at contacts as well as dilation that is related to particle rearrangement and overriding each other. Particle crushing, which increases in importance as confining pressure increases and void ratio decreases, also contributes to the shear strength of soil. According to Rowe (1963), the mobilized friction angle at the onset of dilation, φ_f , varies with particle packing arrangement and the number of sliding contacts. Depending on confining pressure and density, φ_f varies in the range of $\varphi_\mu \leq \varphi_f \leq \varphi_{cv}$ with φ_μ being the interparticle friction angle (or “true friction”) associated with the resistance to

interparticle sliding. Nevertheless, the ultimate failure and flow of granular materials are governed almost entirely by frictional factors. In other words, when the critical state is reached and shearing continues at constant volume with constant stress level, the shear strength is linked to stress level by a coefficient of friction.

Experimental evidence reveals that the critical state friction angle φ_{cv} cannot be uniquely determined from mineral-to-mineral friction angle φ_{μ} that largely depends on particle roughness, as well as on particle shape. For example, Chan and Page (1997) observed the value of φ_{cv} decreases with particle roundness. Granular materials comprising angular-shaped particles usually have higher macroscopic shear strength at a given confining pressure than those comprising round particles. For example, Koerner's work on single mineral soils shows that the angularity of particles may result in a variation in φ_{cv} as much as 8° (Koerner, 1970), because the angularity of particles may cause an interlocked fabric in addition to providing extra restraint to particle rotation and hence enhancing dilation.

It should be noted that the interlocking owing to particle angularity is different from the concept of locked sand introduced by Dusseault and Morgenstern (1979) and Barton (1993), who defined locked sand as the consequence of pressure solution at particle contacts over a long period of geological time, which cannot be created artificially in the laboratory. More details about the mechanical properties of locked sand can be found in Cuccovillo and Coop (1999), Cresswell and Barton (2003), and Cresswell and Powrie (2004).

This Chapter examines the effect of interparticle locking on the shear strength and stress-dilatancy characteristics of granular materials owing to angularity of particles. Based on the experimental results of Sand O and Sand L, an alternative concept of different components of the maximum friction angle is proposed. The results also cast some light on the stress-dilatancy formulation of granular materials of angular particles that may have strong interparticle locking. The discussion in the remainder of this Chapter will only be on specimens fabricated using the moist tamping (MT) method.

From the perspective of thermodynamics, breakage of particles and the breaking down of unbonded fabric structure are both associated with energy dissipation, and hence are considered as potential sources of shear strength even in the absence of dilation (Rowe, 1962). In the range of the stress levels ($\sigma_3 \leq 500$ kPa) used in this study, no noticeable particle breakage was observed; as confirmed by Figure 5.1 that compares the particle size distribution curves of the material before and after tests.

5.2 Experimental results and discussions

5.2.1 Stress-strain and volume change responses

Figure 5.2 shows typical experimental data for Sand O and Sand L of different initial void ratios, sheared at an effective cell pressure of 100 kPa. The stress-strain response is presented as the principal stress ratio $R = \sigma_1 / \sigma_3$ against the axial strain. For Sand O with the relative density $D_r = 74\%$, following the initial volumetric compression at small axial strain, significant dilation occurs when the mobilized stress ratio approaches its maximum value. After the peak on the $R - \varepsilon$ curve, both the stress ratio

and the rate of volume dilation decrease quickly with continuous shearing until the critical state is reached. The peak stress ratio and the amount of volume dilation, which both tend to reduce with the increase of void ratio, vanish completely for a loose specimen with the initial void ratio $e_0 = 0.77$.

For dense specimens of Sand L with $D_r = 84 - 86\%$, when the axial strain is less than 1%, the stress ratio R increases quickly and the corresponding volumetric strain is very small. Further shearing, however, induces significant dilation but a relatively small change in stress ratio R , resulting in a “plateau” on the $R - \varepsilon$ curves. When comparing the responses of Sand L with Sand O, one observes that Sand L requires larger axial strains to mobilize the maximum shear resistance than Sand O of the same relative density, but the post-peak strain softening is gentler than that of Sand O. As shown in Figure 5.2, possible critical states can be defined from the measured stress-strain responses for both materials.

The differences between the behaviour of Sand O and Sand L presented in Figure 5.2 may be attributed to the effect of particle shape. Since the angularity of particles causes more interparticle locking that restrains relative sliding and rotation between particles, larger shear stress is required for Sand L than for Sand O to break the interlocking owing to particle angularity before relative particle movement associated with dilation can take place, which also implies that the mobilized shear resistance is a combination of dilation and interparticle locking. It should be noted that dilation tends to degrade interparticle locking; the “plateau” on the $R - \varepsilon$ curves is the consequence of coupled effects of dilation and the degradation of interlocking. More specifically, the

interlocking is degraded with increasing axial strain, which reduces the shear resistance of the specimen. On the other hand, the mobilized dilation tends to enhance the strength of the material. As a result, the coupling of dilation and interlocking degradation may result in less change in shear resistance with continued shearing. It is interesting to note that these observations are similar to those for locked sand studied by Cresswell and Powrie (2004).

A closer examination of the experimental results in Figure 5.2 reveals that dilation of Ottawa sand (Sand O) starts at a stress ratio smaller than that at critical state, indicating that the mobilized friction angle at the onset of dilation, φ_f , is smaller than the critical state friction angle φ_{cv} . It should be noted that φ_f is similar to the characteristic friction angle φ_{mc} in Chapter 4. Figure 5.3(a), which summarizes the variation of φ_f and the peak friction angle, φ_{peak} , against the initial void ratio e_0 for Sand O from all tests, shows that φ_f gradually approaches φ_{cv} as e_0 increases. This observation is similar to typical test results of unstructured sand (e.g., Rowe 1962). For Sand L, however, the experimental data show that the onset of dilation occurs at mobilized friction angles higher than φ_{cv} (as summarized in Figure 5.3b). Moreover, the difference between φ_f and φ_{cv} increases with a decrease in the void ratio of the material. A comparison of Figure 5.3 (a) with (b) implies that the higher φ_f of Sand L than φ_{cv} likely reflects the influence of interparticle locking owing to particle angularity. It should be mentioned that the friction angle φ_f at the onset of dilation is calculated from the $R - \varepsilon$ curves at

$d\varepsilon_v = 0$, which corresponds to the point of maximum volume compaction or zero angle of dilation φ_f . For loose samples that only have volume compaction, φ_f is determined from the stress–dilatancy plot when the dilatancy factor approaches zero (see the following section for details).

5.2.2 Limiting envelopes in p - q space

The influence of stress level on the friction angle at the onset of dilation can be more clearly displayed in the classical p - q space with p being the mean effective stress and q the deviatoric stress. Figure 5.4 shows the limiting envelopes corresponding to the state of onset of dilation, the peak strength state and the possible critical state (CSL) in the p - q space for both materials. The envelopes for the peak and the onset of dilation are both curved upward, while the CSL can be well represented as a straight line. For Sand L, the limiting envelope at the onset of dilation is above the CSL, which is attributed to the effect of interparticle locking as discussed in previous sections. On the contrary, the limiting envelope at onset of dilation of Sand O is below the corresponding CSL, which is consistent with the results shown in Figure 5.3.

The mobilisation of stress ratios considerably in excess of critical has been reported by Cresswell *et al.* (2004) for a purely locked sand with virtually no cement for both intact samples and reconstituted samples. The tests reported herein demonstrate that the mobilisation of near-peak stress ratios well in excess of critical can occur as a result of fabric structure alone.

5.2.3 Stress-dilatancy plots

The evolution of stress-dilatancy with deformation history is plotted in Figure 5.5 for both materials under an effective confining stress of $\sigma_3 = 100$ kPa. The stress-dilatancy curves for Sand O plotted in Figure 5.5 (a) show a consistent increase in the stress ratio $R = \sigma_1 / \sigma_3$ with dilatancy factor D , which is defined as $D = 1 - d\varepsilon_v / d\varepsilon_1$, prior to the maximum dilation being mobilized. During the stage of post-peak deformation, both R and D decrease until the critical state is reached. All $R - D$ plots are located within an upper and lower bound corresponding to the K_{cv} - and K_{μ} -line, respectively, in which $K_{cv} = \tan^2(\pi/4 + \varphi_{cv}/2)$ and $K_{\mu} = \tan^2(\pi/4 + \varphi_{\mu}/2)$. The R/D ratio, which increases gradually from K_{μ} to K_{cv} with deformation, reaches its maximum at critical state. These observations are generally in agreement with previous experimental studies in the literature; *see, e.g.*, Rowe (1962), Lee and Seed (1967), King and Dickin (1970) among others. It should be noted that the interparticle friction angle $\varphi_{\mu} = 25^\circ$ for Sand O is back-calculated from the dilatancy plot of very dense specimens, which forms the lower bound of all dilatancy curves at different initial void ratios. The value of the back-calculated φ_{μ} is very close to the measured value of 24° for Ottawa sand (Lee and Seed 1967) and the representative value of 26° for quartz sand found in nature (Mitchell 1976).

Similar to Sand O, the measured stress ratio of Sand L also increases with dilatancy factor D until the maximum stress ratio is mobilized, as shown in Figure 5.5 (b). However, the stress-dilatancy plots are all above the K_{cv} -line, indicating $R/D \geq K_{cv}$. Moreover, the R/D ratio tends to decrease during the course of shearing until its

minimum value is reached at the critical state. As discussed in previous sections, the decrease in R/D ratio reflects progressive destructuring of interparticle locking owing to particle angularity. Given that the dilatancy plots of Figure 5.5 (a) are typical for “classical” sand with rounded to surrounded particles, one may argue that the difference in the dilatancy plots presented in Figure 5.5 reflects the influence of particle angularity. More specifically, at a given rate of dilatancy, large particle angularity of Sand L substantially increases the mobilized stress ratio with $R/D \geq K_{cv}$, compared with $K_{\mu} \leq R/D \leq K_{cv}$ for Sand O. In other words, in addition to dilation, particle angularity may increase the shear strength of granular materials significantly, which is consistent with the findings in the literature (*e.g.*, Koerner 1970, and Sukumaran and Ashmawy 2001).

Figure 5.6 presents the stress-dilatancy plots for specimens at given initial void ratios under different confining pressures. Even though an increase in confining pressure suppresses dilation for both materials, the dilatancy characteristics of Sand L, however, are more sensitive to the variation of the confining pressure than those of Sand O. This is because the rotation of angular particles in Sand L can be substantially restrained at increased confining pressure, which in turn causes appreciable reduction in the maximum dilatancy factor D_{max} , as can be seen from Figure 5.6 (b). It is also observed from Figure 5.5(b) and Figure 5.6(b) that the dilatancy curves for Sand L of different void ratios under various confining pressures stay above the K_{cv} -line even at peak stress ratios, which suggests that the interlocking of angular particles of Sand L still largely exists at the peak stress ratio. R/D approaches K_{cv} when the critical state is reached, which is a sign that

interlocking mostly disappears only at the critical state. This observation is similar to that noted by Cresswell and Powrie (2004) for undisturbed sand with locked fabric (i.e., locked sand).

5.2.4 Contributions to shear strength of granular materials

According to Rowe (1962), major contributions to shear strength of granular soils come from interparticle friction, particle crushing, particle rearrangement and dilation. Figure 5.7 shows the general relationships among the strength contributing factors and void ratio proposed by Rowe, who suggested that the friction angle at the onset of dilation, ϕ_f , is generally influenced by particle packing arrangement and the number of sliding contacts. As shown in Figure 5.3a, the experimental data for Ottawa sand composed of particles of low angularity are generally in agreement with Rowe's framework. The triaxial compression test results of Sand L shown in Figure 5.3b, nevertheless, clearly show that Rowe's suggestions may not be applicable to granular materials comprising particles of high angularity, which forms locked fabric and yields additional shear strength. The experimental data shown in Figures 4.15 and 4.16 for specimens fabricated using other methods also support these observations.

Based on the experimental data presented in Figure 5.3 to Figure 5.6, the contributions to shear strength of Sand L from different factors are illustrated in Figure 5.8. The mobilized shear strength above the critical value is the result of both dilation and interparticle locking, which are influenced by confining pressure and density or void ratio. By following the concept proposed by Rowe (1962), an alternative model is proposed as shown in Figure 5.8(a) to accommodate the contribution of interparticle

locking. According to this new model, the friction angle at the start of dilation φ_f , may be larger than φ_{cv} , depending on interparticle locking. Figure 5.8(b) alternatively illustrates the variation of different components of shear strength against mean effective stress.

According to Figure 5.8, the mobilized friction angle at the onset of dilation, φ_f , is affected by interparticle friction, interparticle locking, particle rearrangement and potential particle crushing. φ_f increases as the particles become more angular and as density or interparticle friction increases. An increase in confinement generally reduces the influence of interparticle locking and dilation, while the contributions from particle rearrangement and particle crushing are enhanced. All these are supported by the experimental data of Sand L.

It should be noted that the influence of particle crushing on the strength of granular soils with angular particles might be more noticeable than that is observed for sand of rounded / subrounded particles. The effect of particle crushing, however, is considered to be negligible for the range of confining pressures used in this study.

The results of triaxial tests for both Ottawa standard sand (Sand O) and crushed limestone (Sand L) have identified limiting stress ratio (q/p) envelopes at the onset of dilation corresponding to friction angle φ_f . The experimental results of Sand O confirm Rowe's finding of $\varphi_\mu \leq \varphi_f \leq \varphi_{cv}$. The values of φ_f for Sand L, nevertheless, are consistently larger than φ_{cv} and gradually approach φ_{cv} with the increase of the initial void ratio. As a result, one may conclude that, for granular materials with angular particles that may have significant interparticle locking owing to particle angularity, both

dilation and interparticle locking are important in the maintenance of stress ratios in excess of critical. Once the interlocking structure starts to break down, it is also a mechanism by which the material becomes destructured or weakened to allow shearing. The dilatancy plots for Sand L presented in both Figure 5.5(b) and Figure 5.6(b) imply that the effect of interparticle locking still exists at the peak stress ratio but largely vanishes at the critical state, particularly for dense samples subjected low confining pressures (*e.g.*, $e_0 = 0.71$ and $\sigma_3 = 100$ kPa). The results suggest that, in terms of dissipated energy, the dilatancy characteristics of granular materials with strong interparticle locking associated with particle angularity can be described qualitatively by introducing energy dissipation dedicated to disrupting the structure of the material, as proposed by Cuccovillo and Coop (1999). In other words, the total energy dissipation $d\Phi$ consists of dissipation partly related to interparticle friction $d\Phi_{fric}$ and partly to disrupting interparticle locking $d\Phi_{fab}$; *i.e.*,

$$d\Phi = d\Phi_{fric} + d\Phi_{fab} \quad (5.1)$$

In next section, the concept of energy dissipation associated with interparticle locking will be implemented to modify Rowe's stress-dilatancy model so that the effect of interparticle locking is taken into account.

5.3 Energy dissipation associated with interlocking degradation

5.3.1 Theoretical background

It is known that Rowe's stress-dilatancy model was developed based on the assumption of a purely frictional energy dissipation mechanism and the hypothesis of

minimum energy ratio. By considering the energy consumption Φ_{bk} due to *particle breakage* at the contact between sand particles such that the total energy dissipation is $\Phi = \Phi_{fric} + \Phi_{bk}$, Ueng and Chen (2000) modified Rowe's dilatancy formulation according to

$$\frac{\sigma_1}{\sigma_3} = \left(1 - \frac{d\varepsilon_v}{d\varepsilon_1}\right) \tan^2\left(45^\circ + \frac{\varphi_f}{2}\right) + \frac{d\Phi_{bk}/d\varepsilon_1}{\sigma_3 \left[1 - \tan \varphi_f \tan(45^\circ - \varphi_f/2)\right]} \quad (5.2)$$

or

$$\frac{\sigma_1}{\sigma_3} = \left(1 - \frac{d\varepsilon_v}{d\varepsilon_1}\right) \tan^2\left(45^\circ + \frac{\varphi_f}{2}\right) + \frac{1}{\sigma_3} \frac{d\Phi_{bk}}{d\varepsilon_1} (1 - \sin \varphi_f) \quad (5.3)$$

When replacing the energy dissipation Φ_{bk} due to particle breakage using Φ_{fab} which is due to overcoming interparticle locking, one obtains the stress-dilatancy formulation with interparticle locking being taken into account:

$$\frac{\sigma_1}{\sigma_3} = \left(1 - \frac{d\varepsilon_v}{d\varepsilon_1}\right) \tan^2\left(45^\circ + \frac{\varphi_f}{2}\right) + \frac{1}{\sigma_3} \frac{d\Phi_{fab}}{d\varepsilon_1} (1 - \sin \varphi_f) \quad (5.4)$$

Rowe's formulation is recovered when $d\Phi_{fab} = 0$.

Recalling that $D = 1 - d\varepsilon_v/d\varepsilon_1$ and $K = \tan^2(45^\circ + \varphi_f/2)$, the rate of energy dissipation due to interlocking degradation is given as

$$\dot{\Phi}_{fab} = \frac{d\Phi_{fab}}{d\varepsilon_1} = \frac{R - KD}{1 - \sin \varphi_f} \sigma_3 \quad (5.5)$$

This relation can be used to estimate the energy consumption associated with interlocking.

In order to quantify the energy dissipation term due to interlocking degradation deduced from Eq. (5.5), φ_f must be determined first. As discussed in Chapter 4, the value of φ_f ranges from φ_μ to φ_{cv} . Direct measurement of φ_μ , however, was not practical for this study. An alternative approach estimated the value of φ_μ from the empirical relationship shown Figure 5.9, which is based on available data in the literature presented in Table 5.1. Given the measured critical friction angle of Sand L in a range of 35.5° to 36.5° with the average being 36° , φ_μ was estimated as 31° . It can be shown that

$\dot{\Phi}_{fab}$ varies in the range of $\dot{\Phi}_L \leq \dot{\Phi}_{fab} \leq \dot{\Phi}_U$ with

$$\dot{\Phi}_L = \sigma_3 \frac{R - K_{cv} D}{1 - \sin \varphi_\mu}, \quad \dot{\Phi}_U = \sigma_3 \frac{R - K_\mu D}{1 - \sin \varphi_\mu} \quad (5.6)$$

5.3.2 Energy dissipation due to interlocking: Experimental data

5.3.2.1 Sand O (Ottawa sand)

Figure 5.10 shows $\dot{\Phi}_U$, which is the upper limit of $\dot{\Phi}_{fab}$, of dense Ottawa sand tested at $\sigma_3 = 100, 200$ and 500 kPa , respectively. Given the scattering of the data, the value of $\dot{\Phi}_U$ for dense specimens of Sand O under various confining pressures can be considered as approximately zero, implying that the effect of interlocking is negligible.

5.3.2.2 Sand L

Figure 5.11 presents the variation of $\dot{\Phi}_U$ against axial strains for Sand L specimens fabricated using the moist tamping (MT) method, with e_0 of the specimens being 0.86 and 0.71, respectively. For the effective confining pressure varying from 100

to 500 kPa, $\dot{\Phi}_U$ is quickly mobilized to its maximum values with the increase of axial strain at small strains, then it stays as almost constant for each individual confining stresses. The maximum values of $\dot{\Phi}_U$, however, increase with σ_3 . Figure 5.12 presents the value of $\dot{\Phi}_U$ against σ_3 at the onset of dilation and the peak stress states, yielding a linear relation between $\dot{\Phi}_U$ and σ_3 .

In addition to the effective confining pressure, the initial void ratio of a specimen has significant influence on the $\dot{\Phi}_{fab}$; as can be observed from Figure 5.12. Generally, more energy is consumed to overcome interlocking for a dense specimen. The results presented in Figure 5.13 and Figure 5.14 for Sand L specimens fabricated using DP and WP methods and sheared under the effective confining pressure of $\sigma_3=100$ kPa further confirmed this conclusion. An analysis of the experimental data reveals the following relation

$$\dot{\Phi}_U = ap \exp(-be_0) \quad (5.7)$$

with a and b being experimental constants.

The sample preparation methods, however, tend to affect the energy dissipation for specimens of the same void ratio subjected to the same confining pressure, as shown in Figure 5.15. One observes that specimens prepared by pluviation or tamping tend to have stronger interlocking structure than those prepared via rodding.

5.4 Summary

Based on the experimental work in this chapter, the following conclusions can be made:

- The CTC test results for both Ottawa sand (Sand O) and crushed limestone (Sand L) have identified three distinct limiting stress ratio ($\eta = q / p$) envelopes corresponding to different friction angles; *i.e.*, (1) the start of dilation, φ_f ; (2) the peak stress state, φ_{peak} ; (3) the critical state, φ_{cv} . For dense Sand L, the values of φ_f are considerably larger than φ_{cv} , which is identified as the effect of interparticle locking.
- For granular materials with angular particles and rough surface texture, in addition to interparticle friction and dilatancy, interparticle locking may contribute substantially to the shear resistance of sand.
- For Sand O consisting of rounded particles with weak interparticle locking, the stress-dilatancy plots are bounded between the K_μ - and K_{cv} -lines. For Sand L with strong interlocking due to particle angularity, the measured stress-dilatancy curves are above the K_{cv} -line. At low confining pressures, Sand L exhibits a high peak friction angle associated with greater dilatancy. Under elevated confining pressures, the potential of dilatancy is restrained, but interlocking still exists at least in the range of stresses investigated in this study. The rate of energy dissipation varies almost linearly with confining pressures.
- A theoretical framework was proposed to quantify the energy dissipation associated with overcoming interlocking. Within this framework, Rowe's dilatancy formulation

is modified by introducing a term related to the rate of energy dissipation, which has been determined from experimental data for Sand L under different conditions.

Table 5.1: Reference data for φ_μ and φ_{cv} in literature

φ_μ (Degree)	φ_{cv} (Degree)	Type of material	Reference
26.0	32.0	Mersey river quartz sand	Rowe (1962)
17.0	24.0	Glass ballotini	Rowe (1962)
27.0	32.0	Quartz sand	Rowe (1965)
23.0	29.0	Zircon	Rowe (1969)
36.0	41.0	Feldspar	Lee (1966)
27.4	32.6	Ham River sand	Bishop and Green (1965)
38.0	42.0	Quartz sand	Bromwell (1966)
28.0	36.0	Quartz sand	Bromwell (1966)
27.0	33.0	Brasted River sand	Cornforth (1964)
37.6	41.5	Limestone sand	Billam (1971)
31.2	36.8	Crushed anthracite	Billam (1971)
29.0	34.0	Karlsruhe sand	Hettler and Vardoulakis (1984)
24.0	33.3	Sacramento river sand	Lee and Seed (1967)
24.0	30.0	Ottawa sand	Lee and Seed (1967)
39.0	43.0	Crushed glass	Parikh (1967)
28.0	35.0	Quartz sand	Parikh (1967)
20.0	27.0	Bronze spheres	Parikh (1967)
29.0	34.4	Hostun sand	Schanz and Vermeer(1996)
28.5	34.0	Quartz sand, angular	Hanna (2001)
27.0	33.5	Quartz sand, angular	Hanna (2001)

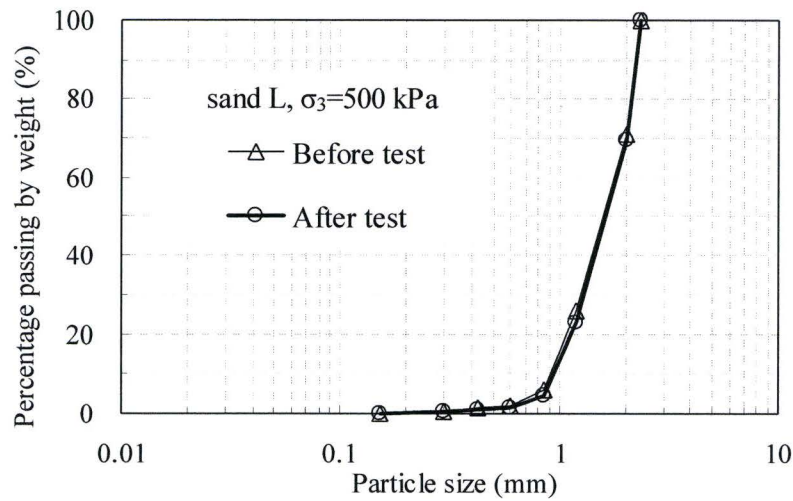


Figure 5.1: Pre- and post- test check on particle size distribution sheared at $\sigma_3=500$ kPa

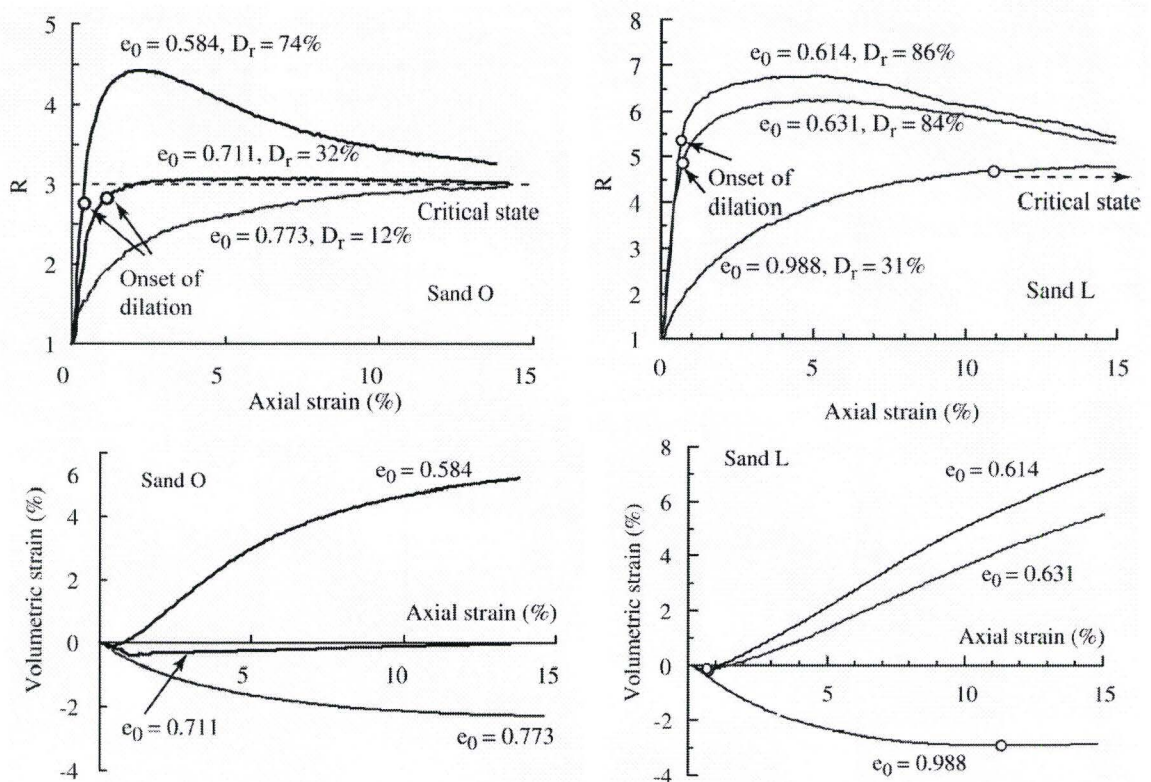


Figure 5.2: Typical data of stress ratio $R = \sigma_1 / \sigma_3$ and volumetric strain plotted against axial strain for Sand O and Sand L at $\sigma_3 = 100$ kPa

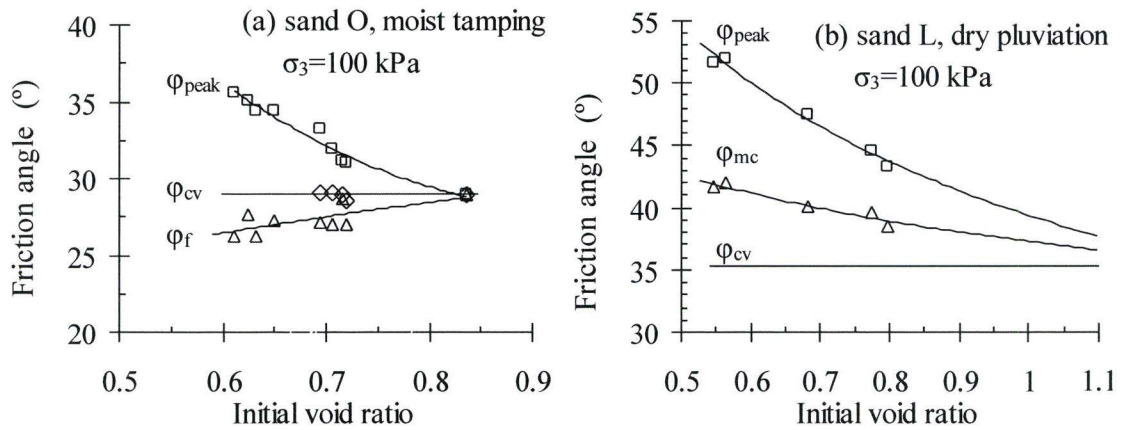


Figure 5.3: Measured contribution to shear strength of Sand O and Sand L of different void ratios at $\sigma_3 = 100 \text{ kPa}$

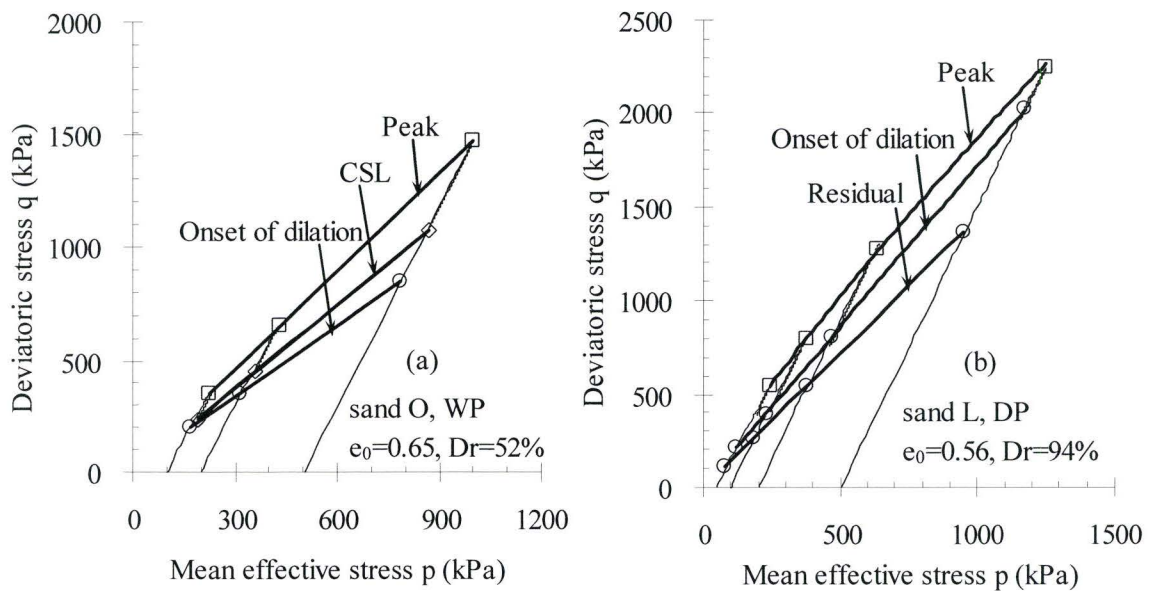


Figure 5.4: Limiting envelopes in p - q space: (a) Sand O, and (b) Sand L

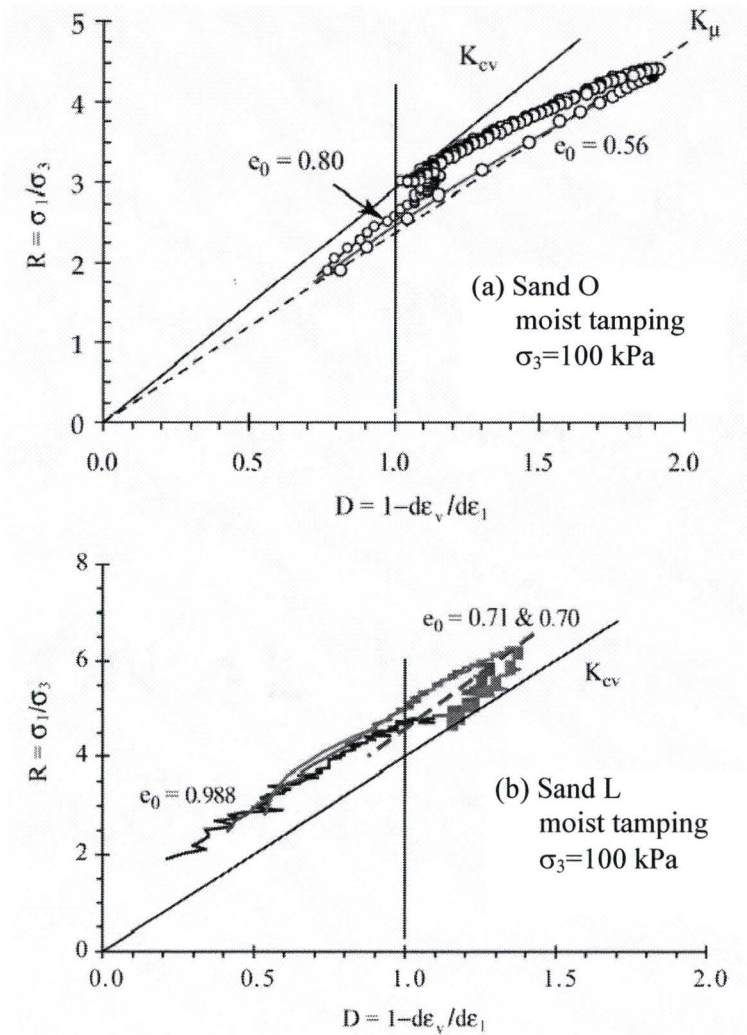


Figure 5.5: Stress-dilatancy plots at $\sigma_3=100$ kPa

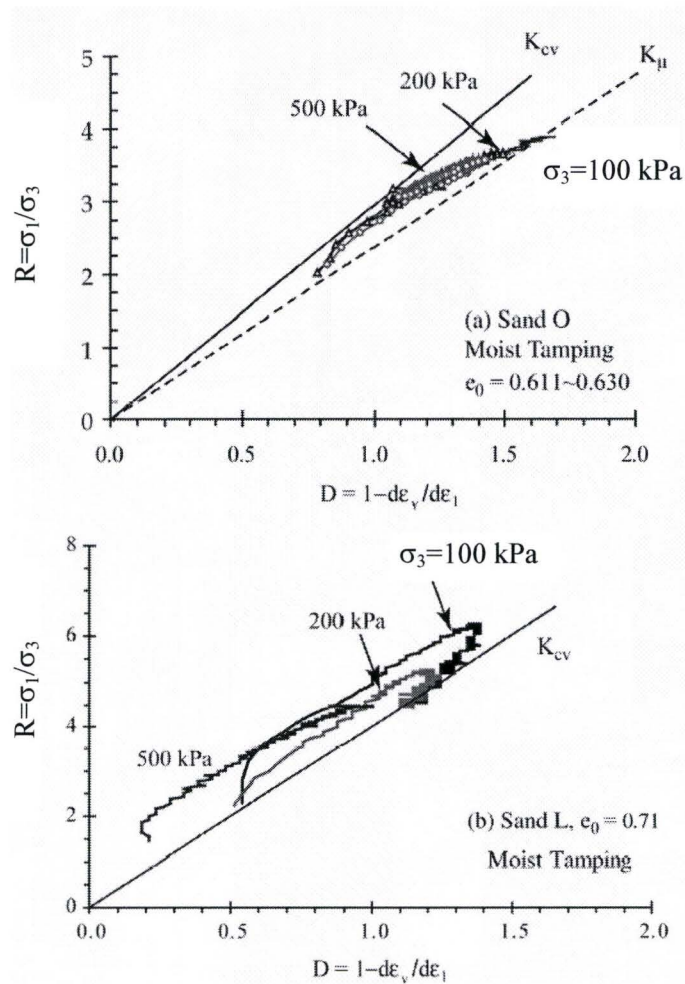


Figure 5.6: Influence of stress level on stress-dilatancy plots: (a) Sand O, $D_r = 62\%$; and (b) Sand L, $D_r = 72\%$

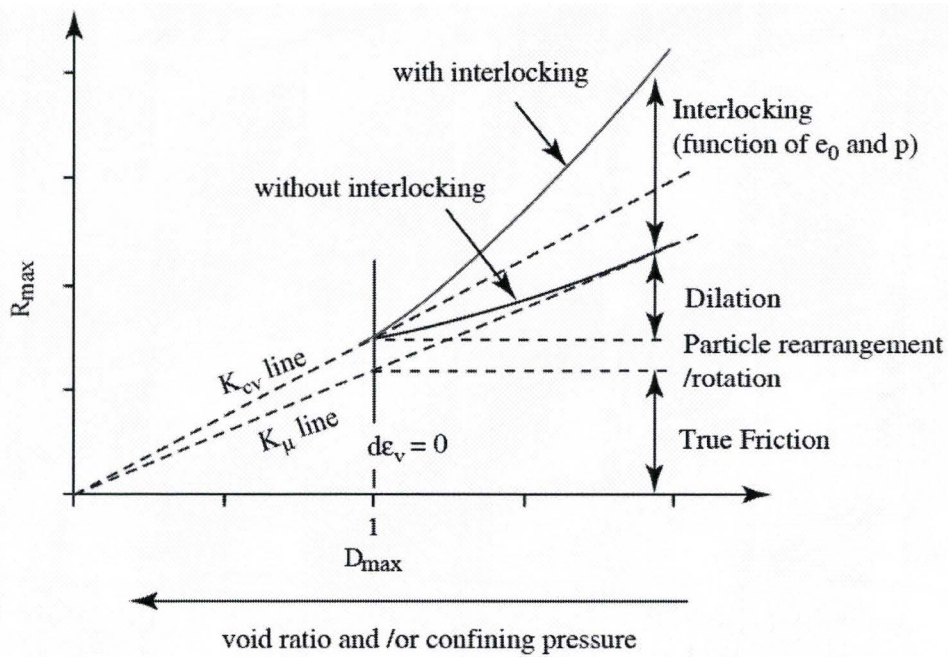


Figure 5.7: Influence of interparticle locking on shear strength of granular materials

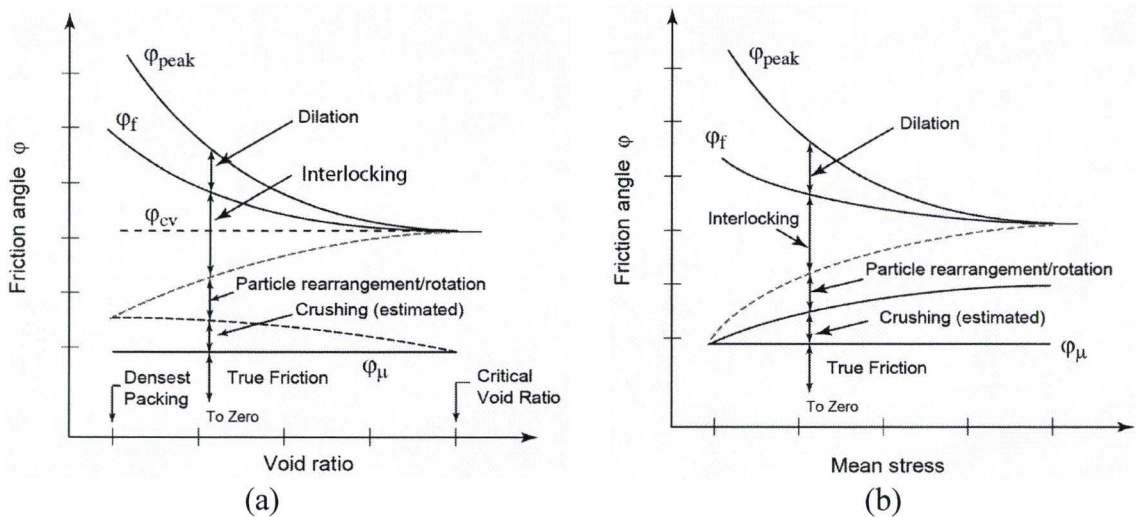


Figure 5.8: An alternative conceptual model for shear strength of granular materials

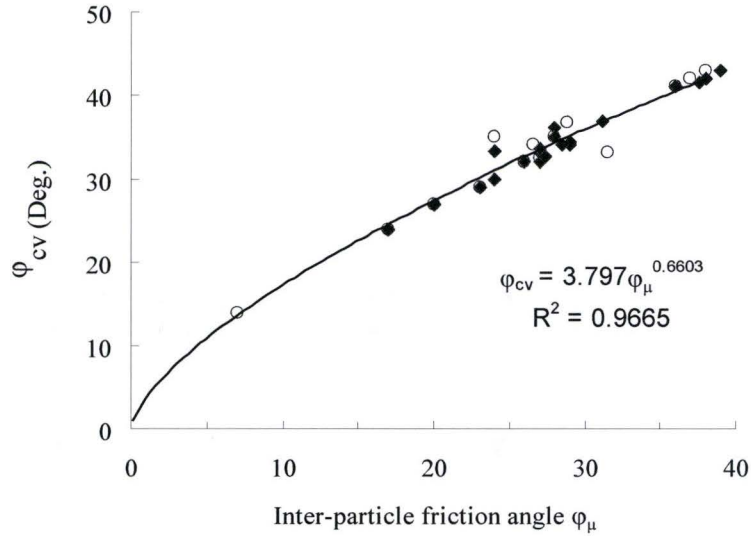


Figure 5.9: Empirical relationship between φ_{μ} and φ_{cv} based on data in the literature

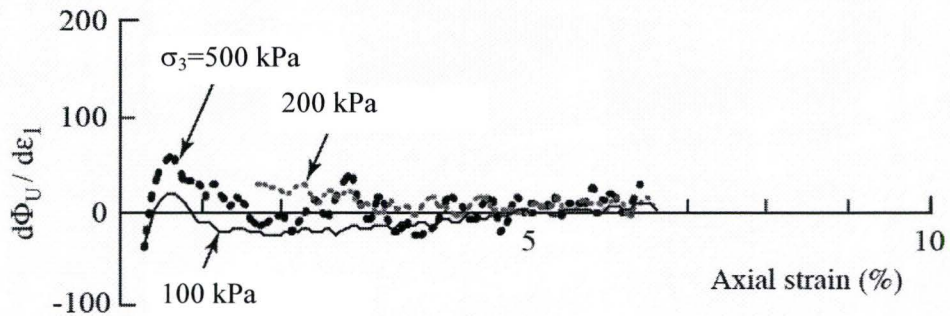


Figure 5.10: Variation of Φ_U of Sand O during triaxial compression at different confining pressures ($e_0 = 0.56$)

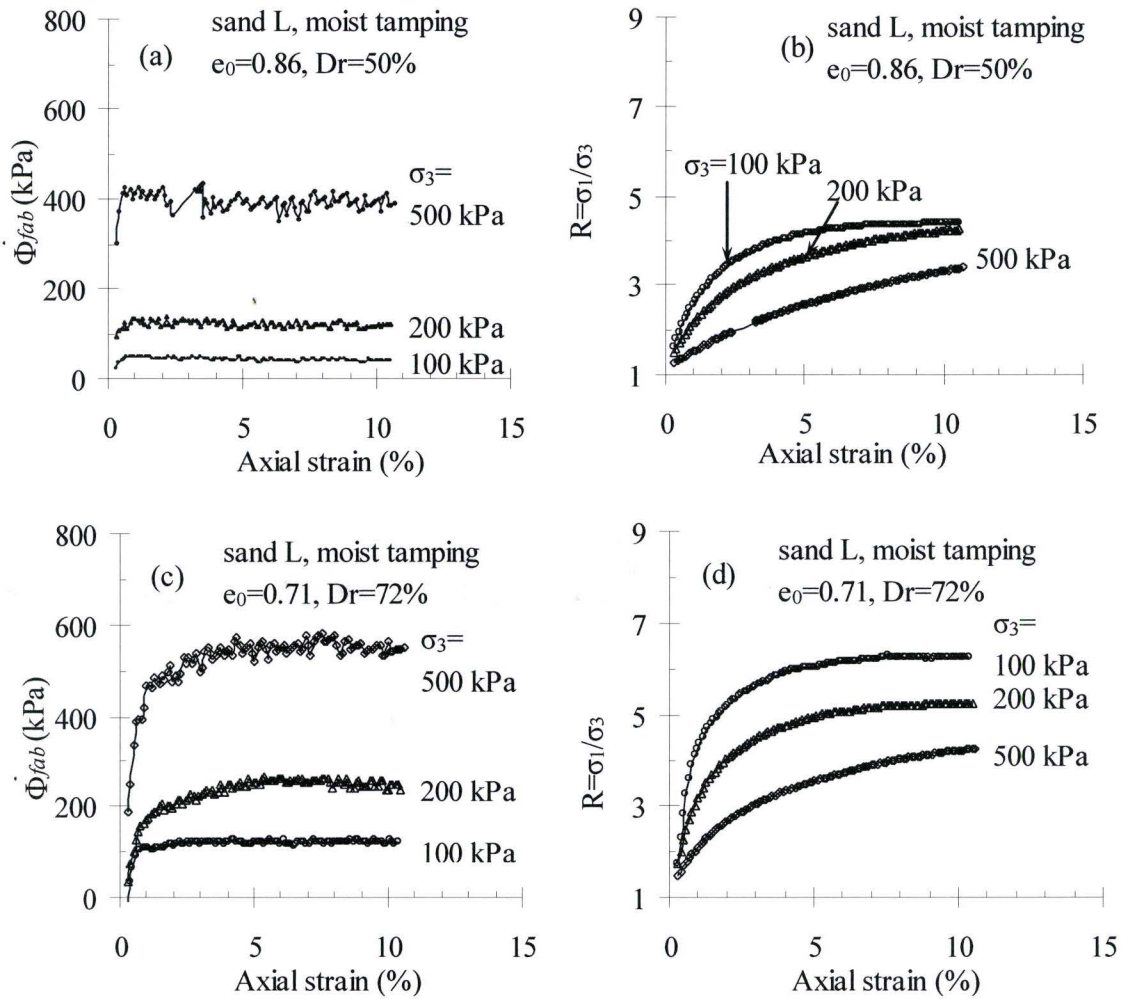


Figure 5.11: Rate of energy dissipation due to fabric degradation of Sand L at different effective confining pressures

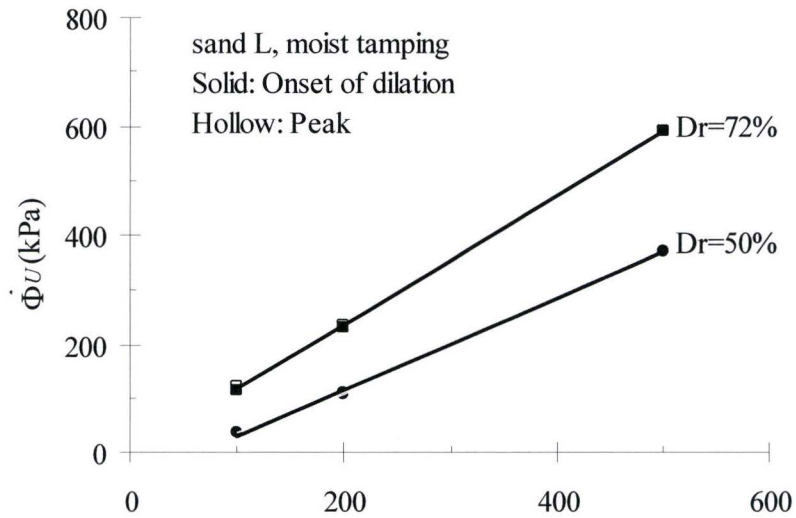


Figure 5.12: Rate of energy dissipation at peak of Sand L sheared at different effective confining pressures $\dot{\Phi}_U$ (kPa)

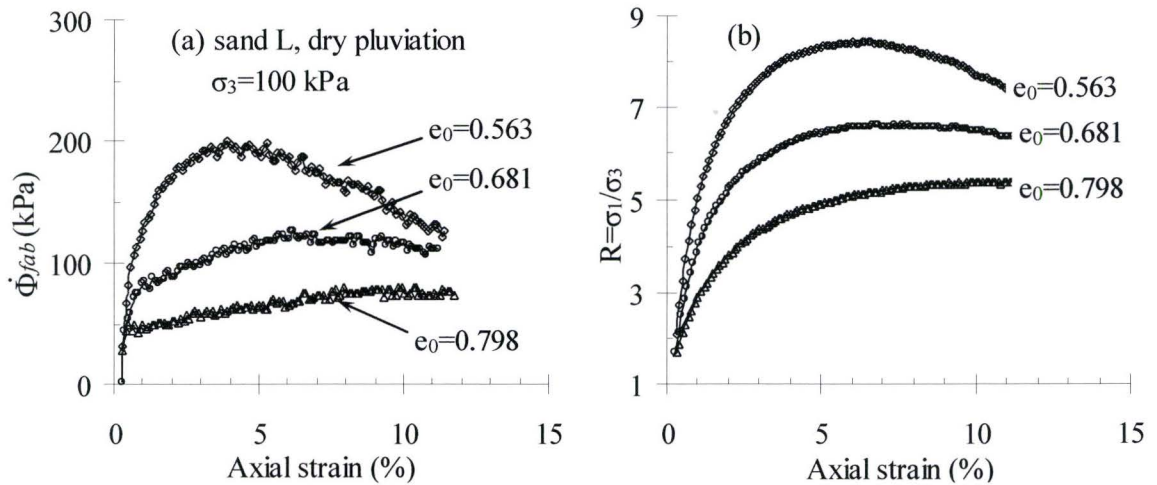


Figure 5.13: Rate of energy dissipation due to fabric degradation of Sand L specimens fabricated by dry pluviation at $\sigma_3=100$ kPa

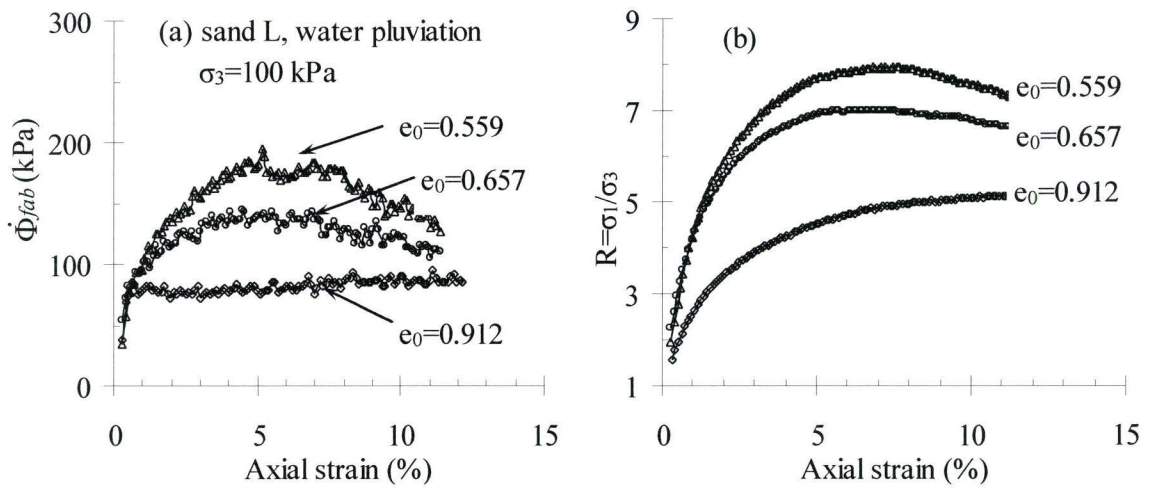


Figure 5.14: Rate of energy dissipation due to fabric degradation of Sand L specimens fabricated by water pluviation at $\sigma_3=100$ kPa

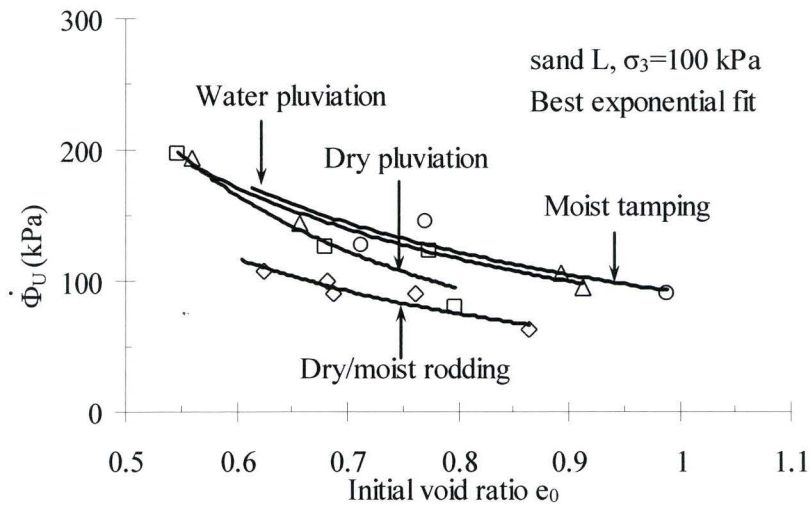


Figure 5.15: The effect of sample preparation methods on energy dissipation due to interlocking

Chapter 6

Strain softening and material instability along proportional strain paths

6.1 Introduction

In general, material stability is ensured if a small stress increment yields a small strain increment. Several modes of instability can be obtained from laboratory and field observations, for example, in conventional drained triaxial tests on dense sand at constant confining stress, the state corresponding to the peak deviator stress signifies the onset of instability. This type of instability, which is accompanied by the development of shear bands at failure has been studied by numerous investigators (Lade 1992, Nova, 1994, and Oda and Kazama, 1998). Instability may also occur during undrained loading of loose sand prior to the attainment of the state of maximum drained obliquity. This type of instability has been referred to as pre-failure instability (Lade and Pradel 1990, Chu *et al.* 1993, and Sasitharan *et al.* 1993).

Under non-undrained conditions, Chu (1992, 1993) and Vaid and Eliadorani (1998) showed that the mechanisms for pre-failure strain softening and instability are the same, except that strain softening occurs in a strain-controlled mode, and instability occurs in a stress controlled mode. On the other hand, hinging on Hill's stability criterion, Darve *et al.* (1995) showed numerically that instability might occur before or after strain softening, which was verified by Lancelot *et al.* (2004) in a series of tests on loose

Hostun RF sand along proportional strain paths at low confining pressures (20 to 100 kPa).

Several definitions of strain softening within the context of plasticity theory have been proposed in the past. Strain softening is usually associated with $d^2W = d\sigma_{ij}d\varepsilon_{ij}^p < 0$ as defined by Valanis (1985), or when the shear resistance of a soil element decreases with further straining after the peak value (i.e., $dq < 0$) (Prevost 1975, Read 1984, Chu *et al.* 1992). Pre-failure strain softening is sometimes referred to as strain softening that occurs before the effective stress path reaches the failure line (Chu and Leong 2001).

This chapter presents a series of tests on Ottawa sand sheared along proportional strain paths with $d\varepsilon_v/d\gamma$ being constant. Specimens of various densities were tested to investigate deformation stability and strain softening along such proportional strain paths. The rate of volumetric strain is achieved by controlling the amount of water flowing in or out of a fully saturated specimen. When defining $\vartheta = d\varepsilon_v/d\gamma$, the strain paths can be classified as follows:

- $\vartheta > 0$: Contractive strain paths along which water flows out of the soil specimen during shearing;
- $\vartheta < 0$: Dilative strain paths along which water flows into the soil specimen during shearing; and
- $\vartheta = 0$: Conventional undrained test.

For axisymmetric conditions, since $d\varepsilon_v = d\varepsilon_1 + 2d\varepsilon_3$ and $d\gamma = d\varepsilon_1 - d\varepsilon_3$, ϑ can be alternatively expressed as a function of the volumetric and the axial strains:

$$g = \frac{2d\varepsilon_v/d\varepsilon_1}{3 - d\varepsilon_v/d\varepsilon_1} \quad (6.1)$$

It should be noted that all stress components in this chapter are referred as effective.

6.2 Hill's material instability along proportional strain paths

When neglecting plastic strain components, Hill's second order work $d^2W = d\sigma_{ij}d\varepsilon_{ij}$ can be rewritten for triaxial stress conditions as

$$d^2W = (dp \frac{d\varepsilon_v}{d\varepsilon_q} + dq)d\varepsilon_q \quad (6.2)$$

with $dp = (d\sigma_1 + 2d\sigma_3)/3$, $dp = d\sigma_1 - d\sigma_3$, $d\varepsilon_q = 2(d\varepsilon_1 - d\varepsilon_3)/3$. In undrained tests, Eq. (6.2) becomes $d^2W = dq \cdot d\varepsilon_q$ since there is no volume change. Consequently, $d^2W = 0$ only when $dq = 0$, indicating that the deviator stress q reaches its maximum q_{\max} when the deformation of the specimen becomes unstable under undrained conditions.

Consider a loading program satisfying

$$d\varepsilon_1 + 2\mathfrak{R}d\varepsilon_3 = 0 \quad (6.3)$$

with $\mathfrak{R} = \text{const}$ and $d\varepsilon_1 = \text{const}$. One can relate g to $\mathfrak{R} = -d\varepsilon_1/(2d\varepsilon_3)$ through

$$g = \frac{d\varepsilon_v}{d\varepsilon_1} = \frac{d\varepsilon_1 + 2d\varepsilon_3}{d\varepsilon_1 - d\varepsilon_3} = \frac{2(\mathfrak{R} - 1)}{2\mathfrak{R} + 1} \quad (6.4)$$

The second order work along such as imposed strain path can be expressed as

$$d^2W = \left(d\sigma_1 - \frac{d\sigma_3}{\mathfrak{R}} \right) d\varepsilon_1 = d \left(\sigma_1 - \frac{\sigma_3}{\mathfrak{R}} \right) d\varepsilon_1 \quad (6.5)$$

One observes that, for any non-zero strain increment $d\varepsilon_1 \neq 0$, the condition of zero second order work is satisfied when $d(\sigma_1 - \sigma_3 / \mathfrak{R}) = 0$, for which

$$(\sigma_1 - \sigma_3 / \mathfrak{R}) = \max \quad (6.6)$$

In other words, the condition of $d^2W = 0$ corresponds to a peak point in the curve obtained by plotting $(\sigma_1 - \sigma_3 / \mathfrak{R})$ versus ε_1 . Hence, a peak in the plot of $(\sigma_1 - \sigma_3 / \mathfrak{R})$ against ε_1 signals a zero second order work, or material instability.

6.3 Material Instability along proportional strain path

This section discusses the results of tests along imposed strain paths $\mathcal{G} = \text{constant}$ on Sand O. The specimens were consolidated under the effective confining pressure of $\sigma_{30} = 100$ kPa, with the initial relative densities after consolidation ranging from about 1% to 96%. Figure 6.1 shows the measured strain paths for dense Ottawa sand specimens with $D_r = 75\%$ and loose ones with $D_r = 1\%$. As can be seen, satisfactory precision was achieved in controlling proportional strain increments during the tests.

6.3.1 Stress-strain responses

Figure 6.3 presents the responses of loose Ottawa sand specimens ($e_0 = 0.58$ and $D_r = 75\%$) along a variety of imposed strain paths ranging from forced dilation to compaction ($\mathcal{G} = -0.46$ to $+1.0$). The specimens were fabricated using the moist tamping method and consolidated under $\sigma_{30} = 100$ kPa. It should be noted $\mathcal{G} = 0$ is in fact the conventional undrained triaxial compression test, while the ultimate case with $\mathcal{G} \rightarrow \infty$ is hydrostatic compression. The response of the material was found to change from stable

behaviour (hardening) for strain paths corresponding to forced compaction ($\mathcal{G} > 0$), to unstable (strain softening) for forced dilative paths.

6.3.1.1 Contractive Proportional Strain Paths

When a medium dense sand of $e_0 = 0.58$ is forced to have contractive volume change along a proportional strain path of $\mathcal{G} = 1.0$, p and q of the corresponding effective stress path increase simultaneously, displaying a typical strain hardening behaviour (see Figure 6.2b). The mobilized friction angle is smaller than φ_{cv} before non-uniform deformation is observed, indicating that shear failure does not occur along this strain path. This phenomenon can be interpreted as follows. According to the results of drained triaxial compression tests, when sheared at an initial effective confining pressure of 100 kPa, a dense Ottawa sand specimen with $e_0 = 0.58$ tends to dilate. If a sample is forced to undergo contractive volume change, one would expect that the confining pressure must be increased to suppress the potential of dilation.

6.3.1.2 Dilative Proportional Paths

As can be observed in Figure 6.2b, for high dilative strain paths ($\mathcal{G} = -0.46$), shearing induces a continuous decrease in the mean effective stress. The deviatoric stress first increases and then decreases until “flow” failure occurs, as if the specimen were a very loose sand subjected to undrained shearing. For strain paths corresponding to moderate enforced dilation rates (e.g., $\mathcal{G} = -0.26$), the behaviour of the material can be divided into three parts defined by points A to E on the effective stress path. Referring to Figure 6.2b, which shows variation of different stress components during the test, both

σ_3 and the mean effective stress p decrease in the initial phase A–B, leading to a general decrease in effective confinement (as shown in Figure 6.2b). At the same time, the axial stress σ_1 and the deviatoric stress q increase steadily. After the transition point B, all stress components increase with axial strain, which is an indication of a typical strain hardening. When the maximum friction angle is mobilized at point P, both the mean effective stress p and the deviatoric stress q , however, continue to increase up to point C at which σ_1 and σ_3 reach their maximum. Stability cannot be sustained after C, with collapse occurring along path CD. The same features are observed from the responses of sand along the strain path of $\vartheta = -0.31$ and -0.34 . However, the deviator stresses at which collapse takes place decreases.

An examination of the excess water pressure responses presented in Figure 6.2c shows that, when ϑ varies between -0.26 and -0.34 , the snap-back of the effective stress paths at Point C in Figure 6.2b correspond to a temporary minimum excess pore pressure u_{min} . The lateral effective stress σ_3 , however, reaches a temporary maximum value at this moment; as shown in Figure 6.2c.

6.3.1.3 Influence of Density

The behaviour of sand along imposed proportional strain paths is found to be affected substantially by void ratio. For a sand specimen of $e_0 = 0.73$ (or $D_r = 26\%$) subjected to initial consolidation pressure of 100 kPa, pre-failure hardening occurs when ϑ is positive or slightly smaller than zero, as shown in Figure 6.3b. The comparison of

Figure 6.2b with Figure 6.3b implies that a dense sand can sustain stable deformation when subjected to a higher rate of dilative volume change.

6.3.1.4 Phase transformation

The phase transformation (PT) lines defined by Ishihara *et al.* (1975) as the loci of states in p - q plane where the behavior changes from contractive to dilative are also shown. In undrained shear the instants of maximum pore pressure, *e.g.*, $du=0$, signify the cessation of the tendency to contract and the start of the tendency to expand. Some workers consider PT state as the minimum mean effective stress point ($dp=0$) in the q - p space (*e.g.*, Lade and Yamamuro 1997). These two interpretations yield slightly different PT points on an effective stress path. In this study, the phase transformation state is referred to the points at which $du = 0$.

Figure 6.4 presents the influence of \mathcal{G} on the stress ratio $\eta_{PT} = (q/p)_{PT}$ at phase transformation states for Ottawa sand subjected to $\sigma_{30}=100$ kPa. For a given initial void ratio, η_{PT} tends to decrease with increasing \mathcal{G} , indicating that forced volume compaction results in PT states at smaller stress ratios and the PT state is not unique along different strain paths. For loose specimens in undrained tests, η_{PT} is very close to the stress ratio $\eta_{cr} = (q/p)_{cr}$ at the critical state. However, η_{PT} might be larger than η_{cr} when the specimens are sheared along dilative strain paths (*i.e.*, $\mathcal{G} > 0$). This finding is different with the observations from in undrained tests that the phase transformation in the $p - q$ space PT line is always located below the critical state line (CSL), *i.e.*, $\eta_{PT} \leq \eta_{cr}$ (see, for example, Ishihara 1993 and Yoshimine and Ishihara 1998).

6.3.2 Strain softening along proportional strain path

The experimental results presented in Figure 6.2 and Figure 6.3 clearly show that, for given void ratio, the stress-strain responses of a specimen may vary substantially from strain-softening to strain-hardening, depending on the imposed rate of volume change. It is recalled herein that strain-softening is referred to as $dq < 0$ (or $q = q_{max}$ at least temporarily) during testing in this study.

Figure 6.5 shows mobilized stress ratio η when $q = q_{max}$, which is the onset of strain softening, against the imposed rate of volume change \mathcal{G} in all tests under $\sigma_{30} = 100$ kPa. The data from undrained tests are also included in this figure for completeness. The data are generally divided into three groups corresponding to softening, hardening and the transition from temporary softening to hardening. When plotting the $(-\psi_{max}) \sim \eta_{max}$ relation obtained from conventional drained triaxial compression tests in Figure 6.5, one observes that the data corresponding to softening and hardening are separated, with the data for specimens exhibiting transitional behaviour being located close to the $(-\psi_{max}) \sim \eta_{max}$ curve. As a results, one may define the criterion of strain softening along imposed strain paths with $\mathcal{G} = \text{constant}$ as

$$\mathcal{G} + \psi_{max} < 0 \quad (6.7)$$

Physically, the above inequality indicates that a specimen exhibits softening behaviour when it is forced to expand more than the maximum dilate it has under drained conditions. On the other hand, if the specimen is forced to expand less that its maximum

dilation, strain hardening takes place. This conclusion is consistent with the experimental data of Chu *et al.* (1992).

In addition to the material properties including void ratio, particle shape and fabric, the mean effective stress level also affects the maximum angle of dilation ψ_{\max} . Consequently, a change of the initial effective confining pressure may result in different stress-strain responses for sand sheared along the same imposed strain path.

The dependency of strain softening on \mathcal{R} and the dilatancy characteristics of sand can be explained as follows. Let us consider a stress state (σ_1, σ_3) with corresponding strains $(\varepsilon_1, \varepsilon_3)$ during deformation. Given the inherent angle of dilation at this state is ψ , a lateral strain increment $d\varepsilon_3$ induced by an increase in the axial strain $d\varepsilon_1$, due to the inherent dilation, can be expressed as

$$d\varepsilon_3 = -\frac{d\varepsilon_1}{2\mathfrak{R}_D}, \quad \mathfrak{R}_D = \frac{2 - \sin\psi}{2(1 + \sin\psi)} \quad (6.8)$$

When deformation is enforced to deform along an imposed strain path $d\varepsilon_1 + 2\mathfrak{R}d\varepsilon_3 = 0$, the stresses must change to yield additional lateral strain

$$\Delta(d\varepsilon_3) = -\frac{d\varepsilon_1}{2\mathfrak{R}} + \frac{d\varepsilon_1}{2\mathfrak{R}_D} \quad (6.9)$$

which corresponds to an additional volumetric strain

$$d\varepsilon_{vc} = 2\Delta(d\varepsilon_3) = \left(\frac{1}{\mathfrak{R}_D} - \frac{1}{\mathfrak{R}} \right) d\varepsilon_1 \quad (6.10)$$

$d\varepsilon_{vc}$ can only be related to a corresponding variation of mean effective stress p that can be computed as

$$dp = \bar{K} d\varepsilon_{vc} = \bar{K} \left(\frac{1}{\mathfrak{R}_D} - \frac{1}{\mathfrak{R}} \right) d\varepsilon_1 = \frac{6\bar{K}(\mathcal{G} + \sin\psi)}{(2 - \sin\psi)(2 + \mathcal{G})} d\varepsilon_1 \quad (6.11)$$

with \bar{K} being a nominal bulk modulus of the material. When $\mathcal{G} < -\sin\psi$ or the specimen is forced to expand more than it can dilate, p has to decrease and thus reducing the shear resistance, which in turn induces strain softening or static liquefaction.

6.3.3 Strain softening and material instability

6.3.3.1 Instability during strain softening

We next examine material instability defined as $d^2W \leq 0$. Figure 6.6 presents the evolution of d^2W , $(\sigma_1 - \sigma_3 / \mathfrak{R})$ and the deviator stress of a loose Ottawa sand specimen ($e_0 = 0.81$) along an imposed strain path of $\mathcal{G} = -0.18$. One observes that $(\sigma_1 - \sigma_3 / \mathfrak{R})$ reaches its maximum when $d^2W = 0$, which confirms the conclusion obtained from Eqs. (6.5) and (6.6) that the condition of $d^2W = 0$ corresponds to a peak point in the curve of $(\sigma_1 - \sigma_3 / \mathfrak{R})$ versus ε_1 . It is interesting to note that strain softening takes place when $q = q_{max}$ prior to $d^2W = 0$ is satisfied. The post-softening deformation instability is also observed for a specimen of the same initial void ratio but sheared along the strain path of $\mathcal{G} = -0.34$, as shown in Figure 6.7. In a conventional undrained compression test, however, the onset of strain softening and Hill's instability occur almost at the same time. One may conclude that shearing along a higher dilative imposed strain path tends to have strain softening behaviour prior to its deformation becomes unstable. This conclusion is confirmed by the experimental results for Ottawa sand with a different initial void ratio $e_0 = 0.68$, as shown in Figure 6-8. It is important to note that both strain softening and

deformation instability take place before the peak friction angle is mobilized, as clearly shown in Figure 6.7 and Figure 6-8. In other words, strain softening and unstable deformation may both take place below the failure envelope. This observation confirms the theoretical analysis of Nova (1994).

Figure 6.9 summarizes the experimental data at the onset of instability and strain softening. Even though the onset of strain softening at $q = q_{max}$ occurs prior to deformation instability at $d^2W = 0$, the mobilized friction angle (or the stress ratio $\eta = q/p$) at the onset of strain softening is smaller than that when $d^2W = 0$. Moreover, both strain softening and deformation instability can take place even for dense sand, depending on the rate of imposed volumetric strain. For example, for dense specimens of $e_0 = 0.58$ (or $D_r = 75\%$), $\mathcal{G} < -0.4$ leads to both strain softening and deformation instability.

6.3.3.2 Instability during strain hardening

The experimental results in Figure 6.2 show that, when dense specimens ($e_0 = 0.58$ and $D_r = 75\%$) are sheared along imposed dilative strain paths with medium \mathcal{G} values, strain softening and deformation instability might be triggered following strain hardening. Herein only the variation of d^2W along imposed strain paths of $\mathcal{G} = -0.26, -0.31$ and -0.33 are examined for clarity. Figure 6.10 presents the variation of d^2W with deviator stresses, together with the effective stress paths. One observes that the zero second order work is satisfied in the course of strain hardening, with strain softening occurring simultaneously with deformation instability; as one can see from the variation

of d^2W and the deviator stress against the axial strain in Figure 6.11 for $\mathcal{G} = -0.26$. Comparing Figure 6.7 and Figure 6-8, Figure 6.10 clearly reveals that unstable deformation and strain softening are triggered after the peak friction angle is mobilized for the three specific proportional strain paths. The continuous decrease in p and q after the peak ($q = q_{max}$) of the effective stress path corresponds to unstable deformation with $d^2W < 0$ and the effective stress path below the failure surface.

It should be emphasised again that strain softening or instability may never take place when \mathcal{G} exceeds a certain threshold; as can be seen from Figure 6.2. Figure 6.12 presents additional experimental results for medium dense specimens of $e_0 = 0.68$ ($D_r = 43\%$), which are consistent with the observations made from Figure 6.10 and Figure 6.11.

6.3.3.3 Hardening following limited strain softening and unstable deformation

The stress-strain responses in some tests show that strain hardening may take place following limited strain softening and unstable deformation. Figure 6.13 presents the effective stress paths and the variation of d^2W for very loose specimens of $e_0 = 0.81$ sheared along proportional strain paths of $\mathcal{G} = 0.08, 0.22, \text{ and } 0.28$. For the case of $\mathcal{G} = 0.28$, both the effective stress path and the variation of d^2W show strain hardening behaviour. When q reaches its maximum at Point B, the condition of $d^2W = 0$ is satisfied, indicating both strain softening and material instability are triggered. Limited strain softening is observed between Points B and C, followed by strain hardening along CD. It is interesting to notice that $d^2W = 0$ at both B and C. Similar deformation phenomenon are also observed when $\mathcal{G} = 0.08$ and 0.22 .

Limited strain softening and material instability followed by strain hardening are not limited to loose specimens, as shown in Figure 6.14 that presents the experimental results of a very dense specimen subjected to a proportional strain path of $\mathcal{G} = -0.51$.

6.4 Instability domain along imposed proportional strain paths

The essentials of the results are summarized next in the deviatoric (q) versus mean effective (p) stress space shown in Figure 6.15. The $p - q$ space is divided into dilation and contraction regions as distinguished by negative and positive \mathcal{G} values respectively. Interestingly, it is found that there are certain forced \mathcal{G}^* paths for which the material response can still be stable, with the threshold \mathcal{G}^* being a function of the initial void ratio of the material. Those effective stress paths, found within the “forced dilation and stable” region (D1 and D2 in Figure 6.15), reflect a dilatant hardening behaviour. The behaviours of sand in region E between D1 and D2 can be stable or unstable, depending on the deformation history. The effective stress paths in Region B with forced contraction are stable, with strain softening after the peak point. In Region C, all effective stress paths are associated with both strain softening and unstable deformation.

6.5 Summary

An experimental study on the behaviour of sand along proportional strain paths was performed on sand specimens of different initial void ratios. Strain softening and material stability in the sense of Hill’s second order work were examined for strain paths of various imposed rate of volume change. The following conclusions are derived from the experimental observations:

- Under undrained condition, potential strain softening and instability are possible for loose sand, and they take place at the same time. For dense sand, conditions of strain softening and zero-second order work can never be satisfied.
- A dilatant sand displaying hardening and stable material behaviour under isochronic (undrained) conditions, as often used as a reference in soil mechanics, may succumb to unstable flow type behaviour along dilative strain paths. More specifically, when the imposed rate of dilation exceeds the inherent rate of dilation of the material, a dense sand specimen will have flow failure similar to a saturated loose specimen subjected to undrained compression. On the contrary, a loose sand may not have a flow failure when it is forced to have contractive volume change along imposed strain paths.
- Strain softening and material instability are different deformation phenomenon and they may not take place at the same time. When loose specimens are forced to follow a dilative strain path, they may have stable deformation during strain softening. In other words, the occurrence of instability is a sufficient but not necessary condition for strain softening, while instability may take place without strain softening.
- Depending on the rate of imposed volume change, unstable deformation might be triggered either before or after the maximum friction angle is mobilized.

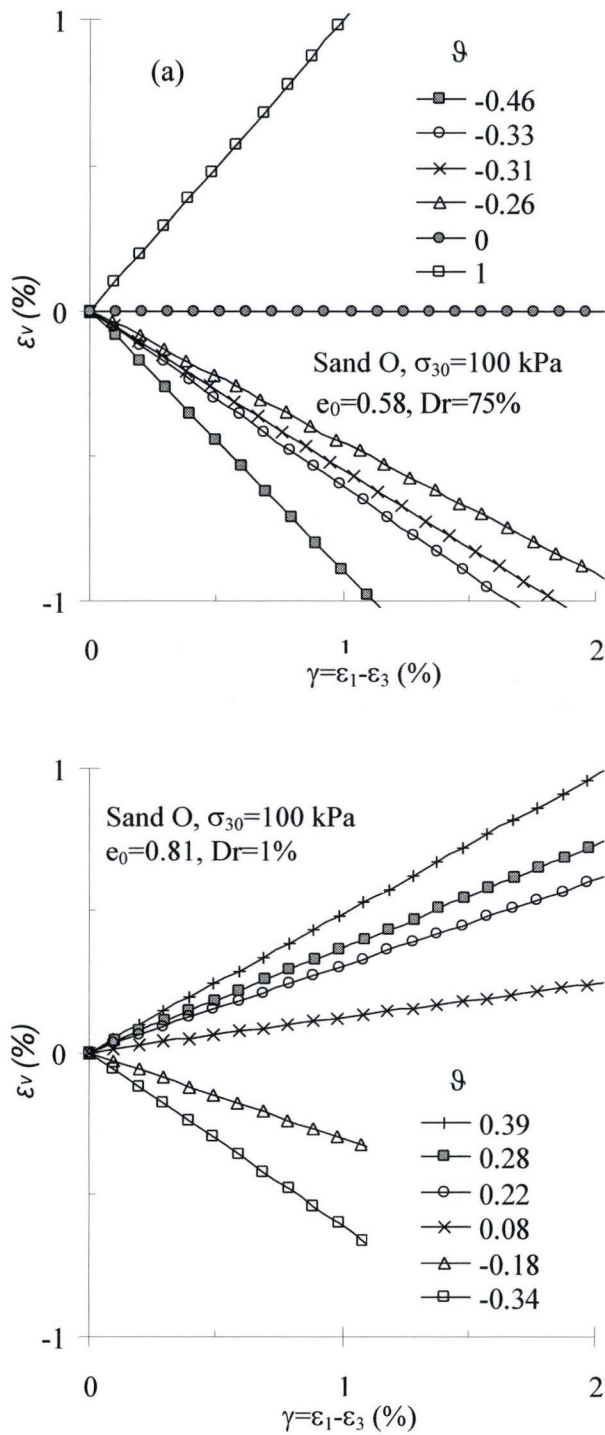


Figure 6.1: Measured strain paths: (a) Dense Ottawa sand; (b) Loose Ottawa sand.

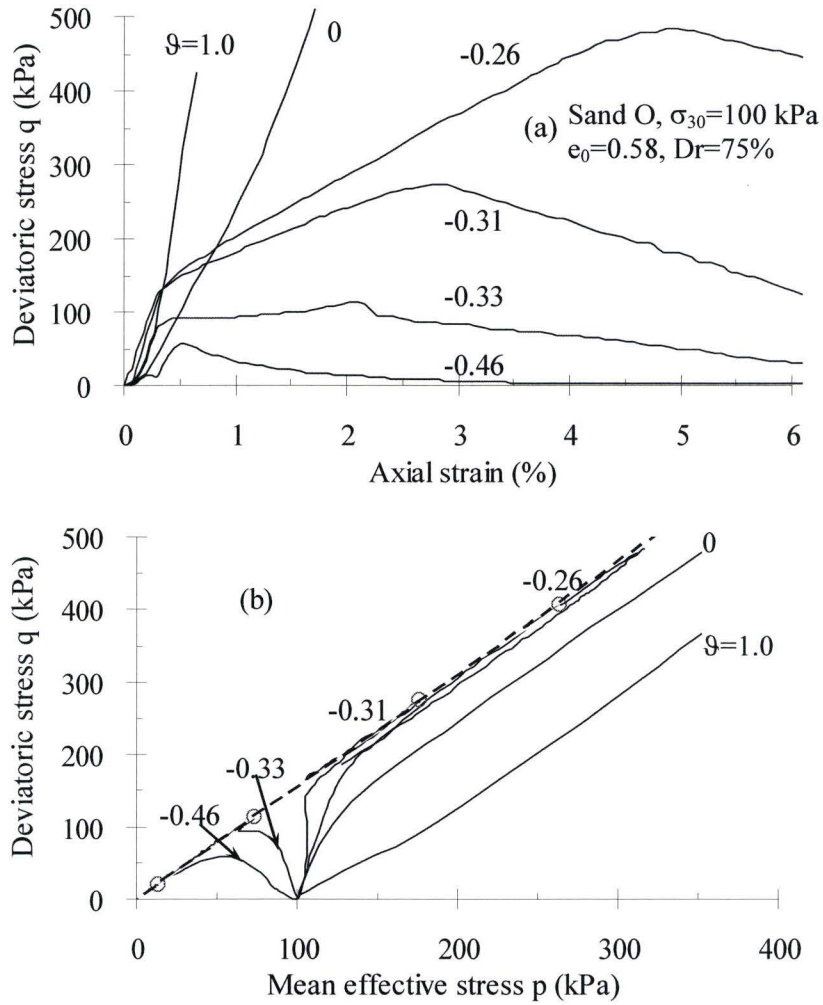


Figure 6.2: Behaviour of dense water pluviated Ottawa sand sheared along imposed proportional strain paths: (a) Stress-strain curves; (b) Effective stress path.

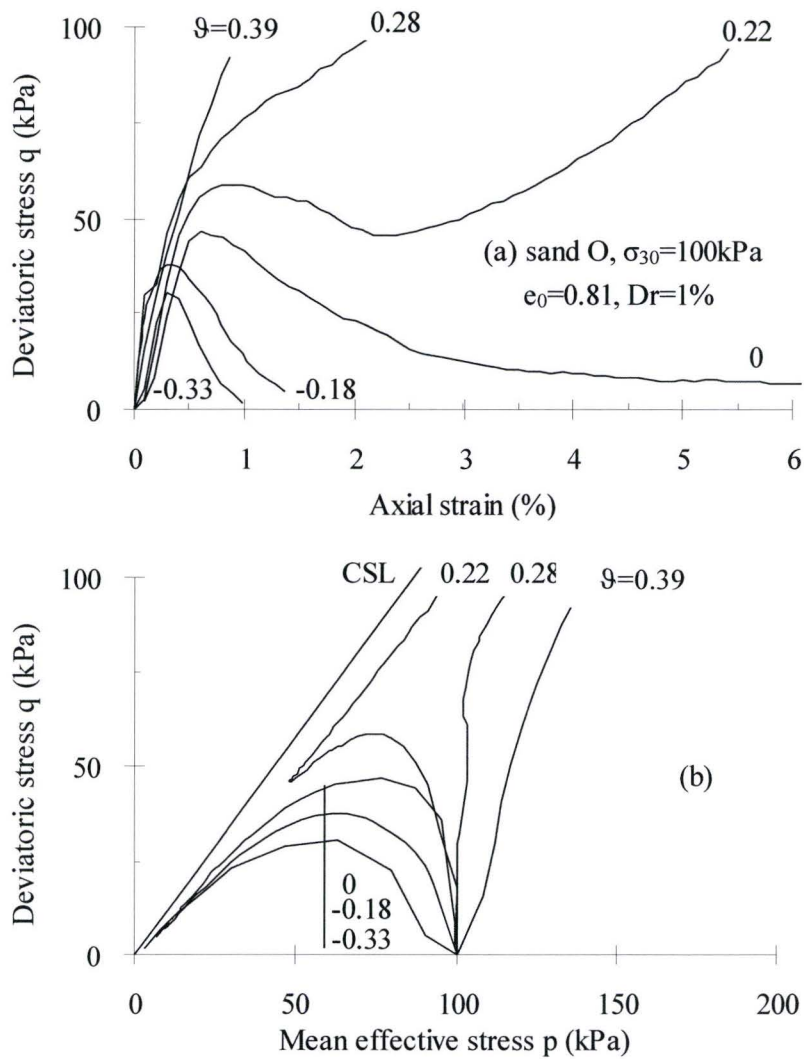


Figure 6.3: Behaviour of loose moist tamped Ottawa sand sheared along imposed proportional strain paths: (a) Stress-strain curves; (b) Effective stress path.

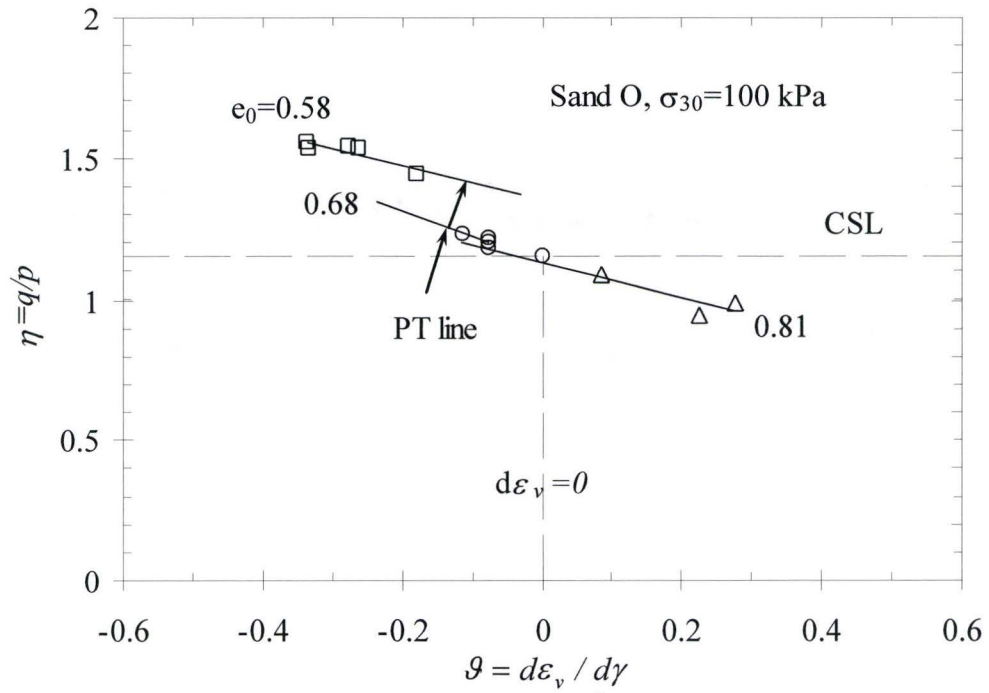


Figure 6.4: Dependency of phase transformation line on initial void ratio and imposed rate of volume change g

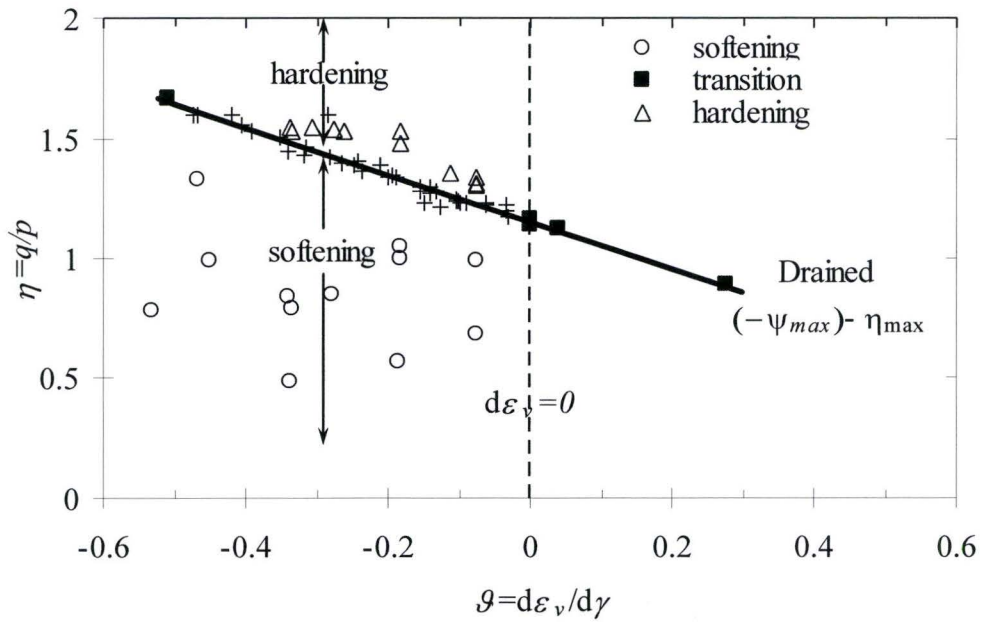


Figure 6.5: Softening/hardening domain in strain path tests

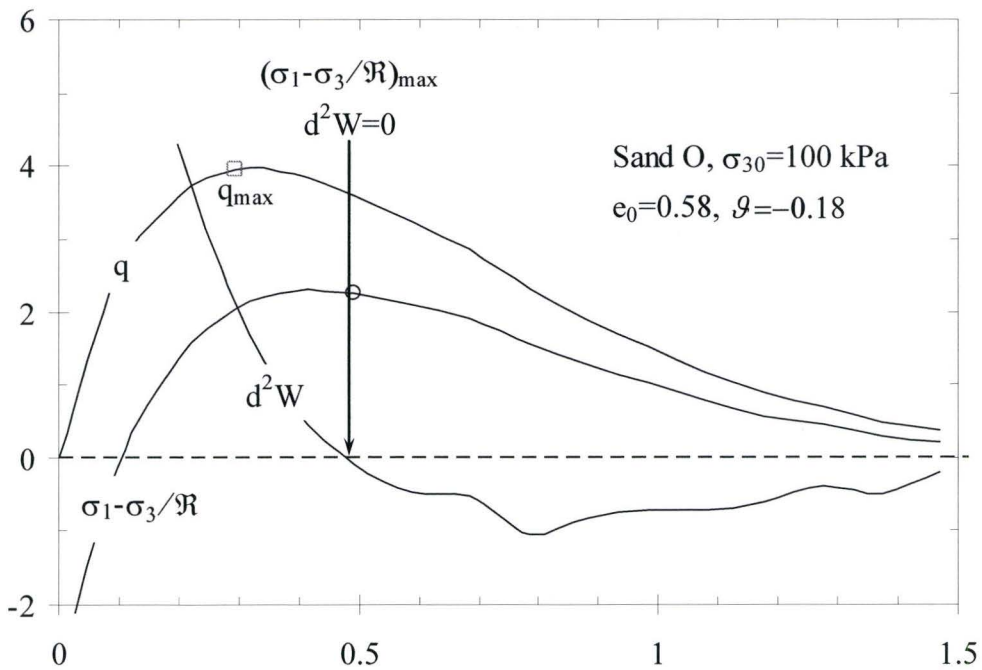


Figure 6.6: Evolution of second-order work, $\sigma_1 - \sigma_3 / \mathcal{R}$, and deviatoric stress along $g = -0.18$

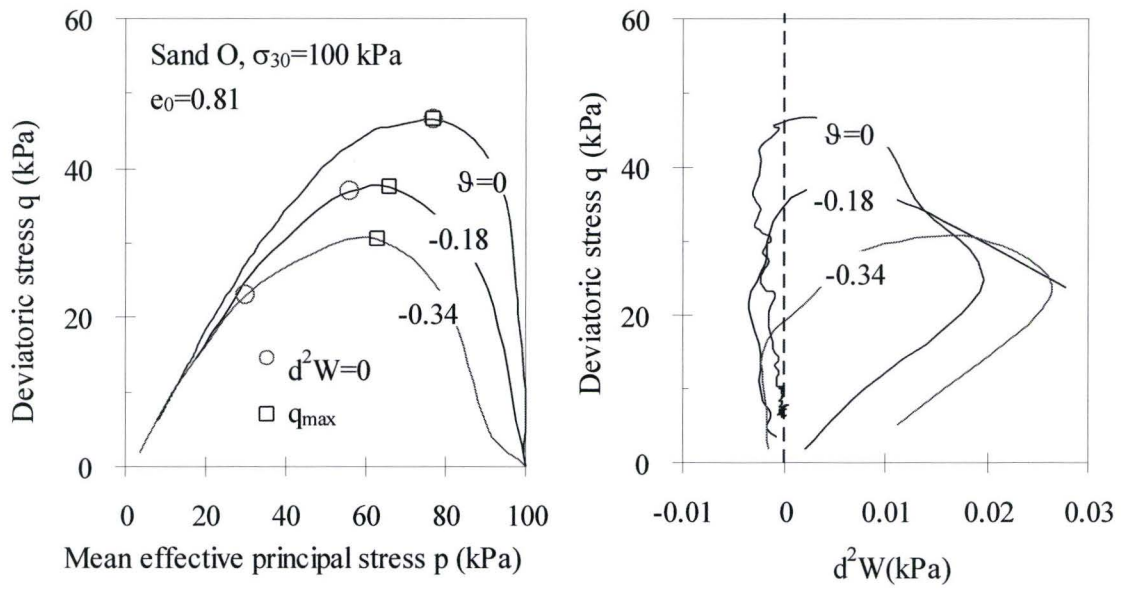


Figure 6.7: Stress path and evolution of d^2W for loose Ottawa sand ($e_0 = 0.81$) sheared along $\vartheta = 0, -0.18$ and -0.34

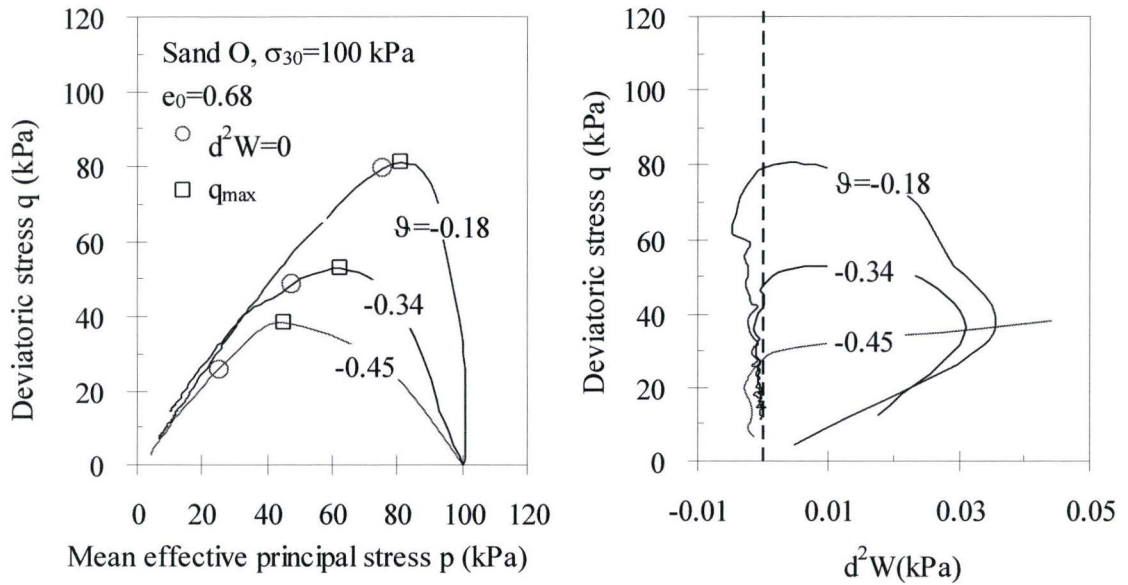


Figure 6.8: Effective stress paths and evolution of d^2W of medium dense Ottawa sand ($e_0 = 0.68$) sheared along $\mathcal{G} = -0.18, -0.34$ and -0.46

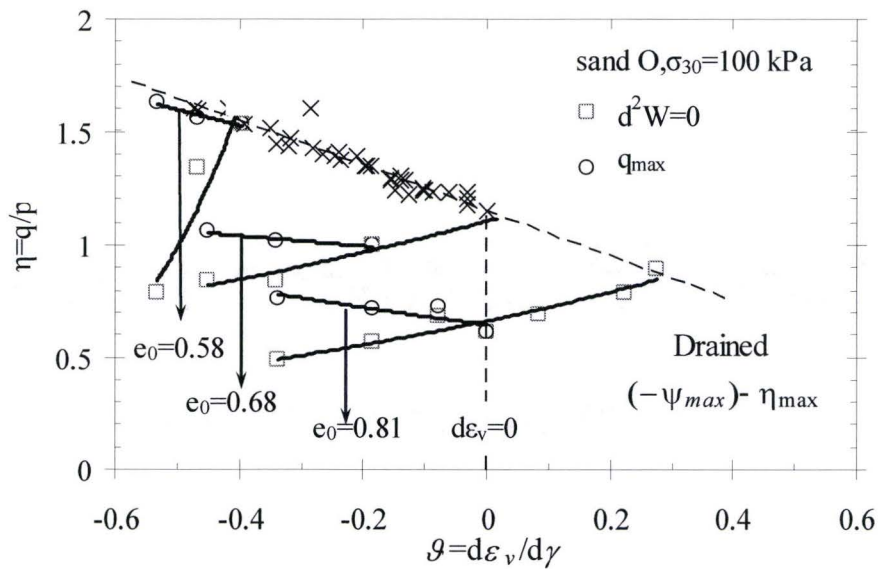


Figure 6.9: Comparison of onset of static liquefaction and instability in $\eta - \mathcal{G}$ space

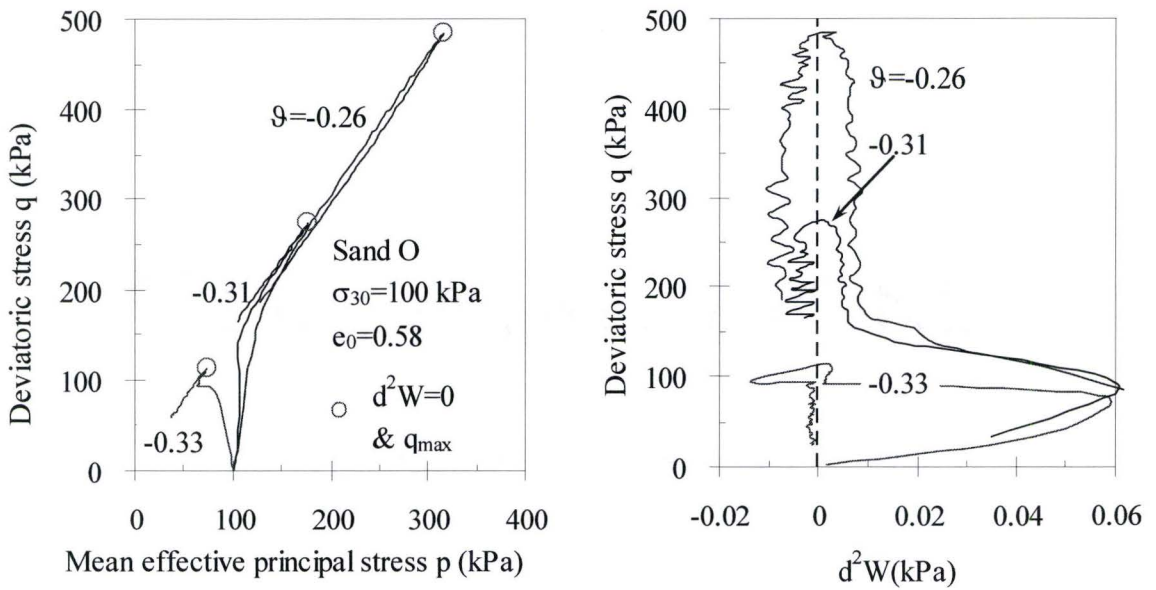


Figure 6.10: Effective stress paths and evolution of d^2W along strain paths of $g = -0.26, -0.31$ and -0.33

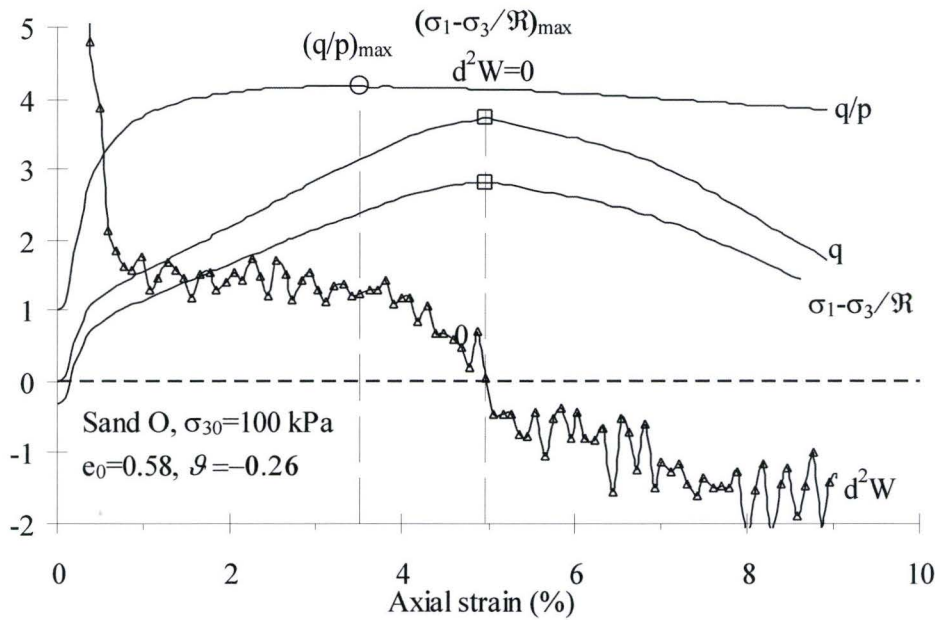


Figure 6.11: Evolution of second-order work, $\sigma_1 - \sigma_3 / \mathcal{R}$, deviatoric stress along strain path: $g = -0.26$; $e_0 = 0.58$

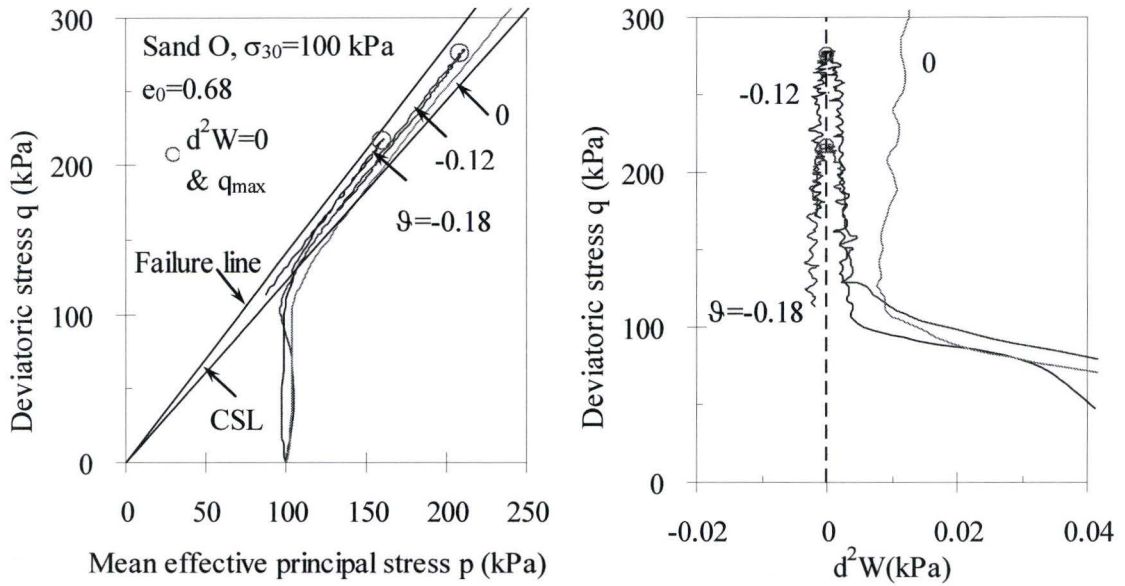


Figure 6.12: Stress path and evolution of the second-order work along strain path: $e_0 = 0.68$, $\vartheta = 0, -0.12, \text{ and } -0.18$

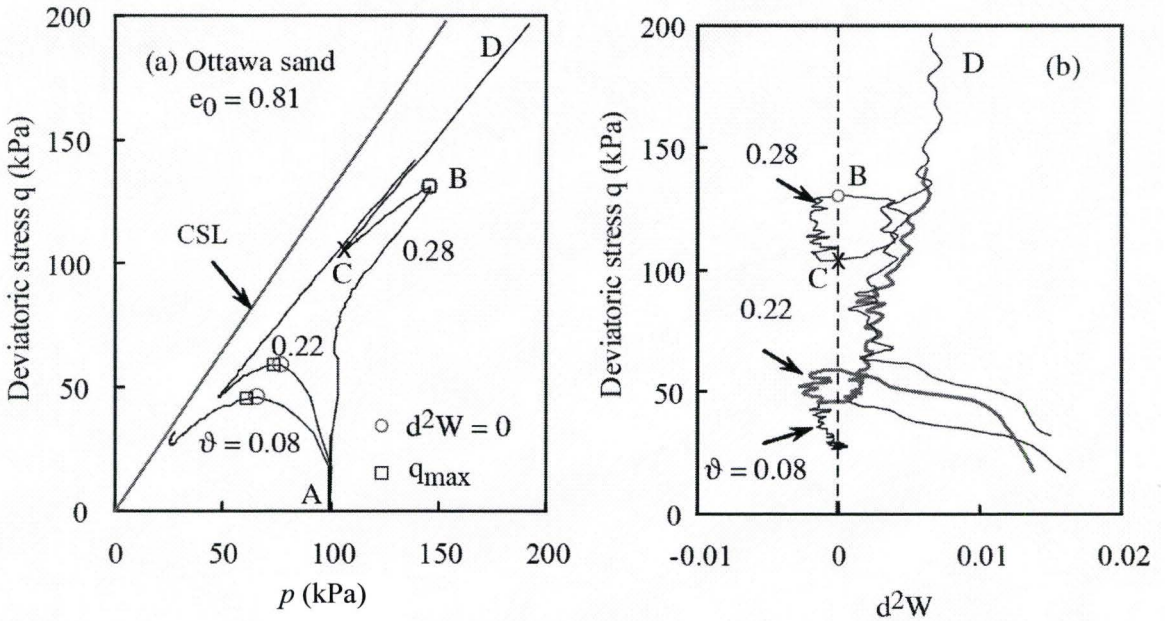


Figure 6.13: Stress paths and evolution of d^2W along various strain path: loose sand ($e_0 = 0.81$), $\vartheta = 0.08, 0.22, \text{ and } 0.28$

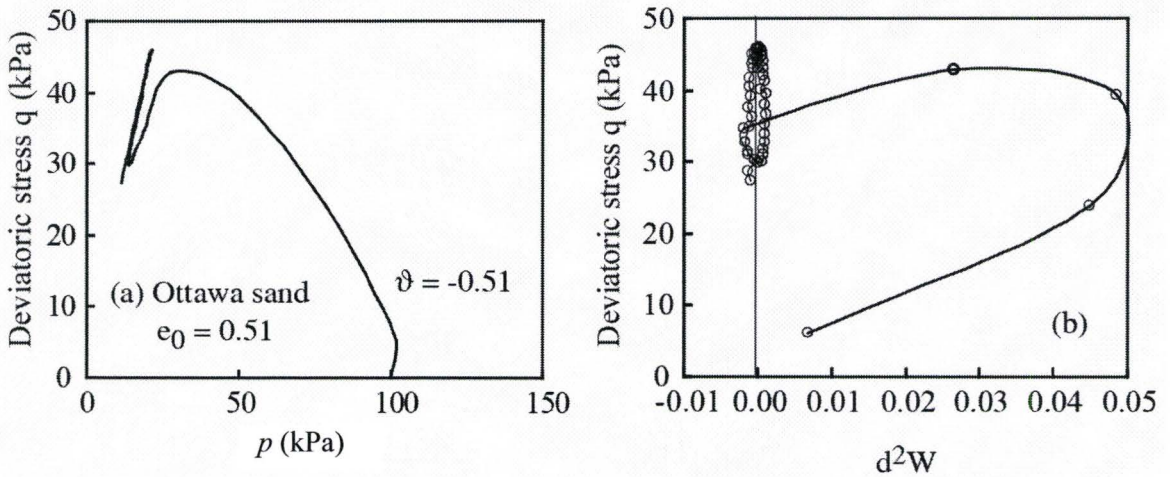


Figure 6.14: Stress paths and evolution of d^2W along various strain path: dense sand ($e_0 = 0.51$), $\vartheta = -0.51$

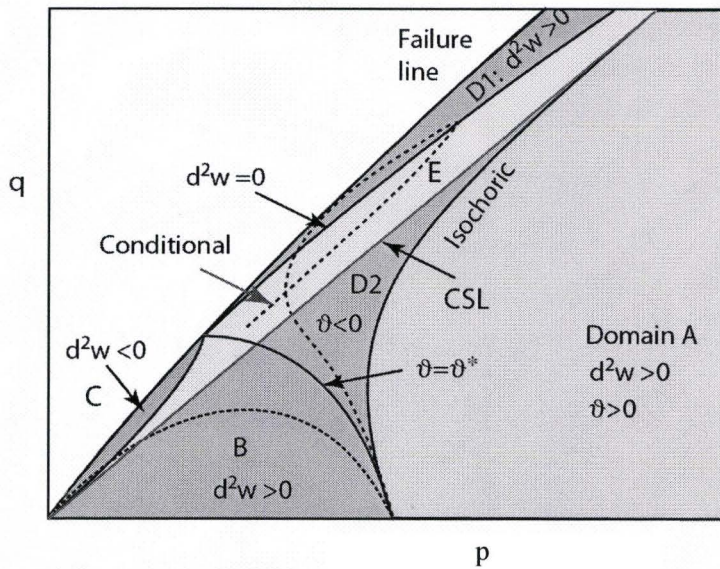


Figure 6.15: Instability domain along imposed proportional strain paths

Chapter 7

Summary and Conclusions

The research reported in this thesis mainly focused on the experimental investigation of the influence of sample preparation methods and interparticle locking on sand behaviour in triaxial compression tests, as well as the behaviour of sand along proportional strain paths.

The influence of sample preparation methods on sand behaviour was assessed by comparing the measured stress-strain-volume change responses of Ottawa sand and crushed limestone in drained triaxial compression tests. A total of eight sample preparation methods are examined, with the most of the specimens being fabricated using water pluviation (WP), moist tamping (MT), and moist rodding (MR). WP and MT methods were used to investigate the influence of sample preparation methods on the undrained behaviour of Ottawa sand. When the influence of particle shape on the behaviour of sand is concerned, the experimental results of sand consisting angular crushed limestone show that strong interparticle locking may develop in the specimen owing purely to particle angularity. The following conclusions can be made based on the research accomplished in this thesis:

1. Different initial fabric formed by different sample preparation methods yield different characteristic of initial fabric of granular soils, which in turn affect the strength and the deformation characteristic of specimens with the same initial physical state.

2. The effect of sample preparation methods on the behaviour of sand varies with the material being tested. For example, the effect of sample preparation methods on crushed limestone with angular particles and rough surface texture is more significant than on Ottawa sand with rounded / subrounded particle and relatively smooth surface texture.
3. Both the moisture condition (dry, moist or saturated) and the densification methods (tamping, tapping or rodding) to obtain the desired density have influences on the initial fabric of specimens. Specimens prepared at “wet” state tend to dilate more and have higher peak friction angle than “dry” specimens densified using the same compaction method. Specimens compacted by rodding have the most random special distribution of particles and hence less dilation.
4. Pluviation under water or in the air tends to yield uniform samples, with clear layering being observed in specimens prepared using moist tamping. For specimens of a given void ratio, shear band is more prone to appear in the ones prepared by moist than those by water or dry pluviation.
5. The results of triaxial tests for both standard Ottawa sand and crushed limestone identified three distinct limiting stress ratio (q/p) envelopes corresponding to different friction angles; *i.e.*, the start of dilation, ϕ_f ; the peak stress state, ϕ_{peak} ; and critical states, ϕ_{cv} . For dense Ottawa sand with no interlocking, ϕ_f is between ϕ_{μ} and ϕ_{cv} . Conversely, for dense crushed limestone with angular particles, ϕ_f is well above ϕ_{cv} within the range of confining pressure (50-500 kPa) in this study.

6. For granular materials with angular particles that may form locked fabric even when reconstituted in the laboratory, the triaxial test results show that dilation is the mechanism by which the material becomes destructured sufficiently to allow shearing. The fabric structure owing to interlocking still largely exists at the peak stress ratio but vanishes at the critical state, particularly for dense samples subjected low confining pressures.
7. When introducing an extra energy dissipation function describing the energy consumption for breaking inter-particle locking, Rowe's stress-dilatancy formulation can be modified to take into account the influence of interlocking. The rate of energy dissipation, $d\Phi_{fab}/d\varepsilon_1$, varies with stress level, density, as well as initial fabric. For a selected sample preparation method, $d\Phi_{fab}/d\varepsilon_1$ increases almost linearly with the effective confining pressure for a given initial void ratio, but decreases with increasing void ratio at a given stress level.
8. $d\Phi_{fab}/d\varepsilon_1$ varies with sample preparation methods. More specifically, specimens prepared by water pluviation and moist tamping have higher $d\Phi_{fab}/d\varepsilon_1$ than those prepared by rodding at a given density and stress level.
9. Depending on the strain path or the deformation history, a dilatant sand displaying hardening and stable material behaviour under isochronic (undrained) conditions, as often used as a reference in soil mechanics, may succumb to unstable flow type behaviour along dilative strain paths. More specifically, when the imposed rate of dilation exceeds the inherent rate of dilation of the material, a dense sand

specimen will have flow failure similar to a saturated loose specimen subjected to undrained compression. On the contrary, a loose sand may not have a flow failure when it is forced to have contractive volume change along imposed strain paths.

10. Strain softening and material instability are different deformation phenomenon and may not take place at the same time. When loose specimens are forced to follow a dilative strain path, it may have stable deformation during strain softening. In other words, the occurrence of instability is a sufficient but not necessary condition for strain softening, while instability may take place without strain softening.

The following work is considered necessary in the future:

1. Further microscopic studies are required to quantify the influence of sample preparation methods on the spatial distribution of sand grains. For example, one may use digital image analysis to obtain the connectivity of particles and hence define a fabric tensor as a measure for the initial fabric.
2. The influence of interparticle locking on soil behaviour should be related to quantitative measures for the angularity of sand particles.
3. Further laboratory experiments on sand consisting of angular particles are required for the purposes of understanding interparticle locking and for the modification of existing stress-dilatancy model to take into account the effect of interlocking.
4. The influence of interparticle locking in triaxial extension and cyclic loading tests has not been studied in this thesis. Additional experimental work may provide

deep insights into the influence of interlocking on the behaviour of sand subjected to cyclic loading.

Bibliography

- Alshibli, K. A. and Sture, S. (2000). Shear band formation in plane strain experiments of sand. *Journal of Geotechnical and Geoenvironmental Engineering*, 126(6): 495-503
- Alarcon-Guzman, A., Leonards, G. and Chameau, J.L. (1988). Undrained monotonic and cyclic strength of sands. *Journal of Geotechnical Engineering Division, ASCE*, 114(10): 1089-1109
- Andersen, A., Bjerrum, L. (1968). Slides in subaqueous slopes in loose sand and silt. Norwegian Geotechnical Institute, No.81: 1-9
- Banerjee, N.G., Seed, H.B., and Chan, C.K. (1979). Cyclic behavior of dense coarse-grained materials in relation to the seismic stability of dams, UCB/EERC.79/13
- Bardet, J. P. (1994). Observations on the effects of particle rotations on the failure of idealized granular materials. *Mechanics of Materials*, 18: 159-182
- Barton, M. E. (1993). Cohesive sands: the natural transition from sands to sandstones. In *Geotechnical engineering of hard soils - soft rocks* (eds. Anagnostopoulos, A. et al.), Rotterdam: Balkema, 367- 374
- Barrett, P. J. (1980). The shape of rock particles, a critical review. *Sedimentology*, 27, 291-303
- Been, K. and Jefferies, M. G. (1985). A state parameter for sands. *Géotechnique*, 35(2): 99-112
- Billam, J. (1971). Some aspects of the behaviour of granular materials at high pressures. *Stress-strain behaviour of soils. Proceedings of the Roscoe Memorial Symposium*, Cambridge University (eds. Parry, R.H.G.). Henley-on-Thames: G.T. Foulis & Co., 69-80
- Bishop, A.W., and Eldin, A.K.G. (1953). The effect of stress history on the relation between ϕ and porosity in sand. *Proceedings of the Third International Conference on Soil Mechanics and Foundation Engineering*, 1: 100-105
- Bishop, A.W. (1954). Correspondence on “Shear characteristic of a saturated silt measured in triaxial compression”. *Géotechnique*, 4: 43-45

- Bishop, A.W. and Green, G.E. (1965). The influence of end restraint on the compression strength of a cohesionless soil. *Géotechnique*, 15 (3): 243-266
- Bishop, A.W.(1966). The strength of soils as engineering materials. *Géotechnique*, 16(2): 91–128
- Bishop, A.W.(1972). Shear strength parameters for undisturbed and remoulded soils specimens. In *Stress-strain behaviour of soils*, (eds. Parry, R. H. G.). London: Foulis, 3-58
- Bishop, J.F.W. and Hill, R.(1951). A theory of the plastic distortion of a polycrystalline aggregate under combined stress. *Philosophical Magazine* 42, 414-427
- Bolton, M.D.(1986). The strength and dilatancy of sands. *Géotechnique*, 36(1), 65–78
- Bromwell, L.G. (1966). The friction of quartz in high vacuum. Research Report B66-18, Dept. of Civil Engineering, M.I.T.
- Casagrande, A.(1936). Characteristics of cohesionless soils affecting the stability of slopes and earth fills. *Contributions to soil mechanics*, Boston Society of Civil Engineers, 257–276
- Casagrande, A. and Carillo, N. (1944). Shear Failure of Anisotropic Materials. *Proc. Boston Soc. of Civil Eng.* 31, 74 - 87
- Casagrande, A. (1975). Liquefaction and cyclic deformation of sands: a critical review. Harvard University, Cambridge, Mass., Harvard Soil Mechanics Series No.88. (originally presented at 5th Pan-American Conference on Soil Mechanics and Foundation Engineering, 1975, Buenos Aires, Argentina).
- Castro, G. (1969). Liquefaction of sands. Harvard Soil Mechanics Series No. 81, Cambridge, Massachusetts
- Cecconi, M. and Viggiani, G.M.B. (2001). Structural features and mechanical behaviour of a pyroclastic weak rock. *International Journal for Numerical and Analytical Methods in Geomechanics*, 25(15): 1525-1557
- Chan, L.C.Y. and Page, N.W. (1997). Particle fractal and load effects on internal friction in powders, *Powder Technology*, 90: 259-266

- Chu, J. and Lo, S-C. R. (1993). Instability of granular soils under strain path testing. *Journal of Geotechnical Engineering, ASCE*, 119(5): 874-892
- Chu, J. and Lo, S.-C. R. (1994). Asymptotic behaviour of a granular soil in strain path testing. *Géotechnique*, 44(1):65-82
- Chu, J. and Leong, W. K. (2001). Pre-failure strain softening and prefailure instability of sand: a comparative study. *Géotechnique*, 51(4):311-321
- Cresswell, A. and Barton, M. E. (2003). Direct shear tests on an uncemented, and a very slightly cemented, locked sand. *Quarterly Journal of Engineering Geology and Hydrogeology*, 36:119-132
- Cresswell, A. and Powrie, W. (2004). Triaxial tests on an unbonded locked sand. *Géotechnique*, 54(2): 107-115
- Cornforth, D.H. (1964). Some experiments on the influence of strain conditions on the strength of sand. *Géotechnique*, 14 (2):143-167
- Cuccovillo, T. and Coop, M. R. (1999). On the mechanics of structured sands. *Géotechnique*, 49(6): 741-760
- Darve, F. (1995). Constitutive modeling and instabilities of soil behaviour. *Computers und Geotechnics*, 17, 203-224
- DeGregorio, V. B. (1990). Loading systems, sample penetration, and liquefaction. *Journal of Geotechnical Engineering, ASCE*, 116(5): 805-821
- De Josselin de Jong, G. (1976). Rowe's stress-dilatancy relation based on friction. *Géotechnique*, 26(3): 527-534
- Dennis, N. D. (1988). Liquefaction evaluation procedure: discussion. *Journal of Geotechnical Engineering, ASCE*, 114(2): 241-243
- Doanh, T., Ibraim, E. and Matiotti, R. (1997). Undrained instability of very loose Hostun sand in triaxial compression and extension. Part 1: experimental observations. *Mechanics of Cohesive-frictional Materials*, 2: 71-92
- Dusseault, M. B. and Morgenstern, N. R. (1978). Shear strength of Athabasca oil sands. *Canadian Geotechnical Journal*, 15: 216-238

- Dusseault, M. B. and Morgenstern, N. R. (1979). Locked sands. *Quarterly Journal of Engineering Geology*, 3(3):117-131
- Emery, J.J., Finn, W.D.L., and Lee, K.W. (1973). Uniformity of saturated sand samples. In *Evaluation of relative density and its role in geotechnical projects involving cohesionless soils*. ASTM STP 523, 182-194
- Frost, J.D., Jang, D.J., Chen, C.C., and Park, J.Y., (1998). Quantitative characterization of microstructure evolution. *Proceedings of International Workshop on Physics and Mechanics of Liquefaction*, Balkema, 169-177
- Frost, J. D. and Park, J. Y. (2003). A critical assessment of the moist tamping technique. *ASTM Geotechnical Testing Journal*, 26(1):1-14
- Garga, V. K. and Zhang, H. (1997). Volume changes in undrained triaxial tests on sands. *Canadian Geotechnical Journal*, 34:762–772
- Goddard, J. D., and Bashir, Y. M. (1990). On Reynolds dilatancy, recent development in structured continua, (eds. Kee, D. De and Kaloni, P. N.), Vol. II, Longman's, London, 23-35
- Guo, P. J. (2000). Modelling granular materials with respect to stress-dilatancy and fabric: a fundamental approach. PhD dissertation, University of Calgary, Canada
- Guo, P. J. and Su, X. (2006). Shear strength, interparticle locking and dilatancy of granular materials. To appear on *Canadian Geotechnical Journal*
- Gutierrez M, Ishihara K, Towhata I. (1991). Flow theory for sand during rotation of principal stress direction. *Soils and Foundations*, 31(4): 121-132
- Gudehus, G. (1996). A comprehensive constitutive equation for granular materials. *Soils and Foundations*, 36(1): 1-12
- Han, C. and Drescher, A. (1993). Shear bands in biaxial tests on dry coarse sand. *Soils and Foundations*, 33(1): 118-132
- Hanna, A. (2001). Determination of plane-strain shear strength of sand from the results of triaxial tests. *Canadian Geotechnical Journal*, 38: 1231-1240
- Hettler, A. and Vardoulakis, I. (1984). Behaviour of dry sand tested in a large triaxial apparatus. *Géotechnique*, 34(2): 183-198

- Hill, R. (1958). A general theory of uniqueness and stability in elastic-plastic solids. *Journal of the Mechanics and Physics of Solids*, 6: 236-249
- Holubec, I. and D'Appolonia, E. (1973). Effect of Particle Shape on the Engineering Properties of Granular Soils. ASTM STP 523, 304-318
- Horn, M.R. (1965a). The behaviour of an assembly of rotund, rigid cohesionless particles. Part I. *Proceedings of the Royal Society of London, Series A*, 286: 62-76.
- Horn, M.R. (1965b). The behaviour of an assembly of rotund, rigid cohesionless particles, Part II. *Proceedings of the Royal Society of London, Series A*, Vol. 286, pp. 79-97.
- Houlsby, G. T. (1991). How the dilatancy of soils affects their behaviour. *Proc. 10th Euro. Conf. on Soil Mech. Found. Eng.*, 4:1189-1202
- Indraratna, B. and Salim, W. (2002). Modelling of particle breakage of coarse aggregates incorporating strength and dilatancy. *Proceedings of the Institution of Civil Engineers, Geotechnical Engineering*, 155(4): 243-252
- Ishihara, K., Tatsuoka, F. and Yasuda, S. (1975). Undrained deformation and liquefaction of sand under cyclic stresses. *Soils and Foundations*, 15(1):29-44
- Ishihara, K. (1993). Liquefaction and flow failure during earthquakes. *Géotechnique*, 43(3):351-415
- King, G. J. W. (1970). Comprison of stress-dilatancy theories. *Journal of Soil Mechanics and Foundation Division, ASCE*, 96(5): 1697-1714
- Koerner, R.M. (1970). Effect of particle characteristics on soil strength. *Journal of Soil Mechanics and Foundation Division, ASCE*, 96(4):1221-1234
- Kuerbis, R., and Vaid, Y.P. (1988). Sand sample preparation—the slurry deposition method. *Soils and Foundations*, 28(4): 107-118
- Ladd, R. S. (1974a). Specimen preparation and liquefaction of sands. *Journal of Geotechnical Engineering, ASCE*, 100(10):1180-1184
- Ladd, R. S. (1974b). Specimen preparation and cyclic stability of sands. *Journal of Geotechnical Engineering, ASCE*, 103(6): 535-547

- Lade, P.V., Nelson, R.B. and Ito, Y.M. (1988). Instability of granular materials with nonassociated flow. *Journal of Engineering Mechanics, ASCE*, 114: 2173-2191
- Lade, P.V. (1989). Instability and failure of soils with nonassociated flow. *Proc., 12th Int. Conf. on Soil Mech. Found. Engr., Rio de Janeiro, Brazil*, 1, 727-730
- Lade, P.V., and Pradel, D. (1990). Instability and plastic flow of soils. I: Experimental observations. *Journal of Engineering Mechanics, ASCE*, 116(11): 2532-2550
- Lade, P.V. (1992). Static instability and liquefaction of loose fine sandy slopes. *Journal of Geotechnical Engineering, ASCE*, 118(1): 51-71
- Lade, P.V., and Yamamuro, J.A. (1997). Effects of nonplastic fines on static liquefaction of sands. *Canadian Geotechnical Journal*, 34: 918-928
- Lancelot, L., Shahrour I. and Mahmoud, M. A. (2004). Instability and static liquefaction on proportional strain paths for sand at low stresses. *Journal of Engineering Mechanics, ASCE*, 130(11): 1365-1372
- Laouafa, F. and Darve, F. (2002). Modelling of slope failure by a material instability mechanism. *Computers and Geotechnics*, 29:301-325
- Lee, I. K. (1966). Stress-dilatancy performance of feldspar. *Journal of the Soil Mechanics and Foundations Division, ASCE*, 2 (1): 79-103
- Lee, K. L. and Seed, H. B. (1967). Drained strength characteristics of sand. *Journal of the Soil Mechanics and Foundations Divisions, ASCE*, 93(6):117-141
- Li, X.S. and Dafalias, Y.F. (2000). Dilatancy for cohesionless soils. *Géotechnique*, 50(4): 449-460
- Mahmood, A., Mitchell, J.K., and Lindblom, Ulf. (1976). Effect of specimen preparation method on grain arrangement and compressibility in sand. *ASTM STP 599*, 169-192
- Marachi, N. D., Chan, C. K. and Seed, H. B. (1972). Evaluation of properties of rockfill materials. *Journal of Soil Mechanics and Foundations Division, ASCE*, 98(1): 95-114
- Marcuson, W.F., III, and Gilbert, P.A. (1972). Earthquake liquefaction potential at Patoka Dam, Indiana. *U.S. Army Waterways Experiment Station, Vicksburg, Miscellaneous Paper S-72-42*

- Marsal, R.J.(1973). Mechanical properties of rockfill. (eds. Hirschfeld, R. C. & Poulos, S. J.) Embankment Dam Engineering, Casagrande Volume, Wiley, New York, 109-200
- Matsuoka, H. (1974). Dilatancy characteristics of soils. *Soils and Foundations*, 14(3): 45-53
- McDowell, G. R. and Bolton, M. D. (1998). On the micromechanics of crushable aggregates. *Géotechnique*, 48(5): 667-679.
- Miura, S., and Toki, S. (1982). A sample preparation method and its effect on static and cyclic deformation–strength properties of sand. *Soils and Foundations*, 22(1): 61-77
- Miura, S., and Toki, S. (1984). Anisotropy in mechanical properties and its simulation of sands sampled from natural deposits. *Soils and Foundations*, 24(3): 69-84
- Miura, K., Maeda K., Furukawa, M., Toki, S. (1998). Mechanical characteristics of sands with different primary properties, *Soils and Foundations*, 38(4):159-172
- Mitchell, J.K. (1976). *Fundamentals of soil behavior*. John Wiley & Sons, New York
- Mooney, M.A., Viggiani, G., and Finno, R.J.(1998). The existence of a unique critical state? *Journal of Geotechnical and Geoenvironmental Engineering*, ASCE, 124(11):1100-1108
- Muhunthan, B., Chameau, J. L. and Masad, E. (1996). Fabric effects on the yield behaviour of soils. *Soils and Foundations*, 36(3): 85–97
- Mulilis, J. P., Seed, H. B., Chan, C. K., Mitchell, J. K., and Arulanandan, K. (1977). Effects of sample preparation on Sand Liquefaction. *Journal of Geotechnical Engineering*, ASCE,103(2): 91-108
- Nakai, T.(1997). Dilatancy characteristics of geomaterials. In *Deformation and Progressive Failure in Geomaterials, IS-Nagoya'97* (eds. Asaoka, A, Adachi, T. and Oda, F.), 899-906
- Newland, P.L. and Alley, B.H., (1957), Volume changes in drained triaxial tests on granular materials. *Géotechnique*, 7(1):17-34
- Nicholson, P.G., Seed, R.B., and Anwar, H.A. (1993). Elimination of membrane compliance in undrained triaxial testing. I. Measurement and evaluation. *Canadian Geotechnical Journal*, 30: 727–738

- Nova, R. (1994). Controllability of the incremental response of soil specimens subjected to arbitrary loading programmes. *J. Mech. behav. Mater.*, 5(2),193-201
- Oda, M. (1972a). Initial fabrics and their relations material. *Soils and Foundations*, 12(1):17-36.
- Oda, M. (1972b). The mechanism of fabric changes during compressional deformation of sand. *Soils and Foundations*, 12(2): 1-18.
- Oda, M. and Kazama, H. (1998). Microstructure of shear bands and its relation to the mechanisms of dilatancy and failure and dense granular soils. *Géotechnique*, 48(4): 465-481
- Papadimitriou, A. G., Dafalias, Y. F. and Yoshimine, M. (2005). Plasticity modeling of the effect of sample preparation method on sand response. *Soils and Foundations*, 45(2): 109-123
- Parikh, P.V. (1967). The shearing behaviour of sand under axisymmetric loading. PhD thesis, Manchester University
- Pradhan,T.B.S., Tatsuoka,F. and Sato,Y. (1989). Experimental stress-dilatancy relations of sand subjected to cyclic loading. *Soils and Foundations*, 29(1): 45-64
- Prevost, J.-H. & Hoeg, K. (1975). Soil Mechanics and Plasticity Analysis of strain softening. *Géotechnique*, 25(2):279-297
- Read, H. E. & Hegemier G. A. 1984, Strain softening of rock, soil and concrete - a review article. *Mechanics of Materials*, 3: 271-294
- Reynolds, O. (1885). On the dilatancy of media composed of rigid particles in contact, with experimental illustrations. *Philosophical Magazine*, 20: 469-481
- Rowe, P. W. (1962). The stress-dilatancy relation for static equilibrium of an assembly of particles in contact. *Proceedings of the Royal Society of London, Series A, Mathematical and Physical Sciences*, 269: 500-527
- Rowe, P. W. (1963). The stress-dilatancy performance of two clays. *ASTM STP* 361:134-143
- Rowe. P. W. (1964). The importance of free ends in triaxial testing. *Journal of the Soil Mechanics and Foundations Engineering division. ASCE*, 90(1):1-27

- Rowe, P. W. (1971). Theoretical meaning and observed values of deformation parameters for soil. Proc. Roscoe memorial symposium on stress-strain behaviour of soils. Cambridge University, 143-194
- Sasitharan, S., Robertson, P.K., Sego, D.C., and Morgenstern, N.R. 1993. Collapse behavior of sand. Canadian Geotechnical Journal, 30: 569-577
- Schanz, T., and Vermeer, P. A. (1996). Angles of friction and dilatancy of sand. Géotechnique, 46(1): 145-151
- Schofield, A. N. (1999). A note on Taylor's interlocking and Terzaghi's "true cohesion" error. Geotechnical News, 17(4)
- Silver, M.L., Tatsuoka, F., Phukunhaphan, A., and Avramidis, A.S.(1980). Cyclic undrained strength of sand by triaxial test and simple shear test. In Proceedings of the 7th World Conference on Earthquake Engineering, Istanbul, 3: 281-288
- Sladen, J.A., D.Hollander, R.D., and Krahn, J. (1985). The liquefaction of sands, a collapse surface approach. Canadian Geotechnical Journal, 22: 564-578
- Sukumaran, B., and Ashmawy, A. K. (2001). Quantitative characterization of the geometry of discrete particles. Géotechnique, 51(7): 171-179
- Terzaghi, K. (1956). Varieties of submarine slope failures. Proceedings, 8th Texas Conference on Soils and Foundation Engineering, University of Texas, Austin, 1-41
- Tsukamoto, Y., Ishihara, K. and Nanaka, T. (1998). Undrained deformation and strength characteristics of soil from reclaimed deposits in Kobe. Soils and Foundations (Special Issue on Geotechnical Aspects of the January 17, 1995 Hyogoken-Nambu Earthquake No. 2): 47-55
- Tatsuoka, F., Iwasaki, T., Yoshida, S., Fukushima, S. and Sudo, H. (1979). Shear modulus and damping by drained tests of clean and specimens reconstituted by various methods. Soils and Foundations, 19(1): 39-54
- Tatsuoka, F. (1987). Discussion on the paper by Bolton. Géotechnique, 37(2): 219-226
- Taylor, D.W. (1948). Fundamentals of Soil Mechanics, Wiley, New York
- Tokue, T. (1979). Deformation behaviours of dry sand under cyclic loading and a stress-dilatancy model. Soils and Foundations, 19(2): 63-78

- Uchida, K. and Vaid, Y.P. (1994). Sand behavior under strain path control. Proc. of 13th Int. Conf. Soil Mech. and Found. Eng., 1, 17-20
- Ueng, T. S. and Chen, T. J. (2000). Energy aspects of particle breakage in drained shear of sands. *Géotechnique*, 50(1):65-72
- Ueng, T. S. and Lee, C. J. (1990). Deformation Behavior of Sand Under Shear-Particulate Approach, *Journal of Geotechnical Engineering, ASCE*, 116(11): 1625-1640
- Vaid, Y. P., Sivathayalan DS, Stedman D. (1999). Influence of specimen-reconstituting method on the undrained response of sand. *Geotechnical Testing Journal*, 22(3):187-195
- Vaid, Y.P., and Eliaborani, A. (1998). Instability and liquefaction of granular soils under undrained and partially drained states. *Canadian Geotechnical Journal*, 35: 1053-1062
- Valanis, K. C. (1985). On the uniqueness of solution of the initial value problem in strain softening materials. *Journal of Applied Mechanics, ASME*, 52: 649-653
- Vardoulakis, I. (1979). Bifurcation analysis of the triaxial test on sand samples. *Acta Mechanica*, 32, 35-54
- Verdugo, R. and Ishihara, K. (1996). The steady state of sandy soils. *Soils and Foundations*, 36(2): 81-92
- Vesic, A.S. and Clough, G.W. (1968). Behaviour of granular material under high stresses. *Journal of the Soil Mechanics and Foundations Division, ASCE*, 94 (3): 664-688
- Wan, R. G., and Guo, P. J. (1998). A simple constitutive model for granular soils: Modified stress-dilatancy approach. *Computers and Geotechnics*, 22(2): 109-133
- Wan, R. G. and Guo, P. J. (1999). A pressure and density dependent dilatancy model for granular materials. *Soils and Foundations*, 39(6):1-11
- Wan, R., Guo, P.J, Al-Mamun, M. (2005). Behaviour of granular materials in relation to their fabric dependencies. *Soils and Foundations*, 45(2): 77-86
- Wong, R. C. K. (2001). Strength of two structured soils in triaxial compression. *International Journal for Numerical and Analytical Methods in Geomechanics*, 25:131-153

- Wong, R. K. S. and Arthur, J. R. F. (1985). Induced and inherent anisotropy in sand. *Géotechnique*, 35, 471-481
- Yoshimine, M. and Ishihara, K. (1998). Flow potential of sand during liquefaction. *Soils and Foundations*, 38 (3): 189-198
- Zhang, H. and Garga, V.K. (1997). Quasi-steady state: a real behaviour? *Canadian Geotechnical Journal*, 34: 749-761
- Zlatovic, S, and Ishihara, K. (1997). Normalized behaviour of very loose non-plastic soils: effects of fabric. *Soils and Foundations*, 37(4): 47-56

Appendix A

Formulae used for the data analysis

In order for the results to be clearly understood, all the main formulae that were used in the analysis were explained in this section. All data analysis was based on right cylinder assumption, induced by volume change and axial strain correction as compared with initial state according to various drainage conditions. Once localization or shear plane was observed, the data thereafter was removed even the test was continued.

A.1 Right cylinder assumption and strain localisation

In order for the cross-sectional area of a sample tested to be calculated, the standard right cylinder assumption was adopted. As large strains accumulate in the sample, they cause strain localisation and its behaviour deviates from this idealized adopted geometry. The sample may also barrel. Barreling and localisation both have a direct impact on volumetric strain calculations.

A.2 Formulae used for the data analysis

Given consolidated volume of sample V_0 , consolidated area A_0 , applied axial force P , axial displacement Δl , and measured volume change ΔV . The initial void ratio e_0 can be calculated as:

$$e_0 = G_s V_0 / m_s - 1 \quad (\text{A.1})$$

where G_s is specific gravity, m_s denotes the measured weight of dry sand.

The axial strain ε_a was calculated based on the change of axial length Δl over the sample length l for both internal and external axial displacements.

$$\varepsilon_a = \frac{\Delta l}{l} = \frac{\Delta l}{l_0 - \Delta l} \quad (\text{A.2})$$

The Volumetric Strain ε_v was in turn calculated by taking the ratio of the change in volume gauge reading ΔV (and therefore the change in volume) over the initially calculated volume of the sample ΔV .

$$\varepsilon_v = \frac{\Delta V}{V} = \frac{\Delta V}{V_0 - \Delta V} \quad (\text{A.3})$$

The corrected area:

$$A = A_0 \frac{1 - \varepsilon_v}{1 - \varepsilon_a} \quad (\text{A.4})$$

The corrected deviatoric stress q was given by the equation:

$$q = \sigma_1 - \sigma_3 = \frac{P}{A_0} \frac{1 - \varepsilon_a}{1 - \varepsilon_v} \quad (\text{A.5})$$

Note for undrained conditions, it reduces to:

$$q = \frac{P}{A_0} (1 - \varepsilon_a) \quad (\text{A.5})$$

It was followed by:

$$p = (\sigma_1 + 2\sigma_3)/3 \quad (\text{A.6})$$

The shear strain γ was calculated based on a combination of the axial strain and the volumetric strain.

$$\gamma = \varepsilon_1 - \varepsilon_3 = (3\varepsilon_a - \varepsilon_v)/2 \quad (\text{A.7})$$

The mobilized friction angle φ_m was calculated by the following equation.

$$\varphi_m = \sin^{-1} \frac{\sigma_1 - \sigma_3}{\sigma_1 + \sigma_3} \quad (\text{A.8})$$

Where σ_1 is the major principal stress and σ_3 the minor principal stress.

The maximum dilatancy angle ψ_{\max} was calculated from the volumetric strain versus axial strain curves. It was calculated from the steepest portion of the volumetric strain curves:

$$\psi_{\max} = -\sin^{-1} \left(\frac{d\varepsilon_v}{d\gamma} \right)_{\max} = \sin^{-1} \left(\frac{-d\varepsilon_v / d\varepsilon_1}{2 - d\varepsilon_v / d\varepsilon_1} \right)_{\max} \quad (\text{A.9})$$